Surgical Implant and Tissue Interface

A Dissertation Presented for the
Doctor of Philosophy
Degree
The University of Tennessee, Knoxville

Remigiusz Maciej Grzeskowiak
May 2020

Copyright © 2020 by Remigiusz Maciej Grzeskowiak.
All rights reserved.

DEDICATION

This work is dedicated to Ilona, Maciej, Kasia and Elizabeth as well as all equine patients who I have been blessed to work with throughout my career.

ACKNOWLEDGEMENTS

I would like to acknowledge everyone who has shown me exceptional support during my scientific adventure. I would like to acknowledge the CEM program at the University of Tennessee, College of Veterinary Medicine for giving me this amazing opportunity to prove myself in the research area. Further, I would like to thank my family, friends and my girlfriend who encourage me every day to chase my dreams and follow my plans. I would also like to thank all my mentors who have guided me throughout my education and who have motivated me to engage in the research projects, especially Drs. Anderson, Adair, Mulon, Schumacher, Harper, Dhar and Biris. Finally, I would like to acknowledge my fellows in the CEM program for their tremendous help with all my projects as well as the students involved in conducted studies for their extraordinary assistance and contagious enthusiasm.

PREFACE

This work provides a comprehensive assessment of surgical implant and tissue interface stability. The implants have been evaluated under different conditions within distinct tissues including cartilage and bone. The first chapter, literature review, offers a broad discussion of current challenges associated with implant placement in tissues as well as novel techniques that have been found to improve the stability of the implant and have a positive influence on the long-term integration.

Placing an implant in tissue leads to injury which must heal over time and healing results in the long-term integration of the implant. Several techniques have been described to improve the integration process, which essentially improves the healing of injured tissue. Some of these techniques concern novel implant designs which increase tissue and implant contact surface and therefore reduce focal stresses applied during insertion, distributing them over larger tissue area. Another common technique to improve long-term integration is coating the implants with various kinds of bioactive agents. Popular examples include growth factors and minerals which have been known to directly stimulate the healing process.

The following two chapters relate to ex-vivo research conducted on several implants placed in cartilage and bone. Suture and thyroid cartilage interface stability was evaluated with a single pullout to failure test on the laryngeal advancement constructs. The conclusions of this study lead to improved implant design which showed higher primary stability than the existing suture. The succeeding study evaluated osseointegration of screw implants placed in a dynamic compression plate to stabilize tibial defect using the peak reverse torque (PRT) method. Self-tapping screws were found to have better osseointegration after 60 days of loading as compared to non-self-tapping screws. Another conclusion of this study revealed that peak reverse torque can be used to measure the axial stability of an orthopedic plate.

Two final chapters relate to in-vivo studies and focus on the osseointegration of novel technology tissue scaffolding. Osseointegration of temporary bone fillers is an absolute prerequisite to enhance bone regeneration. Scaffolds were evaluated without additives in the goat and equine animal model as well as coated with recombinant human bone morphogenetic protein-2 and seeded with allogenic caprine mesenchymal stem cells in a goat animal model.

ABSTRACT

The stability of implant and tissue interface is vital for a long-term implant integration with adjacent tissue and directly impacts the surgical outcome. Literature provides comprehensive research conducted on implants engaged in soft as well as in hard tissues evaluating further their stability. The results helped establish several factors that have been found to be of importance in interface stability.

This comprehensive work incorporated research projects with the main focus on implant and tissue interface stability, which were evaluated using biomechanical assessment tools such as pullout as well as reverse torque measurement tests. Implants were evaluated under ex-vivo conditions, immediately after placement within the tissue as well as under in-vivo conditions, 2- and 6-months following implantation surgery in the goat and equine animal model.

In the following studies, the stability of interface has been found to be primarily influenced by several factors, including the amount of load experienced by the implants, stress applied by the implants to adjacent tissue as well as bioactive coatings. Furthermore, the studies included in this dissertation offer novel technologies that aim to improve interface stability-enhancing implant integration and tissue regeneration. These technologies concern novel design laryngeal clamps used to improve stability of laryngeal advancement constructs and novel technology polyurethane scaffolds coated with bioactive nanophase Hydroxyapatite to significantly enhance bone regeneration.

The research incorporated in this work found that increased tissue and implant contact areas resulted in increased interface stability and better integration. Furthermore, incorporation of bioactive coatings in bone scaffolds significantly enhanced osseointegration ultimately resulting in improved tissue regeneration. Laryngeal clamps with higher cartilage to implant contact area were superior in biomechanical testing as compared with standard suture. Self-tapping screws with an increased bone to implant contact area revealed higher osseointegration after 60 days of loading as compared with Non-self-tapping screws. Bioactive coatings such as nanophase Hydroxyapatite with decellularized bone particles or Mesenchymal Stem Cells were found to significantly enhance osseointegration of bone scaffolds and resulted in improved bone regeneration.

CONTENTS

Chapter One Surgical Implant and Tissue Interface. Literature Review 1
Introduction 2
Surgical Implant and Cartilage Interface 2
Surgical Implant and Ligament Interface 4
Cartilage - and Soft Tissue - Bone Interface 6
Surgical Implant and Bone Interface 8
Factors Affecting Osseointegration 10
Implant Stability in Bone 12
In-Vivo and Ex-Vivo Stability Testing 15
Ex-Vivo Stability Testing 16
Conclusions 19
Figures 20
Bibliography 21
Chapter Two Ex-vivo Mechanical Testing of Novel Laryngeal Clamps Used for Laryngeal Advancements Constructs 35
Abstract 36
Background 36
Results 36
Conclusions 37
Introduction 37
Materials and Methods 38
Preparation of the larynxes 38
Sample Measurements Collection 38
Uniaxial testing 39
Biaxial testing 39
Laryngeal Tie-forward (LTF) 39
Laryngeal Tie-forward modified with suture buttons (LTFB) 39
Laryngeal Tie-forward modified with novel laryngeal clamp (LTFC) 39
Uniaxial Biomechanical Testing 40
Biaxial Biomechanical Testing 41
Statistical Analyses 41
Results 42
Study Population 42
Sample Measurements Collection 42
Uniaxial Biomechanical Testing 43
Biaxial Biomechanical Testing 44
Discussion 44
Conclusions 47
Tables 48
Figures 53
Abbreviations 62
Footnotes 63
Bibliography 64

Chapter Three Biomechanical Evaluation of Peak Reverse Torque (PRT) in a Dynamic Compression Plate - Screw Construct Used in a Goat Tibia Segmental Defect Model 68
Abstract 69
Background 69
Results 69
Conclusions 69
Introduction 70
Materials and Methods 71
Results 73
Discussion 74
Conclusions 76
Tables 77
Figures 79
Abreviations 80
Footnotes 81
Bibliography 82
Chapter Four Assessment of a 3D Hydrophilic Polyurethane Scaffold containing nano-HA and bone particles, with or without BMP2 or mesenchymal stem cells, on Bone Regeneration and Neovascularization of massive (> 5cm) segmental defects 87
Abstract 88
Background 88
Results 88
Conclusions 88
Introduction 88
Materials and Methods 90
Study Population 90
Nano-HA polyurethane scaffold preparation 90
Caprine Mesenchymal Stem Cell Collection and Culture 90
Surgical Procedure and Postoperative care 91
High Definition Infrared Thermography (HD IR Thermography) 92
Radiography 92
Defect densitometry - Dual X-ray Absorptiometry (DXA) 92
Dual-Phase Computed Tomography (CT) Angiography 93
Histology 93
VEGF and BMP-2 concentration measurement 94
Statistical Analysis 94
Results 95
Study Population 95
High Definition Infrared Thermography (HD IR Thermography) 95
Radiography 96
Densitometry - Dual X-ray Absorptiometry (DXA) 97
Dual-Phase CT Angiography 98

Histology 99
VEGF and BMP-2 concentration measurement 100
Discussion 100
Conclusions 104
Tables 105
Figures 110
Abbreviations 123
Footnotes 124
Bibliography 126
Chapter Five Effects of novel 3D bone scaffold on the healing of equine IV metacarpal bones. 133
Abstract 134
Background 134
Results 134
Conclusions 134
Introduction 134
Materials and Methods 135
Study Population and Study Design 135
Study Timeline 135
Bone scaffold implantation surgery 136
Data acquisition throughout the study 136
Data Analysis 137
Tissue Biopsy 137
Histology 138
Statistical Analysis 138
Results 138
Discussion 139
Conclusions 141
Tables 142
Figures 144
Abbreviations 152
Footnotes 153
Bibliography 154
Vita 159

LIST OF TABLES

Table 2-1. Measurements of larynx thickness. 48
Table 2-2. Thickness comparison between laminae of thyroid cartilage. 49
Table 2-3. Side comparison in uniaxial testing. 50
Table 2-4. Comparison of biomechanical results during uniaxial testing. 51
Table 2-5. Comparison of biomechanical results during construct testing. 52
Table 3-1. Peak Reverse Torque categories for NST and ST screws. 77
Table 3-2. Prevalence of cortical fractures within each screw type. 78
Table 4-1. Radiographical ostectomy gap scoring 105
Table 4-2. Radiographical opacity of new bone scoring 105
Table 4-3. Radiographic defect size evaluation. 106
Table 4-4. BMD results comparison. 107
Table 4-5. CT Evaluation 107
Table 4-6. Bone and osteoid formation. 109
Table 4-7. Complications. 109
Table 5-1. Radiographical ostectomy gap filling scoring system. 142
Table 5-2. Radiographical opacity scoring system. 142
Table 5-3. CT ostectomy gap filling scoring system. 143
Table 5-4. Percent of defect filling. 143

LIST OF FIGURES

Figure 1-1. Implant stability in bone. 20
Figure 2-1. Thickness at 10 different anatomical positions. 53
Figure 2-2. Single-side LTF mechanical testing. 54
Figure 2-3. Biomechanical constructs testing. 55
Figure 2-4. Suture Button. 56
Figure 2-5. Views on laryngeal clamps. 57
Figure 2-6. Laryngeal clamps on the thyroid cartilage. 58
Figure 2-7. Before and after constructs testing. 59
Figure 2-8. Comparison of biomechanical performance of uniaxial constructs. .. 60
Figure 2-9. Comparison of biomechanical performance of the constructs. 61
Figure 3-1. Goat tibial defect ostectomy. 79
Figure 4-1. Survival Kaplan-Meier curve. 110
Figure 4-2. Thermography curve. 111
Figure 4-3. Radiographical assessment. 112
Figure 4-4. Defect reduction after surgery. 113
Figure 4-5. BMD comparison at termination points. 113
Figure 4-6. BMD curve. 114
Figure 4-7. Peripheral VEGF curve. 114
Figure 4-8. Peripheral BMP2 curve. 115
Figure 4-9. Defect Comparison. 116
Figure 4-10. Representative defect cMSC healing. 117
Figure 4-11. Defect measurements. 118
Figure 4-12. 3D CT reconstruction. 119
Figure 4-13. 2-month goats histology. 120
Figure 4-14. 6-month goats histology. 121
Figure 4-15. Fluorescence of 6-month specimens. 122
Figure 5-1. Bone scaffold. 144
Figure 5-2. Radiographic assessment of healing. 145
Figure 5-3. Ultrasonographic assessment of healing. 146
Figure 5-4. 3D CT reconstruction. 147
Figure 5-5. Scaffold and control histology. 148
Figure 5-6. Hyaline cartilage formation. 149
Figure 5-7. Thermography graph. 150
Figure 5-8. Radiographic evaluation 2M after surgery. 151
Figure 5-9. Defect density 2M after surgery. 151

CHAPTER ONE
SURGICAL IMPLANT AND TISSUE INTERFACE. LITERATURE REVIEW

Introduction

Surgical implants are routinely used in soft tissue as well as in orthopedic surgery, with a very wide range of applications. Common examples include screws, plates, and suture anchors used in orthopedics as well as sutures used in soft tissue and scaffolds used in tissue regeneration. Integration between implant and tissue is vital for construct stability and directly influences short- and long-term surgical outcomes. Therefore, current research aims to continuously improve the integration process. Optimally, implants will not lead to adverse reactions associated with surgery as well as will stimulate the integration process. Every implant insertion leads to tissue injury, which heals over time resulting in following implant integration. The integration process is associated with a strengthening of the implant-tissue interface. Several factors have been found to negatively as well as positively influence this process in distinct tissues. This literature review provides a comprehensive look into current knowledge about implant and tissue interface and novel approaches to strengthen the interface. Last paragraphs review approaches for biomechanical testing used to evaluate the integration process.

Surgical Implant and Cartilage Interface

Implant integration within cartilage is challenging due to tissue avascular nature as well as dense and rich in proteoglycans extracellular matrix (EM), strong forces applied to joint surface during physiologic joint motion and low coefficient of friction (1,2). Implantation process causes an injury within the tissue which further results in death of adjacent chondrocytes (2). Because of pour vascularization, material which would facilitate regeneration process is not accessible. This includes chondrogenic progenitor cells from circulating blood and marrow as well as resident chondrocytes which cannot migrate through the dense EM. All those factors have been found to negatively affect the integration process.

Anatomically, articular cartilage consists of chondrocytes that are surrounded by an extensive extracellular matrix which takes up to 90 % of tissue volume and contains primary water, aggrecans as well as type II collagen (1). Tissue is organized in four distinct areas which have been defined as the superficial zone, the intermediate zone, the radial zone and the calcified zone. All the anatomic structures have been involved in implant and tissue interface strengthening.

Pour ability of cartilage to regenerate chondral lesions has been confirmed on the lesions bigger than 6 mm in diameter (3). The osteochondral lesions have a better healing prognosis since the injury extends to subchondral bone causing bleeding (1). Blood coming from bone provides growth factors, mesenchymal stem cells and platelets necessary for the regeneration process. The blood clot formed after osteochondral injury can fill the defects with diameter below 23 mm in their entirety (1). Tissue repair is a complicated process which results in a transient fibrocartilaginous tissue as a replacement for hyaline cartilage (1). Fibrocartilage

is mechanically inferior to hyaline cartilage due to higher collagen I to collagen II ratio as well as lower proteoglycan content (4). It may appear that defect is healed after replacing it with fibrocartilage, however due inferior mechanical properties, microcracking will occur around margins between regenerated tissue and hyaline cartilage which will ultimately lead to the full thickness fissures (5-7). Continuous transition on interface of the implant is vital for the integration process because it provides chondrocyte viability (1).

Implant integration within cartilage is highly dependent on collagen fibers attachment to the surface of an implant as well as on chondrocyte migration and repopulation the interface. The implants placed in subchondral bone achieve higher stability than those placed only in cartilage which commonly result in a higher grade of integration (8). Furthermore, it was shown that the size, modulus, coefficient of friction, and poisons ratio of the implant is critically important in long-term integration (8). The implants with a size of 5 mm lead to a very small tissue damage and result in successful fixation within surrounding tissue (8). Chondral as well as osteochondral implants with lower material modulus, and higher coefficient of friction caused more damage to the interface due to higher shear stresses related to joint motion. The increase in Poisson's ratio was associated with a higher damage of surrounding tissue in implants placed in osteochondral defects as compared with the implants placed in chondral defects. The differences in coefficient of friction and poisson's ratio between cartilage and the implant have been attributed to different organization in collagen fiber distribution as well as different collagen content and crosslink density (9).

Implantation process has been associated with tissue injury which under in-vitro conditions resulted in a zone of cell death characterized by a band of necrosis 100-200 microns wide. The necrosis was followed by a gradual cell apoptosis over 14 days period and it extended the band up to 400 microns from the center of injury (10,11). Surviving cells outside the necrotic zone repopulate the matrix but they can only attach to the same lacunae as daughter cells and are not able to invade entire matrix (11). Because of the limitations in resident chondrocytes migration, delivering an implant with new chondrocytes can enhance the integration process (12-14). According to one study, autografts should contain between 5 and 30 million chondrocytes depending on the size of the defect (14). The source of new cells, including animal species from which the graft was harvested as well as the origin of implanting graft (auricular cartilage, tracheal cartilage etc.) are in a critical importance (12,13). The presence of even a small number of senescent cells within a graft has been associated with a negative influence on regeneration due to the pro-inflammatory properties, catabolic phenotype as well as existence of metalloproteinases (15). Cell apoptosis can be inhibited using caspase inhibitors such as ZVAD-fmk, however the current results are not convincing (16).

Collagen network has been also found to be important in creating implant and tissue interface (1). Integration process has been attributed to direct attachment of

collagen fibers to the surface of an implant (1). It was found that fusion of distinct cartilages with different developmental stages may cause lysyl-oxidase mediated collagen crosslinking which negatively impacts integration (17). Modulation of this process before implantation using β–aminopropionitrile, stimulates collagen maturation and increases its adhesive strength (18). Disruption of collagen fibers either through injury or enzymatic digestion leads to 10 times accelerated cellular proliferation and increased chondrocyte mobility which further repopulate the interface enhancing integration and mechanical strength of an implant (19,20). The most common enzymatic approaches include treatment with collagenase, chondroitinase ABC, trypsin or hyaluronidase (19-27). Furthermore, enzymatic treatment improves proteoglycan synthesis for a longer duration (24). It was also found that chemotactic agents such as insulin like growth factor-1 (IGF-1) and recombinant human bone morphogenetic protein -2 (BMP-2) boosted cell migration (28,29).

Several adhesives which improve implant stability have been described and the most commonly used from them is fibrin glue (30). Chemically modified chondroitin sulphate biopolymers with metacrylate and aldehyde groups to connect biomaterials and tissue protein have been also described (30). Collagen adhesion protein (CNA) is a bacterial surface protein synthetized by *Staphylococcus areus* to attach to monomeric chains of collagen (31,32). It is a well characterized protein with a high binding affinity to collagen type I and type II (31,32). Other examples of biologic adhesives include cationized gelatin (33) RGDs (34), multiple peptides in combination (such as RGD, YIGSR, and IKVAV) (35), and extracellular matrix proteins with or without growth factors such as collagen II and fibroblast growth factor (36). The molecules locally presented in synovial fluid which provides lubrication within the joint, included PRG4 (SZP/lubricin/megakaryocyte stimulating factor precursor) have been also associated with implant cartilage integration (37).

Surgical Implant and Ligament Interface

Similarly, like in cartilage, integration of an implant within ligament is challenging due to slow healing rate. This dense tissue is primarily composed of water (70%), collagen (25%) and matrix components which contain proteoglycans, fibronectin (4%) and tenocites (<1%) (38). Tissue structure is highly organized with tenocites as well as collagen fibers aligned longitudinally and interacting with one another through gap junctions, primarily connexin 32 and 43 (39). Slow healing has been attributed to limited vascular supply which is provided only in epiligament (38). Blood flow through the tissue is regulated by autonomic nerve supply and it may be increased during inflammation and tissue repair (40).

Ligament healing leads to a scar formation, which is known to have inferior tensile strength and viscoelastic properties as compared with native ligament tissue (41,42). Healing process corresponds to osteochondral healing and it is initiated

with internal bleeding as well as blood clot formation (41). During this time, tissue debris resulted from injury is being removed and angiogenic cells together with fibroblasts are attracted to produce matrix consisting of fibrous connective tissue. Collagen ratio in a scar is changed and contains predominantly collagen type III, V, and VI with significantly lower amount of type I (41). During slow further regeneration (up to 2 years), number of cells and vessels decreases, and the collagen alignment improves as well as collagen ratio changes to predominantly collagen type I (41).

Due to slow healing rate of injured tissue and significantly inferior mechanical properties, ligaments are not capable to resist physiologic tensile stresses and require immediate stabilization. Current regenerative research has targeted mostly collagen cross-links, predominant presence of type V collagen, and scar tissue formation (42-44). Level of collagen cross-links have been shown to decrease over 1 year after injury what resulted in the inferior mechanical properties of scar tissue (42). Predominant presence of type V collagen has been further attributed to a smaller fiber diameter due to smaller size fibrils (43). The inferior properties of scar tissue have been associated with presence of non-tensile structures such as blood vessels, fat cells, disorganized collagen fibers and cellular infiltrates (mostly fibroblasts) (44).

Regenerative research has found that cellular infiltrate within scar tissue are well responsive to growth factors, such as platelet derived growth factor (PDGF), basic fibroblastic growth factor (bFGF), epidermal growth factor (EGF) as well as transforming growth factor beta (TGF-beta) which stimulate their proliferation and collagen synthesis (44-46). Platelet rich plasma as a blood derived product, contains rich amount of majority of above-mentioned growth factors and therefore it has been shown to also stimulate the regenerative process (46). Further bioactive agents positively influencing ligament and tendon regeneration include hyaluronic acid (HA), collagen as well as mesenchymal stem cells (46).

Besides the bioactive agents used to stimulate tissue regeneration, several implants have been utilized to provide immediate stabilization of injured tissue and common examples include sutures and allografts. Sutures are used to reattach the ends of a torn ligament to reduce gap between the fragments and increase contact surface. Allografts are used in ligaments containing a defect to also reduce gap and increase contact surface. Gap size and decreased contact surface have been associated with a higher amount of scar formation which has a negative influence on strength of healed ligament up to 2 years after the injury (47).

Suturing process generates direct tissue trauma and cell death in tendons (48). Necrosis creates acellular zone in adjacent tissue within 72 hours which may persist for up to 1 year (48). This phenomenon was explained with tension applied across the suture grasp (49). Healing was not observed in the acellular zone for up to 1 year after surgery due to a pour vascularization, dense extracellular matrix

and aligned tendon cells (49,50). Acellular zone however led to an extended inflammation which has been found to result in adhesion formation (50). It has not been defined whether a predisposed location exist within ligament or tendon for this process to occur (50).

Suture and ligament or suture and tendon interface have been found to be the weakest link in initial surgical repair due to lack of implant stability and cyclic motion (46,50). Studies, which have tested suture and ligament interface, have found that braided suture was significantly more abrasive than monofilament and caused a sawing effect during cyclical loading (51). This effect ultimately led to suture pulling through the soft tissue and failure of the construct (51). This could be resolved, increasing contact surface between the implant and tissue applying for example more complicated suture knots. They appeared to be more stable as compared with the simple knots, in a study which looked at differences between massive cut (MAC) and modified Mason-Allen (MMA) sutures in rotator cuff repair (52).

Recent research has also introduced bio scaffold, porcine small intestine submucosa (SIS), which had promising results in tissue healing (46). Further proposed scaffold materials which had a positive influence on regeneration include biodegradable metallic scaffolds, porous magnesium or magnesium oxide (46). The aim of bio implants as well as bioactive agents is to enhance implant stability within tissue which would ultimately enhance the healing.

Cartilage - and Soft Tissue - Bone Interface

Bone, cartilage and ligament are often found in such anatomic structures as subchondral bone or ligament attachments. However, the relationship between tissues is not only anatomical but also physiological. Cooperation between them leads to a coordinated motion of the musculoskeletal system. Interaction between their interfaces can be further explained by transmission of mechanical forces. Cartilage is mostly suspected to compressive as well as shear stresses during joint kinematics, which are absorbed by the tissue and further transmitted to trabecular bone. Ligaments and tendons are mostly suspected to tension stresses during physiologic joint motion and muscle contraction which is further absorbed by the tissue and transmitted to bone.

The communication and similarities between cartilage and bone have been already seen at the genetic level (54). Under in vitro conditions, osteoblasts are known to stimulate chondrocytes differentiation (55). Furthermore, in patients with osteoarthritis (OA) certain genes expressed by the osteoblasts harvested from sclerotic areas of subchondral bone have been found to modulate functions of chondrocytes (56). The genetic similarities between osteoblasts and chondrocytes can be explained with a similar developmental pathway merged with a common progenitor cell and confirm the communication theory between both tissues and cell types (54).

As stated in paragraph above cartilage is defined as an avascular tissue which receives nutrients and oxygen through synovial fluid and from vasculature present in subchondral bone and calcified cartilage (54,57). Density of vasculature in subchondral bone has been directly influenced by the loading conditions (58). Further increase in vasculature density, protease expression, matrix degradation and increase in bone deposition adjacent to vasculature have been observed in bone with severe OA (59). Efficient transport across calcified cartilage from subchondral bone was proven in a study which measured concentration of hepatocyte growth factor within cartilage (60). In addition to vasculature, sensory nerves have been observed in the vascular channels at osteochondral junction which have been further associated with osteoarthritic pain in patients with OA (59).

Ligament and bone interface is highly organized in a specific structure named enthesis (61). Entheses connect tissues with different biomechanical profiles and are therefore suspected to complex stresses (62). These include tensile stresses applied to ligament and compressive stresses applied to bone (61). The complex stresses within structures require from entheses to have a gradient in tissue organization in order to effectively transmit forces across the interface and maintain communication between cells with different phenotype (61). Gradient in tissue organization relates to four transition zones, including ligament, non-mineralized fibrocartilage, mineralized fibrocartilage, and bone (61).

Differences between all four zones have been explained with the stress distribution within enthesis. Tensile stresses are highest within ligament and gradually decrease towards bone (63). Gradual increase in mineralization across the interface is constant with gradual decrease in collagen fiber organization moving from ligament to bone and results in a smooth mechanical stress distribution (64,65). Furthermore, presence of hyaline cartilage between calcified tissue and bone is associated with tissue adjustment to compression stress. In general, the differences are associated with ECM content, predominant collagen type (I,II,III and X) as well as cellular material (tenocytes, fibroblasts, fibrochondrocytes, osteoblasts, osteoclast and osteocytes) (61).

Research in regenerative medicine and orthopedic surgery currently aims at designing devices which could be used to surgically repair and reattach injured soft tissue to bone, mimicking the sophisticated and complicated structure of enthesis. Up to date however, such devices which would ideally mimic the enthesis have not been designed yet and the surgical repair of enthesis results in a mechanically inferior fibrovascular tissue formation at the repair site (66). Suture anchors are currently the most commonly used surgical implants to reattach the ligaments. The implants consist of two parts connected through an eyelet, the anchor part which is buried in bone and the suture part which reattaches ligament. The biomedical engineering has utilized a combination of micro- and nano-interfaces in designed devices to gradually distribute complex forces. Several

materials have been employed in the research including ceramics, natural polymers (alginate, silk, collagen) and synthetic polymers [poly(ε-caprolactone) (PCL), poly-L-lactic acid (PLLA), polyglycolic acid (PGA), and polylactid-co-glycolid acid (PLGA)] (61). Similarly, on the ligament site, utilized materials include natural (collagen, silk) and synthetic polymers [polyglycolic acid (PGA), poly-L-lactic acid (PLLA)] as well as decellularized native tendon or ligament (61).

The target is to create hybrid materials with different mechanical properties to optimally mimic gradient in enthesis mechanical properties (61). Specifically, using a combination of polymer and ceramic with different Young's modulus would better mimic the gradual mineralization across enthesis (67). An example includes a recent research done on complex and stratified collagen scaffold which incorporated following materials, collagen, collagen cross-linked with chondroitin sulfate and collagen mixed with HA (68). The stratified structure resulted in a smooth stress distribution and distinct cells adhesion within the implant. Further scaffolds are in shape of films, hydrogels, sponges or foam porous scaffolds, meshes and micro/nanofibers.

The surface of an implant has been also modified with nanocomposites which successfully increased scaffold porosity, surface area, and roughness resulting in superior physicochemical properties, increased protein adsorption and nutrient exchange (67,69). The bioactive agents such as mesenchymal stem cells (MSC), tenocytes, dermal fibroblasts have been also used to improve implant stability (61,66). Next, several growth factors have been used including transforming growth factor-b (TGF-b), growth differentiation factor (GDF), platelet derived growth factor (PDGF), fibroblast growth factor (FGF), and connective tissue growth factor (CTGF) (61,66). Finally, proteins have been incorporated into the implants including bone morphogenetic protein (BMP-2,-7), parathyroid hormone related protein (PTHrP), Indian hedgehog (Ihh) as well as transcription factor (Sox9). All above mentioned bioactive agents have been shown to increase cell proliferation and protein expression as well as increased extracellular matrix (ECM) production in soft tissues (70,66).

Surgical Implant and Bone Interface

Surgical implant and bone interface is very important for the construct stability. Implants, such as orthopedic screw, plates and nails have been used in orthopedics as well as in orthodontics to repair injured bone and ceramic tooth. If bone insult is associated with a tissue loss, the defects are filled with either autologous or allogeneic bone grafts, depending on the size of a defect and preference of the surgeon. Injured bones, especially long, weight-bearing bones with a compromised structure, are unable to mechanically withstand the loading conditions. Therefore, surgical repair of long bones warrants additional mechanical support and ultimately creates an environment which stimulates bone healing. In orthodontics, the ceramic teeth are being implanted for esthetic reasons.

Proper fixation can be only achieved with stable implants and literature defines implant stability as primary (mechanical) and secondary (biological). Implant stability has been widely studied in the literature and it has been found that the micro-motion between bone and implant exceeding 150 μm will negatively influence secondary stability (71-74). The excessive motion leads to increased tensile and shear stresses which are associated with a fibrous membrane formation around the implant, otherwise called fibroplasia (75,76). Fibroplasia can further result in further implant displacement decreasing implants secondary stability (75,76).

Implant integration within bone has been found to be dependent three properties of the materials, including osteoinduction, osteoconduction and osseointegration (71,77-80). Osteoinduction has been defined as ability of the material to stimulate undifferantied and pluripotent cells to form the bone-forming cell lines (77). Osteoconduction has been defined as material ability to allow for bone tissue growth on the outer surface as well as within the pores and interconnected channels (77-80). Both terms are difficult to differentiate under in-vivo conditions, because injury created during implant placement or bone fracture begins cellular and extracellular bone healing cascade which already contain osteoinductive growth and differentiation factors (77,81,82).

Osseointegration has become one of the most important terms defining bone and implant interface (71,77-80). This term has been widely studied in orthodontic surgery as well as less frequently in orthopedics (80,83-88). The pioneers who discovered the process are Brånemark et al, however Albrektsson et al evaluated the process under light microscope and defined it as direct contact between bone and implant (89,90). In order to say that an implant is well osseointegrated, direct bone formation line around the implant has to be really thin and ranged between 10 and 20 μm (77). It can occur directly on the implant as direct osteogenesis or from surrounding bone as distance osteogenesis (71). Osseointegration is strongly associated with osteoinduction and osteoconduction (71,77). The biomechanical definition of osseointegration describes it as a process which leads to rigid fixation achievement of the alloplastic material which can be maintained during physiologic loading (91).

Osseointegration process has been further distinguish in several biologic stages which are corresponding to bone healing. Those include hematoma formation, mesenchymal tissue development, intramembranous woven bone formation as well as lamellar bone formation (72,92). First stage is initiated with internal bleeding caused by implant insertion. Blood cells involving red blood cells, platelets as well as inflammatory cells such as polymorphonuclear granulocytes and monocytes reach the implant surface through extravascular migration (82).

Migrated cells are being entrapped on implants surface and activated there. Activation is followed by secretion of cytokines and other growth factors, such as

insulin like growth factor (IGF I and II), fibroblast growth factor (FGF), transforming growth factors beta (TGF-β), and platelet derived growth factor (PDGF) (82). Bone morphogenetic protein-2 and -7 that belong to TGF-β family have gained a special interest in orthopedic research due to their excellent osteoinductive properties. Activation of platelets induces several morphological and biochemical changes which consist of adhesion, aggregation as well as induction of phosphotyrozine, intracellular calcium increase, and phospholipids hydrolysis (82). Present cellular material ultimately shapes a fibrin matrix which works as a biologic and osteoconductive scaffold that also stimulates osteogenic cells to produce bone around the implant (osteoinduction)(82).

Originally created matrix consist of poorly mineralized osteoid tissue structurally similar to bone cement lines and laminae, which forms a continuous 0.5 mm thick layer containing mainly calcium, phosphorus, osteopontin and bone sialoprotein (92). This thin osteoid tissue layer is being gradually calcified by osteoblasts directly on implants surface. Osteoblasts furthermore support this process by collagen matrix deposition (92). Calcification process is followed by the vascular and stem cells invasion in the non-calcified spaces (93). Vascularization is a vital part of ostoegenesis which has a significant impact on osseointegration process (94,95).

Direct and distance osteogenesis occurs simultaneously with host bone resorption conducted by osteoclasts and the processes are separated with a clear demarcation line. Early mineralized osteoid tissue is being gradually transformed into a woven bone which not only is a space filler but also maintains integrity between host tissue and implant providing a mechanical support during the early loading phase (94,95). Three-dimensional woven bone works furthermore as a scaffold for cell attachment and bone deposition (94,96). These early processes related to bone formation begin as soon as 10-14 days after implantation (95). Within three months after the surgery, woven bone is being gradually remodeled into a lamellar bone (95). During the remodeling phase, new osteons circle around the implant with long axis parallel to implants surface. Osseointegration of an implant is confirmed with a thin line of bone containing osteoclasts, osteoblasts, mesenchymal stem cells as well as lymphatic/blood vessels in immediate surroundings. This line can further extend up to 1 mm away from implants surface (77,96).

Factors Affecting Osseointegration

Osseointegration is a complicated process which has been found to be positively influenced by several factors such as topography of implant surface, material, shape, length, diameter, material surface treatment and coatings (hydroxyapatite, bone morphogenetic protein-2) (97), status of adjacent bone (98), mechanical stability and loading conditions applied to the implant (90), adjuvant treatments

such as bone grafting, osteogenic biological coatings (99-101) as well as pharmacological agents such as simvastin and bisphosphonates (102,103).

Macroscopic and microscopic topography of the implant has a vital impact on integration with adjacent bone. It has been proven that a rough surface of the implant stimulates osseointegration through several known mechanisms. Rough surface regulates osteoblast activation, proliferation and differentiation and these processes have been associated with activation of integrin receptors that bind to sequences/domains arginine-glycine-aspartate (ArgGly-ASP or RGD) of proteins (104,105). These Arg-Gly-Asp or RGD are expressed in several bone matrix proteins, including collagen I, fibronectin, osteopontin and bone sialoprotein. After implantation they are immobilized on material surface to promote cell adhesion via ligand receptor reaction (105,106). Activated integrins regulate phosphokinase C and A through phospholipase C and A2 pathways (104).

Rough surface have been further associated with a higher expression of bone formation indicators such as osteocalcin and alkaline phosphatase (101). It also increases implant area in contact with host bone (BIC) supporting primary stability (107,108). Several methods such as spraying with titanium plasma, coating with hydroxyapatite, machine processing such as polishing, sandblasting and acid etching have been described to increase roughness of the surface (108,109).

Smooth surface on the other hand induces more commonly distance osteogenesis in contrast to rough surface (110). Optimal size of microscopic pores an implant have been defined as 80 µm and above to enhance bone formation on implants surface (111). Recent studies have further shown that utilizing multiple surface topography such as a combination of micro and nano topography even more enhances osseointegration process. Nano pores have a direct impact on selective adhesion of osteoblasts and positively influence their proliferation and differentiation (112). Interestingly, even small amount of micro motion (around 30 µm) has been associated with enhanced osseointegration, however any motion above 150 µm significantly impairs the process (72-74).

Gap size between implant and bone also influences osseointegration process. If an implant is placed in a tight contact with bone, only poor bone formation or even bone resorption has been observed, whereas presence of a small gap between implant body and host bone allows for a new trabeculae formation and therefore supports biological fixation. Gaps should however not exceed 500 µm to not reduce the quality of newly formed bone as well as to not delay gap filling process (95,113). Increased gap size significantly reduces bone and implant contact surface (BIC) which has been defined as significant parameter of osseointegration. The process can be also evaluated with bone density measurements, histomorphometry, mineral apposition rate as well as biomechanical tests such as torque measurements, push-out or pullout tests, and resonance frequency test.

The type of material has also a significant influence on osseointegration. To the physical properties which are of importance in the process belong materials modulus, ideally would be similar to cortical bone, high volumetric porosity (70-80%), high frictional characteristics as well as excellent biocompatibility (114). Recently discovered porous tantalum (c.p. tantalum) has been found to be currently the best osseointegrative material (114). Another method to enhance osseointegration, material coatings, such as hydroxyapatite coating which has been also shown to significantly stimulate the process due to excellent osteoconductive and osteoinductive properties.

The literature provides several factors that in contrast have a negative impact on osseointegration process, and those include previously mentioned excessive micro motion (above 150 μm) and related to it increased interfacial strain, inappropriate porosity of the porous coating, radiation therapy (76, 114-116), medications such as cyclosporine A, methotrexate, cis-platinum, warfarin, low molecular weight heparins as well as non-steroidal anti-inflammatory drugs (NSAID) (116-122). The most common nonselective COX-1 and COX-2 inhibitors include diclofenac and phenylbutazone. Diclofenac delayed bone healing in cortical and cancellous bone around titanium implants inserted in the rats after continuous administration for 5 days (122). Phenylbutazone on the other hand reduced the mineral apposition rate in horses after 14 days of continuous administration (123).

Further negative for osseointegration factors include osteoporosis, rheumatoid arthritis, advanced age, nutritional deficiency, smoking and renal insufficiency (124-127). In osteoporosis, the balance between anabolic and catabolic bone metabolism is impaired, causing increased activity of osteoclasts and reduced neovascularization process (81). All of above-mentioned factors lead to failure of peri-implant osteogenesis which has been associated with decreased number and activity of osteogenic cells, increased osteoclastic activity, imbalance between anabolic and catabolic local factors, abnormal bone cell proliferation rate as well as impaired vascularization of peri-implant tissue (97). Osseointegration is a dynamic process named otherwise as biological fixation because it occurs over time after implant placement and it results in secondary stability of the implant.

Implant Stability in Bone

The bond between implant (orthopedic screw or dental implant) and bone is defined with primary and secondary stability. Primary stability is obtained by the implant immediately after placement in bone and it has been influenced by several factors such as surgical technique, implant design, surface texture, loading and related to it micro motion as well as quality of surrounding bone (128-131). Primary stability has been also defined as “mechanical stability” because occurs immediately after implant placement and it is not affected by the osseointegration process (132). Furthermore, because primary stability is associated only with

mechanical properties, it can be easily evaluated under in-vivo as well as ex-vivo conditions.

One of the factors strongly correlated with primary stability is surgical technique and especially insertional torque. Surgical drilling not only causes damage to surrounding bone but also increases temperature within adjacent tissue (132). Death of bone cells occurs when temperature exceeds 47 °C over a time of 1 min (133). Furthermore, surgeons commonly undersize drilling osteotomy prior to implant placement to increase insertion torque during implant placement and increase primary stability. Several studies have found that better primary stability is achieved when osteotomy is 10% smaller than the outside diameter of an implant. Further decreasing the size of osteotomy to 25% of the outside diameter has not given additional benefits (134).

A high insertional torque of dental implants has also been found to have a destructive effect on direct peri-implant tissue causing micro fractures and subsequent bone resorption (135-137). Orthodontic research recommends a lower insertional torque because it is more osteoprotective, resulting in better osseointegration over time (138-140).

Situation looks slightly different in orthopedics. Several articles in orthopedic research have looked at the difference in primary stability of self-tapping and non-self-tapping screws. Self-tapping screws have been found to have a significantly higher insertional torque and through that higher primary stability (128,141-143). Higher insertion torque was attributed to torque required to cut the threads in bone with a cutting flute at the top of implant (128,141). Non-self-tapping screws lack this cutting flute and their placement is preceded with pre-tapping process which is conducted using a tap device (128,141). The tap devices have longer threads creating a micro gap between screw and bone, which results in a significantly lower insertion torque but also in a micro motion and increased interfacial strain (130,131,135,141). Micro gap decreases further the BIC and leads to a lower primary stability of the implant (144).

Encountered discrepancies between the stability of an implant in orthodontics and orthopedics can be explained with bone anatomy and implant design. The craniofacial bones contain mostly cancellous bone which has lower bone mineral density (BMD) in contrast to the long bones which due to a higher content of cortical bone, have higher BMD (145,146). Lower BMD has been also associated with lower BIC. Both have been strongly correlated with primary implant stability and insertion torque (IT) (147,148). Because the craniofacial bones have lower BMD, the peak IT is generally lower than in load bearing bones, and they are more prone to the destructive effect of higher IT. Furthermore, increased IT does not result in increased BIC and primary stability of the implants used in orthodontics. In orthopedics denser bones are more resistant to the higher IT which results in higher BIC and primary stability of the implant.

Primary stability can be evaluated under in-vivo as well as ex-vivo conditions using common mechanical testing methods such as resonance frequency analysis (RFA), percussion test (Periotest), insertion torque (IT) and cutting torque resistance analysis (CRA). Under Ex-vivo conditions followed methods can be utilized including pullout, pushout and bending. Results of implant primary stability measured with RFA under in-vivo conditions are displayed as implant stability quotient (ISQ) which is a graphical (Figure 1) and numerical representation of implant stability and related micro motion. ISQ ranges from 1 to 100, where 1 is a mobile implant and 100 implies maximum stability. ISQ cutoff has been defined as 47 and below this value the implant has no sufficient primary stability (149,150).

As new bone is being formed around the implant, secondary stability is being achieved (Figure 1, all figures are placed in the appendix) (85). Secondary stability is related to long-term stability of the implant and bone interface and it is obtained during the process of osseointegration (132,137). Secondary stability has been named otherwise “biological stability” due to healing influence on the process (132). Since both processes occur simultaneously, the same factors which impact osseointegration, will have an impact on secondary stability (79,97-103).

Several studies have found a significant association between primary and secondary stability (132,135,137). In other words, lesser micro motion leads to better osseointegration. Recent systematic review reports a correlation between primary and secondary stability measured with RFA to be significant and equaled 0.847 (137). Several other studies which looked at survival rate of dental implants with or without primary stability have found that primary stability is not the only factor influencing osseointegration (131,132).

The literature does not provide a specific definition of lack of primary stability. One study classified lack of primary stability of the dental implants into four categories, and those included no rotation [1], light rotation with a feeling of resistance [2], rotation without resistance [3], and rotation combined with lateral oscillation [4] (151). The implants which were assigned to second, third and fourth category were defined as implants having no stability (151). Other research defined lack of stability as a torque below 10 Ncm and slight lateral mobility (152).

Another recent study looked at 3111 dental implants and reported 79.8% survival rate of the implants with no primary stability (71 out of 89) over 3 years compared with 93.4% (2823 out of 3022) survival rate of the implants with primary stability over 3 years (153). More detailed analysis of the without primary stability revealed a significant difference in survival rate of implants coated (91.8%) and not coated (53.6%) with Hydroxyapatite (HA) (153). This confirms relevance of texture of the implant surface in osseointegration process as well as implies that HA coating may improve osseointegration process even in the implants without primary stability.

Rough surface as a beneficial effect in obtaining osseointegration similarly among the implants with or without primary stability. The process can be evaluated with a limited number of mechanical tests under in-vivo as well as ex-vivo conditions, including resonance frequency analysis (RFA) or percussion test (Periotest). Significantly more tests can be conducted to evaluate the process ex-vivo, including peak reverse torque (PRT), pullout, pushout, torsion and bending test.

In-Vivo and Ex-Vivo Stability Testing

Mechanical testing of implant stability provides several options which can be conducted under in-vivo as well as ex-vivo conditions (88,154-157). The tests include resonance frequency analysis (RFA), percussion test (Periotest), insertion torque (IT) as well as cutting torque resistance analysis (CRA). Those tests evaluate implants micro motion as well as encountered resistance during placement of the implant. The tests have been therefore used to evaluate primary as well as secondary stability.

The method most commonly used in dentistry to evaluate primary and secondary implant stability is resonance frequency analysis (RFA). It has been developed and described by Meredith et al in 1998 (154). It utilizes an L shaped transducer device connected with a vibrating element and receptor. The vibrating element applies a continuous and repeatable impact wave or a single impact force to the assessed implant and the receptor in device records resonance signal from the implant and bone component (154,158). Originally, the resonance was measured in Hz unit, but over time this was replaced by a new, developed by Osstell et al., ISQ unit which corresponds with implant stability quotient (149,150).

Another test utilized in orthodontics to measure primary stability is Periotest. The test was originally developed and described by Schulte et al. to evaluate natural tooth mobility (155). The device contains a metallic rod that applies controlled tapping force to the object. The response to tapping is measured by a sensor within the hand piece and it is converted to periotest value (PTV). PTV ranges from -8 (low mobility) to +50 (high mobility) (88,155). The PTV values of an osseointegrated implant fall in the range of -5 to +5 (88). The scientific articles have assumed that PTV precisely reflects the BIC (156).

Cutting Torque Resistance Analysis (CRA) was developed by Friberg at all in 1995 (157). This method measures a torque required to cut a thread in the implant osteotomy site during a low-speed threading. It gives a valuable information about the quality of adjacent bone (157). CRA has been used significantly less frequently than insertion torque (IT) measuring method. The methods described above are used primarily in orthodontics and the research in orthopedics is lacking.

Insertion torque (IT) measures peak resistance torque during implant placement (142,158,159). IT has been measured only during implant placement therefore it does not assess development of osseointegration and secondary stability of the

implant (142). It has been widely studied in orthodontics as well as in orthopedics. Utilization of this method has developed recommendations regarding optimal insertion torque during specific implant placement. For instance, the orthodontic studies recommend optimal torque for implant placement of 0.032 Nm (159). The IT values in orthopedics are significantly higher and dependent on the size of placed screw within the orthopedic plate, e.g. 1.70 Nm for 3.5 mm screw or 4.0 Nm for 4.5 mm screw (160,161). It is a feasible method which can be used to assess primary stability of an implant under in-vivo as well as ex-vivo conditions.

Ex-Vivo Stability Testing

Hence secondary stability occurs over time, it can be only evaluated after the implant had been placed in tissue. Based on above provided literature review, osseointegration process occurs as early as 14 days after implantation and it may take up to 3 months. There are several mechanical tests which can be utilized under both in-vivo as well as ex-vivo conditions and most significant are described in the paragraph above. Several other methods not only test the implant integration, but also the integrity of entire construct repaired with the implant, can be only conducted under ex-vivo conditions. Those methods require a mechanical testing system such as Instron machine and include pullout, pushout, torsion and bending tests. Peak reverse torque can be also performed using a torque measuring screwdriver.

Peak reverse torque (PRT) has been successfully used in the research on orthodontic as well as orthopedic implants (86,87,129-131,162,163). This method measures torque required to remove an implant from bone and to break the bond between bone and osseointegrated implant (86,87,129-131,162,163). PRT has been shown to be strongly influenced by the grade of osseointegration (86,129-131). It is a very sensitive method to evaluate not only a single orthodontic or orthopedic implant but also the entire orthopedic plate-screw stability as it has been recently proven (86).

Osseointegration has been negatively influenced by loading conditions and micro motion of the implant as stated in the paragraph above. The differences in loading between single implants used to fix dynamic compression (DC) orthopedic plate, should affect the osseointegration process (86). Hence, the axial strength of a DC plate can be predicted with axial strength of the weakest screw in the construct, PRT provides more insight information about the stability of entire tested construct (86).

Further mechanical testing methods discussed in this literature review are used to test entire constructs such as a long bone repaired with orthopedic plate and screws (128) as well as soft tissue constructs such as anchoring the thyroid

cartilage with laryngeal clamps (164) or collateral ligaments with the suture anchors (165). The tests have to be conducted under ex-vivo conditions because their aim is to test construct stability until it fails (128,164,166-168). Pullout tests have been used to test single implants or entire constructs in several orthopedic as well as soft tissue studies (128,164,166-168). Pullout is caused by displacement of the actuator in the testing frame which applies tensile stresses to tested implant or entire construct (169). Tests are being conducted until implant is being entirely removed from tissue and construct fails (164,166,167). Rate of displacement should be adjusted accordingly to the testing method created for specific construct.

During tests several mechanical parameters are measured, and the most important involve maximum tension load, actuator displacement and construct stiffness. Maximum tension load has been defined as maximum tensile load measured at implant or construct failure (170). The actuator displacement corresponds with distance measured from its original position to its position at the end of conducted study and construct stiffness corresponds with calculated load over displacement slope (164,170).

A recent study used this method to evaluate stability of rostral laryngeal advancement constructs (tie-forward), the surgery commonly performed on horses suffering from dorsal displacement of soft palate (DDSP) (164). The method of construct failure was associated with the suture and cartilage interface, due to shear stresses applied by the suture to surrounding tissue. As a solution to this problem a novel technology laryngeal clamp have been proposed (164). Laryngeal clamps distribute tensile stress applied to them during swallowing, over a larger area and therefore protect thyroid cartilage (164). The clamps increase stiffness of entire construct, reducing the risk of construct displacement in postoperative period (164).

Another test utilized to evaluate single implants or entire construct in bone as well as soft tissue is torsional loading (169-172). In torsion, load applied to the specimen causes its rotation about axis, previously specified in methodology (172). Torsion creates a complex composition of internal stresses which involve compression, tension and shear. Maximum values of all stresses have been found on the surface of tested specimen and they are being reduced towards neutral axis. Maximum shear stresses act on a plane perpendicular and parallel to neutral axis, whereas maximum normal stresses (tensile and compressive) act 45° to the axis of tested specimen. A recent study compared stability of an interference screws versus unicortical buttons used to reattach the biceps tendon in human

cadaveric model. The study utilized torsion method to assess the stability of both implants with the conclusions that unicortical button provides a higher stability fixation (172).

Bending tests have been widely used in biomechanical testing in orthopedic research (166,173-175). The unique testing method also generates composition of stresses which involve compression and tension (169,170). During bending, compression stress is applied to upmost surface of the specimen, adjacent to the actuator and tension is applied to opposite site, far from actuator (169,170). This method has been used to test the entire constructs as opposed to single implant (165,173-175). Current mechanical testing devices are capable of conducting two different bending methods including 3- and 4-point bending.

The difference between 3- and 4-point bending is related to number of loading points attached to actuator (175). In 3-point bending, the actuator contains one loading point between two holding points, creating therefore three stressing points on the tested specimen. Bending moment is concentrated in the area directly under one loading point (175). This results in a higher focused bending stress. In contrast, in 4-point bending, the actuator contains two loading points and two holding points, therefore four stress points (165,173-175). Bending moment is equally distributed between two loading points, increasing the distribution area of bending stress (175). A recent study utilized 4-point bending method to evaluate bending stiffness of metacarpophalangeal collateral ligament repair construct which utilized suture anchors (165). The study compared the ultimate bending resistance of native collateral ligaments and compared it to the constructs repaired with the suture anchors. Further findings included no significant difference in resistance to bending between constructs repaired with different suture anchors (165). Conclusion of this study was that suture anchors can be used to enhance immediate postoperative stabilization of injured collateral ligaments (165).

The literature review provides several options for mechanical testing of implant stability. Methods can be utilized to test the bone or soft tissue constructs as well as single implants. Depending on question stated in the research and implant of interest, the method can be chosen and adjusted accordingly. All the tests can be used in a simple load to failure mode or in cycles with relaxation and creep mode. In some situations, cyclical tests mimic in-vivo conditions better than simple load to failure.

Conclusions

Surgical implantation leads to tissue injury and results in cellular death adjacent to surgical site. Improved healing through enhanced cellular regeneration will stimulate implant stabilization within tissue. Bleeding is the first step of healing in all tissues described above and it has direct influence on the healing process. Limited bleeding after tissue injury in avascular tissues such as cartilage and ligament makes the integration process challenging. This literature review provided several novel approaches on cartilage, ligament as well as in bone to improve implant integration. Current knowledge reveals that design of implant, close to native structure of targeted tissue has a better chance for integration. This however cannot always be achieved, and, in such situations, bioactive coatings may be a solution to stimulate the integration process.

Figures

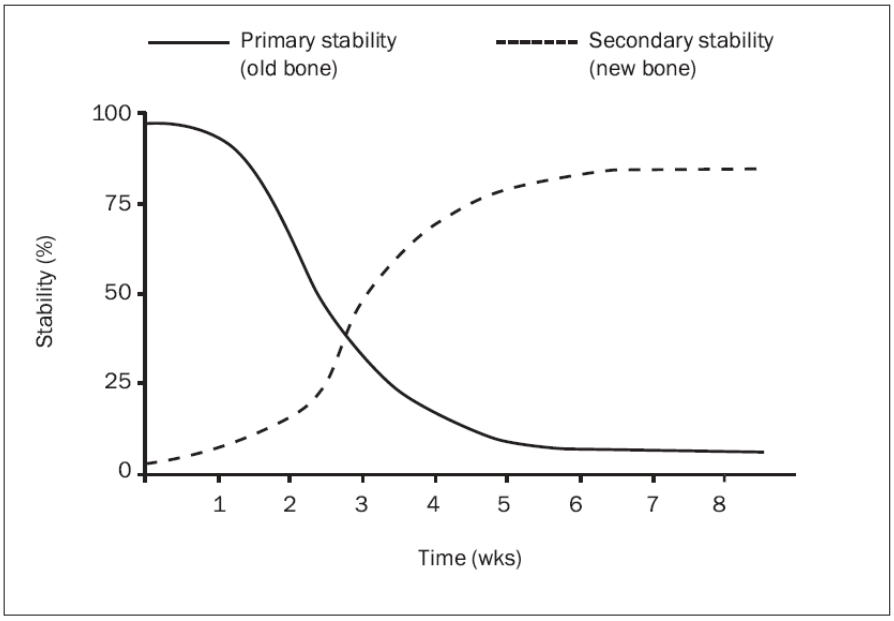


Figure 1-1. Implant stability in bone.

Graph presents gradual changes in primary (mechanical) vs secondary (biological) stability of an implant placed in bone. Primary as well as secondary stability have an influence on total implant stability. There is a decrease in total stability between 2 and 4 weeks after implantation. Graph imported from Raghavendra S, et al. Early Wound Healing Around Endosseous Implants: A review of the Literature. The International Journal of Oral & Maxillofacial Implants 2005; 20(3):425-430. The permission to use the figure was granted by the publisher.

Bibliography

References

1. Khan IM, Gilbert SJ, Singharo SK, Duance VC, Archer CW. Cartilage integration: Evaluation of the reasons for failure of integration during cartilage repair. A Review. European Cells and Materials 2008; 16:26-39
2. Wang D, Williams CG, Yang F, Elisseeff J. Enhancing the Tissue-Biomaterials Interface: Tissue-Initiated Integration of Biomaterials. Adv Funct Mater 2004; 14(12):1152-1158
3. Jackson DW, Lalor PA, Aberman HM, Simon TM. Spontaneous repair of full-thickness defects of articular cartilage in a goat model. A preliminary study. J Bone Joint Surg Am 2001; 83-A:53-64.
4. LaPrade RF, Bursch LS, Olson EJ, Havlas V, Carlson CS. Histologic and immunohistochemical characteristics of failed articular cartilage resurfacing procedures for osteochondritis of the knee: A case series. Am J Sports Med 2008; 36:360–368.
5. Shapiro F, Koide S, Glimcher MJ. Cell origin and differentiation in the repair of full-thickness defects of articular cartilage. J Bone Joint Surg Am 1993; 75:532-553.
6. Zhang Z, McCaffery JM, Spencer RG, Francomano CA. Growth and integration of neocartilage with native cartilage in vitro. J Orthop Res 2005; 23:433–439.
7. Solheim E, Hegna J, Oyen J, Austgulen OK, Harlem T, Strand T. Osteochondral autografting (mosaicplasty) in articular cartilage defects in the knee: Results at 5 to 9 years. Knee 2010; 17:84–87.
8. Vahdati A., Wagner DR. Implant size and mechanical properties influence the failure of the adhesive bond between cartilage implants and native tissue in a finite element analysis. Journal of Biomechanics 2013; 46, 1554-1560
9. Wong M, Ponticiello M, Kovanen V, Jurvelin JS. Volumetric changes of articular cartilage during stress relaxation in unconfined compression. Journal of Biomechanics33,1049–1054.
10. Redman SN, Dowthwaite GP, Thomson BM, Archer CW. The cellular responses of articular cartilage to sharp and blunt trauma. Osteoarthritis Cartilage 2004; 12:106-116.
11. Tew SR, Kwan AP, Hann A, Thomson BM, Archer CW. The reactions of articular cartilage to experimental wounding: role of apoptosis. Arthritis Rheum 2000; 43:215-225.
12. Zhang Z, McCaffery JM, Spencer RG, Francomano CA. Growth and integration of neocartilage with native cartilage in vitro. J Orthop Res 2005; 23:433-439.
13. Peretti GM, Randolph MA, Caruso EM, Rossetti F, Zaleske DJ. Bonding of cartilage matrices with cultured chondrocytes: an experimental model. J Orthop Res 1998; 16:89-95

14. Bentley G, Biant LC, Carrington RW, Akmal M, Goldberg A, Williams AM, Skinner JA, Pringle J. A prospective, randomised comparison of autologous chondrocyte implantation versus mosaicplasty for osteochondral defects in the knee. J Bone Joint Surg Br 2003; 85:223-230.
15. D'Lima DD, Hashimoto S, Chen PC, Lotz MK, Colwell CW. Prevention of chondrocyte apoptosis. J Bone Joint Surg Am 2001; 83(Suppl 2):25-26.
16. Darabi R, Perlingeiro RC. Lineage-specific reprogramming as a strategy for cell therapy. Cell Cycle. 2008; 7(12):1732-7.
17. DiMicco MA, Sah RL. Integrative cartilage repair: adhesive strength is correlated with collagen deposition. J Orthop Res 2001; 19:1105-1112.
18. McGowan KB, Sah RL. Treatment of cartilage with beta-aminopropionitrile accelerates subsequent collagen maturation and modulates integrative repair. J Orthop Res 2005; 23:594-601.
19. Bos PK, DeGroot J, Budde M, Verhaar JA, van Osch GJ. Specific enzymatic treatment of bovine and human articular cartilage: implications for integrative cartilage repair. Arthritis Rheum 2002; 46:976-985.
20. Qiu W, Murray MM, Shortkroff S, Lee CR, Martin SD, Spector M. Outgrowth of chondrocytes from human articular cartilage explants and expression of alpha smooth muscle actin. Wound Repair Regen 2000; 8:383-391.
21. Silverman RP, Bonassar LJ, Passaretti D, Randolph MA, Yaremchuk MJ. Adhesion of tissue-engineered cartilage to native cartilage. Plast Reconstr Surg 2000; 105:1393-1398.
22. Bos PK, DeGroot J, Budde M, Verhaar JA, van Osch GJ. Specific enzymatic treatment of bovine and human articular cartilage: implications for integrative cartilage repair. Arthritis Rheum 2002; 46:976-985.
23. Qiu W, Murray MM, Shortkroff S, Lee CR, Martin SD, Spector M. Outgrowth of chondrocytes from human articular cartilage explants and expression of alpha smooth muscle actin. Wound Repair Regen 2000; 8:383-391.
24. Lee DA, Bentley G, Archer CW. Proteoglycan depletion alone is not sufficient to stimulate proteoglycan synthesis in cultured bovine cartilage explants. Osteoarthritis Cartilage 1994; 2:175-185.
25. Lee MC, Sung KL, Kurtis MS, Akeson WH, Sah RL. Adhesive force of chondrocytes to cartilage. Effects of chondroitinase ABC. Clin Orthop Relat Res 2000; 370:286-294.
26. Hunziker EB, Kapfinger E. Removal of proteoglycans from the surface of defects in articular cartilage transiently enhances coverage by repair cells. J Bone Joint Surg Br 1998; 80:144-150.
27. Obradovic B, Martin I, Padera RF, Treppo S, Freed LE, Vunjak-Novakovic G. Integration of engineered cartilage. J Orthop Res 2001b; 19:1089-1097.
28. Fortier LA. Insulin-like growth factor-1 enhances cell-based repair of articular cartilage. J Bone Joint Surg Br 2002; 84:276–288.

29. Sellers RS, Zhang R, Glasson SS, Kim HD, Peluso D, D'Augusta DA, Beckwith K, Morris EA. Repair of articular cartilage defects one year after treatment with recombinant human bone morphogenetic protein-2 (rhBMP-2). J Bone Joint SurgAm2000; 82:151–160.
30. Drobnic M, Radosavljevic D, Ravnik D, Pavlovcic V, Hribernik M. Comparison of four techniques for the fixation of a collagen scaffold in the human cadaveric knee. Osteoarthritis and Cartilage 2006; 14,337–344.
31. Switalski LM, Speziale P, Hook M. Isolation and characterization of a putative collagen receptor from Staphylococcus aureus strain Cowan 1. J Biol Chem 1989; 264:21080–21086.
32. Patti JM, Jonsson H, Guss B, Switalski LM, Wiberg K, Lindberg M, Hook M. Molecular characterization and expression of a gene encoding a Staphylococcus aureus collagen adhesin. J Biol Chem 1992; 267:4766–4772.
33. Chen JP, Su CH. Surface modification of electrospun PLLA nanofibers by plasma treatment and cationized gelatin immobilization for cartilage tissue engineering. Acta Biomater 2011; 7:234–243.
34. Kambe Y, Yamamoto K, Kojima K, Tamada Y, Tomita N. Effects of RGDS sequence genetically interfused in the silk fibroin light chain protein on chondrocyte adhesion and cartilage synthesis. Biomaterials 2010; 31:7503–7511.
35. Santiago LY, Nowak RW, Rubin JP, Marra KG. Peptide-surface modification of poly(caprolactone) with laminin-derived sequences for adipose-derived stem cell applications. Biomaterials 2006; 27:2962–2969
36. Ma Z, Gao C, Gong Y, Shen J. Cartilage tissue engineering PLLA scaffold with surface immobilized collagen and basic fibroblast growth factor. Biomaterials 2005; 26:1253–1259.
37. Schaefer DB, Wendt D, Moretti M, Jakob M, Jay GD, Heberer M, Martin I. Lubricin reduces cartilage—cartilage integration. Biorheology 2004; 41:503-508.
38. Hildebrand KA, Frank CB. Scar formation and Ligament healing. CJS 1998; 41(6): 425-429
39. Waggett AD, Benjamin M, Ralphs JR. Connexin 32 and 43 gap junctions differentially modulate tenocyte response to cyclic mechanical load. Eur J Cell Biol 2006; 85(11):1145-1154.
40. McDougall JJ, Ferrell WR, Bray RC. Sympathetically mediated constrictor responses in normal and ACL-deficient rabbit knees. Proceedings of the 31st Annual Meeting of the Canadian Orthopaedic Research Society, Hamilton, Ont., 1997. p. 51.
41. Hildebrand KA, Frank CB. Scar formation and Ligament healing. CJS 1998; 41(6): 425-429
42. Hildebrand KA, Frank CB. Biology of ligament injury and repair. In Johnson R, Lombardo J, editors. Current review of sports medicine. 2nd ed. Philadelphia: Current Medicine; 1998. p.121-31.

43. Frank C, McDonald D, Wilson J, Eyre D, Shrive N. Rabbit medial collateral ligament scar weakness is associated with decreased collagen pyridinoline crosslink density. J Orthop Res 1995; 13:157-65.
44. Shrive N, Chimich D, Marchuk L, Wilson J, Brant R, Frank C. Soft tissue “flaws” are associated with the material properties of the healing rabbit medial collateral ligament. J Orthop Res 1995; 13:923-6.
45. Hildebrand KA, Frank CB. Biology of ligament injury and repair. In Johnson R, Lombardo J, editors. Current review of sports medicine. 2nd ed. Philadelphia: Current Medicine; 1998. p. 121-31.
46. Ponce BA, Hosemann CD, Parthasarathy R, Tate JP, Sheppard ED, Eberhardt AW. A Biomechanical Analysis of Controllable Intraoperative Variables Affecting the Strength of Rotator Cuff Repairs at the Suture-Tendon Interface. Am J Sports Med. 2013; 41(10):2256-2261
47. Frank CB, Bray RC, Hart DA, Shrive NG, Loitz BJ, Matyas JR, et al. Soft tissue healing. In Fu FH, Harner CD, Vince KG, editors. Knee surgery. Baltimore: Williams & Wilkins; 1994. p.189-229.
48. Wong JK, Cerovac S, Ferguson MW, McGrouther DA. The cellular effect of a single interrupted suture on tendon. J Hand Surg Br 2006; 31(4):358-367.
49. Rawson S., Cartmell S., Wong J. Suture techniques for tendon repair; a comparative review. Muscles, Ligaments and Tendons Journal 2013; 220(3):220-228
50. Wong JK, Alyouha S, Kadler KE, Ferguson MW, Mc-Grouther DA. The cell biology of suturing tendons. Matrix Biol 2010; 29(6):525-536.
51. Savage AJ, Spruiell MD, Schwertz JM, McGwin G, Eberhardt A, Ponce BA. The Effect of Sliding Knots on the Suture-Tendon Interface Strength. Am J Sports Med. 2013; 41(2):296-301
52. Kowalsky MS, Dellenbaugh SG, Erlichman DB, et al. Evaluation of suture abrasion against rotator cuff tendon and proximal humerus bone. Arthroscopy. 2008;24(3):329-334.
53. Bisson LJ, Manohar LM, Wilkins RD, Gurske-Deperio J, Ehrensberger MT. Influence of suture material on the biomechanical behavior of suture tendon specimens: a controlled study in bovine rotator cuff. Am J Sports Med. 2008;36(5):907-912.
54. Mahjoub M, Berenbaum F, Houard X. Why subchondral bone in osteoarthritis? The importance of the cartilage bone interface in osteoarthritis. Osteoporosis Int 2012; (Suppl 8): S841-S846
55. Westacott CI, Webb GR, Warnock MG, Sims JV, Elson CJ. Alteration of cartilage metabolism by cells from osteoarthritic bone. Arthritis Rheum 1997; 40:1282–1291
56. Sanchez C, Deberg MA, Bellahcene A, Castronovo V, Msika P, Delcour JP, Crielaard JM, Henrotin YE. Phenotypic characterization of osteoblasts from the sclerotic zones of osteoarthritic subchondral bone. Arthritis Rheum 2008; 58:442–455

57. Malinin T, Ouellette EA. Articular cartilage nutrition is mediated by subchondral bone: a long-term autograft study in baboons. Osteoarthr Cartil 2000; 8:483–491
58. Lane LB, Villacin A, Bullough PG. The vascularity and remodelling of subchondrial bone and calcified cartilage in adult human femoral and humeral heads. An age- and stress-related phenomenon. J Bone Joint Surg Br 1977; 59:272–278
59. Walsh DA, Bonnet CS, Turner EL, Wilson D, Situ M, McWilliams DF. Angiogenesis in the synovium and at the osteochondral junction in osteoarthritis. Osteoarthr Cartil 2007; 15:743–751
60. Guevremont M, Martel-Pelletier J, Massicotte F, Tardif G, Pelletier JP, Ranger P, Lajeunesse D, Reboul P. Human adult chondrocytes express hepatocyte growth factor (HGF) isoforms but not HgF: potential implication of osteoblasts on the presence of HGF in cartilage. J Bone Miner Res 2003; ƒ18:1073–1081
61. Tellado SF, Balmayor ER, Griensven MV. Strategies to engineer tendon/ligament-to-bone interface: Biomaterials, cells and growth factors. Advanced Drug Delivery Reviews 2015; 94:126-140
62. H.M. Shaw, M. Benjamin, Structure–function relationships of entheses in relation to mechanical load and exercise. Scand. J. Med. Sci. Sports 2007; 17 (4):303–315.
63. Benjamin M, Ralphs JR. Fibrocartilage in tendons and ligaments—an adaptation to compressive load. J. Anat. 1998; 193:481–494.
64. G.M. Genin, et al., Functional grading of mineral and collagen in the attachment of tendon to bone, Biophys. J. 2009; 97(4):976–985.
65. M. Benjamin, et al., Where tendons and ligaments meet bone: attachment sites (‘entheses’) in relation to exercise and/or mechanical load, J. Anat. 2006; 208(4):471–490.
66. Harris E, Liu Y, Cunnife G, Morrisey D, Carrol S, Mulhall K, Kelly DJ. Biofabrication of Soft Tissue Templates for Engineering the Bone-Ligament Interface. Biotechnology and Bioengineering 2017; 114(10): 2400-2411
67. Amini AR, Laurencin CT, Nukavarapu SP. Bone tissue engineering: recent advances and challenges. Crit. Rev. Biomed. Eng. 2012; 40(5):363–408.
68. Kim BS, et al. Human collagen-based multilayer scaffolds for tendon-to-bone interface tissue engineering. J. Biomed. Mater. Res. 2014; A102(11):4044–4054.
69. Caplan MR, Shah MM. Translating biomaterial properties to intracellular signaling. Cell Biochem. Biophys.2009; 54(1–3):1–10.
70. Woo SLY. Tissue engineering: use of scaffolds for ligament and tendon healing and regeneration. Knee Surg Sports Traumatol Arthrosc 2009; 17:559–560
71. Mavrogenis AF, Dimitriou R, Parvizi J, Babis GC. Biology of implant osseointegration. J Musculoskelet Neuronal Interact 2009; 9(2):61-71

72. Cameron HU, Pilliar RM, MacNab I. The effect of movement on the bonding of porous metal to bone. J Biomed Mater Res 1973; 7:301-11.
73. Maniatopoulos C, Pilliar RM, Smith DC. Threaded versus porous-surfaced designs for implant stabilization in bone-endodontic implant model. J Biomed Mater Res 1986; 20:1309-33.
74. Soballe K, Hansen ES, Brockstedt-Rasmussen H, Joergensen PH, Bünger C. Tissue ingrowth into titanium and hydroxyapatite-coated implants during stable and unstable mechanical conditions. J Orthop Res 1992; 10:285-99.
75. Giori NJ, Ryd L, Carter DR. Mechanical influences on tissue differentiation at bone-cement interfaces. J Arthroplasty 1995; 10:514-22.
76. Pilliar RM, Lee JM, Maniatopoulos C. Observations on the effect of movement on bone ingrowth into poroussurfaced implants. Clin Orthop Relat Res 1986; 208:108-13.
77. Albrektsson T., Johansson C. Osteoinduction, osteoconduction and osseointegration. Eur Spine J 2001; 10:S96-S101
78. Wilson-Hench J. Osteoinduction. In: Williams DF (ed) Progress in biomedical engineering, vol 4. Definitions in biomaterials. Elsevier 1977, Amsterdam, p 29
79. Brånemark R, Braenemark P-I, Rydevik B, Myers RR. Osseointegration in skeletal reconstruction and rehabilitation: A review. Journal of Rehabilitation Research and Development 2001; 38(2): 175-181
80. Novaes AB Jr, de Souza SLS., de Barros RRM, Pereira KKY, Iezzi G, Piattelli A. Influence of Implant Surfaces on Osseointegration. Braz Dent J 2001; 21(6): 471-481
81. Fini M, Giavaresi G, Torricelli P, Borsari V, Giardino R, Nicolini A, Carpi A. Osteoporosis and biomaterial osteointegration. Biomed Pharmacother 2004; 58:487-93.
82. Davies JE. Mechanisms of endosseous integration. Int J Prosthodont 1998; 11:391-401.
83. Adell R, Lekholm U, Rockler B, Braenemark PI. A 15 year study of osseointegrated implants in the treatment of the edentulous jaw. Int J Oral Surg 1981; 10:387-416.
84. Rupp F, Liang L, Geis-Gerstorfer J, Scheideler L, Huettig F. Surface characteristics of dental implants: A review. Dental Materials 2018; 34:40-57
85. Raghavendra S, Wood MC, Taylor TD. Early Wound Healing Around Endosseous Implants: A review of the Literature. The International Journal of Oral & Maxillofacial Implants 2005; 20(3):425-430
86. Grzeskowiak RM, Wheeler C, Taylor E, Lillich J, Roush J, Biris AS, Anderson DE. Biomechanical evaluation of peak reverse torque (PRT) in a dynamic compression plate-screw construct used in a goat tibia segmental defect model. BMC Vet Res 2019; 15:321
87. White AA, Kubacki MR, Samona J, Telehowski P, Atkinson PJ. Removal torque of nail interlocking screw is related to screw proximity to the fracture and screw breakage. J Engineering in Medicine. 2016;230(6):599–603.

88. Olive J, Aparicio C. Periotest method as a measure of osseointegrated oral implant stability. Int J Oral Maxillofac Implants 1990;5(4):390–400.
89. Braenemark PI, Hansson BO, Adell R, Breine U, Lindström J, Hallén O, Öhman A. Osseointegrated titannium implants in the treatment of the edentulous jaw. Scand J Plast Reconstr Surg 1977; 11 [Suppl 16]:1–175
90. Albrektsson T, Braenemark PI, Hansson HA, Lindstroem J. Osseointegrated titanium implants. Requirements for ensuring a long-lasting, direct bone anchorage in man. Acta Orthop Scand 1981; 52:155–170
91. Zarb G, Albrektsson T. Osseointegration – a requiem for the periodontal ligament? – An editorial. Int J Periodont Rest Dentistry 1991; 11:88–91
92. Meyer U, Joos U, Mythili J, Stamm T, Hohoff A, Fillies T, Stratmann U, Wiesmann HP. Ultrastructural characterization of the implant/bone interface of immediately loaded dental implants. Biomaterials 2004; 25:1959-67.
93. Murai K, Takeshita F, Ayukawa Y, Kiyoshima T, Suetsugu T, Tanaka T. Light and electron microscopic studies of bone-titanium interface in the tibiae of young and mature rats. J Biomed Mater Res 1996; 30:523-33.
94. Gailit J, Clark RA. Wound repair in the context of extracellular matrix. Curr Opin Cell Biol 1994; 6:717-25.
95. Franchi M, Fini M, Martini D, Orsini E, Leonardi L, Ruggeri A, Giavaresi G, Ottani V. Biological fixation of endosseous implants. Micron 2005; 36:665-71.
96. Probst A, Spiegel HU. Cellular mechanisms of bone repair. J Invest Surg 1997; 10:77-86.
97. Marco F, Milena F, Gianluca G, Vittoria O. Periimplant osteogenesis in health and osteoporosis. Micron 2005; 36:630-44
98. Linder L, Obrant K, Boivin G. Osseointegration of metallic implants. II. Transmission electron microscopyin the rabbit. Acta Orthop Scand 1989; 60:135-9
99. Khan SN, Cammisa FP Jr, Sandhu HS, Diwan AD, Girardi FP, Lane JM. The biology of bone grafting. J Am Acad Orthop Surg 2005; 13:77-86
100. Arrington ED, Smith WJ, Chambers HG, Bucknell AL, Davino NA. Complications of iliac crest bone graft harvesting. Clin Orthop 1996; 329:300-9
101. Younger EM, Chapman MW. Morbidity at bone graft donor sites. J Orthop Trauma 1989; 3:192-5
102. Eberhardt C, Habermann B, Müller S, Schwarz M, Bauss F, Kurth AH. The bisphosphonate ibandronate accelerates osseointegration of hydroxyapatite-coated cementless implants in an animal model. J Orthop Sci 2007; 12:61-6.
103. Basarir K, Erdemli B, Can A, Erdemli E, Zeyrek T. Osseointegration in arthroplasty: can simvastatin promote bone response to implants? Int Orthop 2007;
104. Boyan BD, Sylvia VL, Liu Y, Sagun R, Cochran DL, Lohmann CH, Dean DD, Schwartz Z. Surface roughness mediates its effects on osteoblasts via protein kinase A and phospholipase A2. Biomaterials 1999; 20:2305-10.

105. Tosatti S, Schwartz Z, Campbell C, Cochran DL, Vandevondele S, Hubbel JA, et al. RGD-containing peptide GCRGYGRGDSPG reduces enhancement of osteoblast differentiation by poly(Llysine)-graft-poly(ethylene glycol)-coated titanium surfaces. J Biomed Mater Res A 2004; 68:458-472.
106. Rezania A, Thomas CH, Branger AB, Waters CM, Healy KE. The detachment strength and morphology of bone cells contacting materials modified with a peptide sequence found within bone sialoprotein. J Biomed Mater Res 1997; 37:9-19.
107. Park JY, Davies JE. Red blood cell and platelet interactions with titanium implant surfaces. Clin Oral Implants Res 2000; 11:530-9.
108. Cochran DL, Nummikoski PV, Higginbottom FL, Hermann JS, Makins SR, Buser D. Evaluation of an endosseous titanium implant with a sandblasted and acid-etched surface in the canine mandible: radiographic results. Clin Oral Implants Res 1996; 7:240-52.
109. Soballe K, Overgaard S, Hansen ES, Brokstedt-Rasmussen H, Lind M, Bunger C. A review of ceramic coatings for implant fixation. J Long Term Eff Med Implants 1999; 9:131-51.
110. Franchi M, Bacchelli B, Martini D, Pasquale VD, Orsini E, Ottani V, Fini M, Giavaresi G, Giardino R, Ruggeri A. Early detachment of titanium particles from various different surfaces of endosseous dental implants. Biomaterials 2004; 25:2239-46.
111. Galois L, Mainard D. Bone ingrowth into two porous ceramics with different pore sizes: an experimental study. Acta Orthop Belg 2004; 70:598-603.
112. De Oliveira PT, Nanci A. Nanotexturing of titanium-based surfaces upregulates expression of bone sialoprotein and osteopontin by cultured osteogenic cells. Biomaterials 2004; 25:403-413.
113. Berglundh T, Abrahamsson I, Lang NP, Lindhe J. De novo alveolar bone formation adjacent to endosseous implants. Clin Oral Implants Res 2003; 14:251-62.
114. Levine BR, Sporer S, Poggie RA, Della Valle CJ, Jacobs JJ. Experimental and clinical performance of porous tantalum in orthopedic surgery. Biomaterials 2006; 27:4671-81.
115. Otsuki B, Takemoto M, Fujibayashi S, Neo M, Kokubo T, Nakamura T. Pore throat size and connectivity determine bone and tissue ingrowth into porous implants: three-dimensional micro-CT based structural analyses of porous bioactive titanium implants. Biomaterials 2006; 27:5892-900.
116. Kudo M, Matsui Y, Ohno K, Michi K. A histomorphometric study of the tissue reaction around hydroxyapatite implants irradiated after placement. J Oral Maxillofac Surg 2001; 59:293-300.
117. Sumner DR, Turner TM, Pierson RH, Kienapfel H, Urban RM, Liebner EJ, Galante JO. Effects of radiation on fixation of non-cemented porous-coated implants in a canine model. J Bone Joint Surg Am 1990; 72:1527-33.

118. Eder A, Watzek G. Treatment of a patient with severe osteoporosis and chronic polyarthritis with fixed implant-supported prosthesis: a case report. Int J Oral Maxillofac Implants 1999; 14:587-90.
119. McDonald AR, Pogrel MA, Sharma A. Effects of chemotherapy on osseointegration of implants: a case report. J Oral Implantol 1998; 24:11-3.
120. Callahan BC, Lisecki EJ, Banks RE, Dalton JE, Cook SD, Wolff JD. The effect of warfarin on the attachment of bone to hydroxyapatite-coated and uncoated porous implants. J Bone Joint Surg Am 1995; 77:225-30.
121. Dahners LE, Mullis BH. Effects of nonsteroidal antiinflammatory drugs on bone formation and soft-tissue healing. J Am Acad Orthop Surg 2004; 12:139-43.
122. Pablos AB, Ramalho SA, König B Jr, Furuse C, de Araújo VC, Cury PR. Effect of meloxicam and diclofenac sodium on peri-implant bone healing in rats. J Periodontol 2008; 79:300-6.
123. Rohde C, Anderson DE, Bertone AL, Weisbrode SE. Effects of phenylbutazone on bone activity and formation in horses. AJVR 2000; 61(5):537-543
124. Rosenqvist R, Bylander B, Knutson K, Rydholm U, Rooser B, Egund N, Lidgren L. Loosening of the porous coating of bicompartmental prostheses in patients with rheumatoid arthritis. J Bone Joint Surg Am 1986; 68:538-42.
125. Zhang H, Lewis CG, Aronow MS, Gronowicz GA. The effects of patient age on human osteoblasts' response to Ti-6Al-4V implants in vitro. J Orthop Res 2004; 22:30-8.
126. Mombelli A, Cionca N. Systemic diseases affecting osseointegration therapy. Clin Oral Implants Res 2006; 17(Suppl.2):97-103.
127. Wong MM, Rao LG, Ly H, Hamilton L, Ish-Shalom S, Sturtridge W, Tong J, McBroom R, Josse RG, Murray TM. In vitro study of osteoblastic cells from patients with idiopathic osteoporosis and comparison with cells from non-osteoporotic controls. Osteoporos Int 1994; 4:21-31.
128. Andrea CR, Stover SM, Galuppo LD, Taylor KT, Rakestraw PC. Comparison of insertion time and pullout strength between self-tapping and non–selftapping AO 4.5-mm cortical bone screws in adult equine third metacarpal bone. Vet Surg. 2002; 21:189–94.
129. Stenlund P, Murase K, Stalhandske C, Lausmaa J, Palmquist A. Understanding mechanisms and factors related to implant fixation a model study of removal torque. J Mech Behav Biomed Mater. 2014; 34:83–92.
130. Okazaki J, Komasa J, Sakai D, Kamada A, Ikeo T, Toda L, Suwa F, Inoue M, Etoh T. A torque removal study on the primary stability of orthodontic titanium screw mini implants in the cortical bone of dog femurs. Int J Oral Maxillofac Surg. 2008; 37:647–50.
131. Chowdhary R, Jimbo R, Thomsen C, Carlsson L, Wennerberg A. Biomechanical evaluation of macro and micro-designed screw-type implants: an insertional torque and removal torque study in rabbits. Clin Oral Impl Res. 2013; 24:342–6.

132. Al-Sabbagh M., Eldomiaty W., Khabbaz Y. Can Osseointegration be achieved without primary stability? Dent Clin N Am 2019; 63:461-473
133. Anitua E, Carda C, Andia I. A novel drilling procedure and subsequent bone autograft preparation: a technical note. Int J Oral Maxillofac Implants 2007;22(1):138.
134. Turkyilmaz I, Aksoy U, McGlumphy EA. Two alternative surgical techniques for enhancing primary implant stability in the posterior maxilla: a clinical study including bone density, insertion torque, and resonance frequency analysis data. Clin Implant Dent Relat Res 2008;10(4):231–7.
135. Cha JY, Pereira MD, Smith AA, et al. Multiscale analyses of the bone-implant interface. J Dent Res 2015:94:482-490
136. Yuan X, Pei X, Zhao Y, et al. Biomechanics of immediate postextraction implant osseointegration. J Dent Res 2018; 97:987-994
137. Monje A, Ravida A, Wang HL, et al. Relationship between primary/mechanical and secondary/biological implant stability. The International Journal of Oral & Maxillofacial Implants 2019; 34, Supplement
138. West JD, Oates TW. Identification of stability changes for immediately placed dental implants. Int J Oral Maxillofac Implants 2007; 22:623-630
139. Bayarchimeg D, Namgoong H, Kim BK, et al. Evaluation of the correlation between insertion torque and primary stability of dental implants using a block bone test. J Periodontal Implant Sci 2013; 43:30–36.
140. Sakoh J, Wahlmann U, Stender E, Nat R, Al-Nawas B, Wagner W. Primary stability of a conical implant and a hybrid, cylindric screw-type implant in vitro. Int J Oral Maxillofac Implants 2006; 21:560–566.
141. Phillips JH, Rahn BA. Comparison of compression and torque measurements of self-tapping and Pretapped screws. Plast and Reconstr Surg. 1989;83(3): 447–58.
142. Boyle JM III, Frost DE, Foley WL, et al. Torque and pullout analysis of six currently available self-tapping and emergency screws. J Oral Maxillofac Surg. 1993; 51:45–50.
143. Bahr W. Pretapped and self-tapped screws in the human midface: torque measurements and bone screw interface. Int J Oral Maxillofac Surg. 1990;19: 51–3.
144. Johansson CB, Gretzer C, Jimbo R, Mattison I, Ahlberg E. Enhanced implant integration with hierarchically structured implants: a pilot study in rabbits. Clin Oral Implants Res. 2012; 23:943–53.
145. Klemetti E, Vainio P, Lassila V, Alhava E. Cortical bone mineral density in the mandible and osteoporosis status in postmenopausal women. Scand J Dent Res. 1993; 101(4):219-23.
146. Chen H, Zhou X, Fujita H, Onozuka M, Kubo KY. Age-Related Changes in Trabecular and Cortical Bone Microstructure. Hindawi International Journal of Endocrinology 2013; 213234:1-9

147. Miyamoto I, Tsuboi Y, Wada E, et al. Influence of cortical bone thickness and implant length on implant stability at the time of surgery–clinical, prospective, biomechanical, and imaging study. Bone 2005;37(6):776–80.
148. Norton MR. The influence of low insertion torque on primary stability, implant survival, and maintenance of marginal bone levels: a closed-cohort prospective study. Int J Oral Maxillofac Implants 2017;32(4):849–57.
149. Zix J, Hug S, Kessler-Liechti G, Mericske-Stern R. Measurement of Dental Implant Stability by Resonance Frequency Analysis and Damping Capacity Assessment: Comparison of Both Techniques in a Clinical Trial. he International Journal of Oral & Maxillofacial Implants 2008; 23(3): 525-530
150. Sennerby L., Meredith N. Implant stability measurements using resonance frequency analysis: biological and biomechanical aspects and clinical implications. Periodontology 2000; 47:51–66
151. Rodrigo D, Aracil L, Martin C, et al. Diagnosis of implant stability and its impact on implant survival: a prospective case series study. Clin Oral Implants Res 2010; 21(3):255–61.
152. Verardi S, Swoboda J, Rebaudi F, et al. Osteointegration of tissue-level implants with very low insertion torque in soft bone: a clinical study on SLA surface treatment. Implant Dent 2018; 27(1):5–9.
153. Orenstein IH, Tarnow DP, Morris HF, et al. Three-year post-placement survival of implants mobile at placement. Ann Periodontol 2000; 5(1):32–41.
154. Meredith N. Assessment of implant stability as a prognostic determinant. Int J Prosthodont 1998;11(5):491–501.
155. Romanos GE, Nentwig G-H. Immediate functional loading in the maxilla using implants with platform switching: five-year results. Int J Oral Maxillofac Implants 2009; 24(6):1106–12
156. Morris HE, Ochi S, Crum P, et al. Bone density: its influence on implant stability after uncovering. J Oral Implantol 2003; 29(6):263–9.
157. Friberg B, Sennerby L, Roos J, et al. Evaluation of bone density using cutting resistance measurements and microradiography: an in vitro study in pig ribs. Clin Oral Implants Res 1995; 6(3):164–71
158. Tseng YC, Ting CC, Du JK, Chen CM, Wu JH, Chen HS. Insertion torque, resonance frequency, and removal torque analysis of microimplants. Kaohsiung J Med Sci. 2016; 32:469–74
159. Ottoni JM, Oliveira ZF, Mansini R, et al. Correlation between placement torque and survival of single-tooth implants. Int J Oral Maxillofac Implants 2005;20(5): 769–76.
160. Zhang JY, Tornetta P, Jones B, Zheng Y, Whitten A, Cartner J, Ricci WM. Locking Hole Inserts: Effect of Insertion Torque on Fatigue Performance and Insert Loosening in Locking Plates. J Orthop Trauma 2019; 33:120-124
161. Disegi JA. Metallic Instruments and Implants In: Auer J.A., Stick J.A. Equine Surgery 4th Edition, Elsevier Saunders, Missouri 2012; pages: 1040-1046

162. Carlsson L, Rostlund T, Alberktsson B, Alberktsson T. Removal torques for polished and rough titanium implants. Int J Oral Maxillofac Implants. 1988; 3:21–4.
163. Morberg R, Albrektsson T. A histomorphometric and removal torque analysis of c.p. titanium implants inserted in reamed bone beds with and without acrylic cement. J Mater Sci: Mater M. 1992; 3(3):170–4.
164. Grzeskowiak RM, Schumacher J, Mulon PY, Steiner RC, Cassone L, Anderson DE. Ex-vivo mechanical testing of novel laryngeal clamps used for laryngeal advancements constructs. Front. Vet. Sci. 2020; 7:139.
165. Grzeskowiak RM, Rifkin RE, Mulon PY, Harper DP, Adair HS, Anderson DE. In Vitro Biomechanical Testing of Equine Metacarpophalangeal Collateral Ligaments and Collateral Ligaments Repair Using Suture Anchors. Manuscript accepted in BMC Vet Res.
166. Lin CC, Lin KJ, Chen WC, Wei HW, Lin KP, Tsai CL. Larger screw diameter may not guarantee greater pullout strength for headless screws – a biomechanical study. Biomed Tech (Berl) 2017; 62(3):257-261
167. Gustafson PA, Veenstra JM, Bearden CR, Jastifer JR. The Effect of Pitch Variation and Diameter Variation on Screw Pullout. Foot Ankle Spec 2019; 12(3):258-263
168. Prasanthi P, Garlapati R, Nagesh B, Sujana V, Kiran Naik KM, Yamini B. Effect of 17% ethylenediaminetetraacetic acid and 0.2% chitosan on pushout bond strength of biodentine and ProRoot mineral trioxide aggregate: An in vitro study. J Conserv Dent. 2019; 22(4):387-390
169. Smith G, Markel M, Roe S, Budsberg S. Biomechanics for Surgeons. ACVS Symposium, October 24th, 1993.
170. Timmie-Topoleski LD, Tsao AK, Friis EA, Jones LC. 3-Fundamental principles of mechanical testing. Mechanical Testing of Orthopaedic Implants 2017:33-47
171. Watanabe F, Hiroyasu K, Ueda K. The fracture strength by a torsion test at the implant-abutment interface. Int J Implant Dent 2015; 1(1):25
172. Khalid MA, Morris RP, Black N, Maassen NH. Biomechanical Evaluation of Humerus Fracture after Subpectoral Biceps Tenodesis with Interference Screw Versus Unicortical Button. Arthroscopy. 2020 Jan 20. pii: S0749-8063(19)30962-4
173. Robinson ST, Svet MT, Kanim LA, Metzger MF. Four-point bending as a method for quantitatively evaluating spinal arthrodesis in a rat model. Comp Med (2015) 65:46-50.
174. Darrow BG, Weigel JP, Greenacre CB, Xie X, Liaw PK, Biskup JJ. Ex-vivo Biomechanical Comparison of Titanium Locking Plate, Stainless Steel Nonlocking Plate, and Tie-in External Fixator Applied by a Dorsal Approach on Ostectomized Humeri of Pigeons (Columba livia). J Avian Med Surg (2019) 33:29-37.

175. Gee C, Weddell JN, Swain MV. Comparison of three- and four-point bending evaluation of two adhesive bonding systems for glass-ceramic zirconia bi-layered ceramics. Dent Mater (2017) 33:1004-1011.

CHAPTER TWO
EX-VIVO MECHANICAL TESTING OF NOVEL LARYNGEAL CLAMPS USED FOR LARYNGEAL ADVANCEMENTS CONSTRUCTS

The manuscript has been accepted for publication in peer-review journal, Frontiers of Veterinary Research in March 2020. Utilization of the manuscript in dissertation was granted by the publisher. Student is the first author on the manuscript, meaning that student conducted research project as well as wrote the manuscript. Authors also filed a patent for the Laryngeal Clamp device.

Grzeskowiak RM, Schumacher J, Mulon PY, Steiner RC, Cassone L, Anderson DE. Ex-vivo Mechanical Testing of Novel Laryngeal Clamps used for Laryngeal Advancements Constructs. Front. Vet. Sci. 2020; 7:139.
doi: 10.3389/fvets.2020.00139

Grzeskowiak R.M., Schumacher J., Anderson D.E. (2019). Pending US patent process for laryngeal clamp device.

ORIGINAL RESEARCH ARTICLE
Front. Vet. Sci., 12 March 2020 | https://doi.org/10.3389/fvets.2020.00139



Ex-vivo Mechanical Testing of Novel Laryngeal Clamps Used for Laryngeal Advancement Constructs

Remigiusz M. Grzeskowiak[1*], James Schumacher[1], Pierre-Yves Mulon[1], Richard C. Steiner[1], Lynne Cassone[2] and David E. Anderson[1]

[1]Department of Large Animal Clinical Sciences, College of Veterinary Medicine, The University of Tennessee, Knoxville, Knoxville, TN, United States
[2]Veterinary Diagnostic Laboratory, College of Agriculture, Food and Environment, The University of Kentucky, Lexington, KY, United States



Stable suture and cartilage interface is vital for implant integration and directly influences the outcome of surgical procedures. Rostral laryngeal advancement (tie-forward) is a very common procedure in horses that suffer under dorsal displacement of the soft palate. This procedure relies on anchoring thyroid cartilage to basihyoid bone and advancing entire larynx in the rostral and dorsal direction. Suture implants aim to mimic the action of thyrohyoideus muscles which have been proven to be dysfunctional in horses diagnosed with the disease. Failure of the procedure has been further attributed to suture and thyroid cartilage interface and more precisely to suture pulling through the cartilage. The conducted study aimed to evaluate the stability of tie-forward constructs performed with standard suture implants as well as suture implants stabilized with suture buttons. Further objective embraced report of construct failure mode and comparison of the biomechanical performance of the abovementioned techniques to novel design, laryngeal clamps.

Abstract

Background

Rostral laryngeal advancement, also known as laryngeal tie-forward, is used to treat horses for intermittent dorsal displacement of the soft palate and has a morbidity rate of about 6%. We hypothesized that a novel laryngeal clamp would prevent morbidity associated with the sutures tearing through the thyroid cartilage. Larynges (n = 35 horses) were used for ex-vivo testing. For uniaxial testing, 15 equine larynges were tested in one of three laryngeal tie-forward constructs [standard laryngeal tie-forward; modified laryngeal tie-forward using a suture-button; and modified laryngeal tie-forward using a laryngeal clamp]. For biaxial testing, 20 larynges were tested in one of two treatment groups: laryngeal tie-forward and laryngeal tie-forward using a laryngeal clamp. Constructs were tested in single cycle-to-failure. Statistical analyses were performed using ANOVA for uniaxial testing and t-tests for biaxial testing.

Results

The laryngeal tie-forward using a laryngeal clamp construct was superior to laryngeal tie-forward and laryngeal tie-forward using a suture-button constructs in resistance to pullout in uniaxial testing. The laryngeal tie-forward using a laryngeal clamp presented a significantly different method of failure than the standard laryngeal tie-forward in the biaxial testing. Failure modes for each construct were primarily by suture failure at the clamp (laryngeal tie-forward using a laryngeal clamp), suture pullout through the thyroid cartilage, or, less commonly, tearing of the cricothyroid ligament (laryngeal tie-forward). In uniaxial testing, the laryngeal tie-forward using a laryngeal clamp failed most commonly due to tearing of the cricothyroid ligament, whereas the standard laryngeal tie-forward and the laryngeal tie-forward using a suture-button failed due to the tearing of the cartilage. The laryngeal clamps provided greater stiffness, load at yield, and tensile stress at yield than did the standard construct.

Conclusions

Laryngeal clamps may offer an alternative to standard methods of anchoring the thyroid cartilage when performing the laryngeal tie-forward procedure. Further testing and clinical trials are needed to elucidate the utility of the laryngeal tie-forward using a laryngeal clamp.

Introduction

Intermittent dorsal displacement of the soft palate (IDDSP) is a multifactorial disease occurring in 10-20% of racehorses (1-7) and 28% of competing draft horses (8). Females and young horses (2 - 4 years old) have been reported to be more affected than male and older horses (9). The etiology of this disease is multifactorial, and proposed causes include reduced activity of the thyrohyoideus muscles (10-12), reduced activity of the palatine and palatopharyngeal muscles (13), and reduced activity of the hypoglossal nerve (14).

The suggested medical and surgical treatments of affected horses are many, because the pathophysiology associated with IDDSP is complex (15-22). Surgical treatments include myectomy of the laryngeal retractor muscles (18-20), staphylectomy (21,22), palatoplasty (21,22), and rostral advancement of the larynx, commonly referred to as the laryngeal tie-forward (LTF) procedure (10-12). The success rate of the LTF procedure in preventing IDDSP is reported to be in the range of 80-82%, which is better than the rate associated with the other procedures (11,12). This procedure advances the larynx dorsally and rostrally using a biaxial suture construct in which two non-absorbable sutures, one inserted through the caudoventral aspect of the right lamina of the thyroid cartilage and the other inserted in a similar manner through the left lamina of the thyroid cartilage and anchored to each other at the basihyoid bone, mimic the action of the thyrohyoideus muscles (10,11). The incidence of complications associated with this surgery has been reported to be about 6%, and the primary complication has been the failure of one or both sutures to retain the larynx in its new position (23,24).

The LTF procedure is most often performed using polyethylene or polyester sutures (10,11,25,26), and according to previous reports, the procedure can fail if one or both sutures break or tear through the thyroid cartilage. The LTF procedure reported by Woodie et al. (2005) and Cheetham et al. (2008) has been modified recently in an attempt to increase the mechanical strength of the construct (5,11,26,27). Rossignol et al. (2012) modified the procedure by anchoring the suture to the thyroid cartilage with metallic implants (i.e., "suture buttons"; LTFB), which resulted in improvement of the mechanical stability of the construct during mechanical testing (27). Rossignol et al. (2012) found, however, that the strength of the modified LTFB construct was inferior to that of the standard LTF construct and reported that the method of failure in both types of constructs was pullout of the suture from the thyroid cartilage (25). An implant that reduces the risk of a

pullout from the thyroid cartilage is needed, because the method of failure of the LTF procedure in all tested constructs has been pullout of the construct through the thyroid cartilage.

We hypothesized that a custom-designed, novel laryngeal clamp (LTFC) would distribute tensile forces over a large area of the thyroid cartilage, thereby eliminating morbidity associated with failure at the suture-cartilage interface. The objectives of the study were to design and manufacture a novel laryngeal clamp and to study the mechanical characteristics of the LTF constructs (LTF, LTFB, LTFC) anchored to only one lamina of the thyroid cartilage (uniaxial testing) and to mechanically test the strength of two different constructs (LTF, LTFC) anchored to both laminae of the thyroid cartilage (biaxial testing). We expected that the difference in ex-vivo uniaxial mechanical testing between the constructs would be significantly different but testing between right-sided and left-sided constructs would not be significant. We expected the results of ex-vivo mechanical testing between the standard construct and the construct modified with clamps would be significantly different in biaxial mechanical tests.

Materials and Methods

Preparation of the larynxes

Thirty-five larynges, each with its hyoid apparatus attached, were collected from horses within 24 hours after the horses were euthanized for a reason unrelated to the respiratory tract. Of these 35 larynges, 15 were used in proof-of-concept, uniaxial mechanical studies, and 20 were used in biaxial mechanical studies. Signalment data, including age, weight, breed, and sex, were available for horses supplying the larynxes (n = 20) used for biaxial testing. Larynges were frozen at -20o C until mechanical testing was performed (25,27-32) and were thawed at room temperature for 24 hours prior to testing. The larynges were wrapped in isotonic saline-soaked gauze after they were thawed to keep them moist until tested.

Sample Measurements Collection

Before performing uniaxial tests, the thickness of the laminae of 15 thyroid cartilages was measured at 3 locations, 10 mm apart, on the caudoventral margin of the laminae, close to the insertion of the sternothyroideus muscles, using a digital caliper[a]. The thickness of the laminae of the 20 thyroid cartilages used for biaxial testing was measured in a similar fashion but in 10 different locations on each lamina to assess the properties of the thyroid cartilage (Figure 2-1, Table 2-1, all figures and tables are placed in the appendix). Locations 1 and 2 were at the ventral and axial aspect of the thyroid cartilage. Locations 3 to 5 were at the dorsal aspect of the thyroid cartilage, and locations 6 to 10 were at the caudoventral aspect of the right and left laminae, close to the insertion of the sternothyroideus muscle. Measurements were obtained to determine the space between the arms of the U-shaped clamp necessary to insert the clamp onto the thyroid cartilage (Figure 2-1).

Uniaxial testing

Fifteen larynges were randomly assigned to one of three treatment groups according to the construct tested, and each side of the larynx to which the construct was applied was tested separately. Uniaxial tests on the suture-cartilage interface included the following: 1) standard LTF using USP no. 5 polyester suture[b], 2) LTF modified with a suture button (LTFB), and 3) LTF modified with a custom-designed laryngeal clamp (LTFC) (Figure 2-2). The uniaxial testing was performed to evaluate the performance of a single implant anchored to the thyroid cartilage and to assess the difference in the mechanical performance between the left and right laminae of the thyroid cartilage.

Biaxial testing

Twenty larynges were randomly assigned to one of two treatment groups according to the construct tested, and both sides of the larynx to which the construct was applied were tested simultaneously. The constructs tested included the LTF construct using USP no. 5 polyester suture[b] and the LTFC. The ceratohyoid and thyrohyoid bones were removed from the basihyoid bone, which was mounted on the loading frame of an electromechanical testing machine[c]. The free ends of the sutures passing through the laminae of the thyroid cartilage were attached to the basihyoid bone (Figure 2-3).

Laryngeal Tie-forward (LTF)

The LTF procedure was performed in a manner similar to the technique described by Woodie et al. (2005) and Cheetham et al. (2008) (11, 12). Using this technique, USP No. 5 polyester suture[b] was inserted twice through the right or left lamina of the thyroid cartilage, at the caudoventral aspect of the lamina, using a ½-circle, trocar-point, needled to create a single loop around the caudoventral margin of the lamina close to the tendon of insertion of the sternothyroideus muscle (Figure 2-3).

Laryngeal Tie-forward modified with suture buttons (LTFB)

The LTFB procedure was performed in a manner similar to the technique described by Rossignol et al. (2012) (27). Using this technique, USP No. 5 polyester suture[b] was threaded through the eyelet of the suture-button (2-mm thick rounded plate with 2, 1.5-mm diameter holes), and the free ends of the sutures were inserted through the eye of a ½-circle, trocar-point needle[d] The needle was passed once through the caudoventral margin of the right or left lamina of the thyroid cartilage in a manner similar to that described using the LTF, and by applying tension to the suture, the button became seated firmly on the ventral aspect of the caudal edge of the thyroid cartilage (Figure 2-4).

Laryngeal Tie-forward modified with novel laryngeal clamp (LTFC)

The laryngeal clamps, composed of 316-stainless steel, were a broad U-shaped device designed to wrap around the caudoventral border of the laminae of the

thyroid cartilage. One arm of the clamp was 10 mm long, the other was 14 mm long, and the gap with the “U” between the arms was 7 mm (Figure 2-5). The clamp was inserted around the caudoventral border of the right or left lamina of the thyroid cartilage close to the site of insertion of the sternothyroideus muscle, so the short arm lay dorsal to the lamina and the long arm ventral to the lamina. The dorsal arm contained two, 2-mm diameter holes spaced 2 mm apart, which together served as an eyelet for the suture, and the ventral arm contained a slit through which the suture was easily passed (Figure 2-5). The suture was attached to the clamp by threading one end of the suture through one hole in the eyelet and the other end through the adjacent hole, so the ends emerged between the arms of the clamp. The ends of the suture were then threaded through the eye of a ½-circle, trocar-point needled, which was passed once through the right or left lamina of the thyroid cartilage close to the insertion of the sternothyroideus muscle. The needle emerged approximately 5-10 mm rostral to the caudal margin of the lamina (Figure 2-6). The needle was removed, and the ends of the suture were passed through the slit in the dorsal arm of the clamp. The clamp became seated firmly around the caudal edge of the thyroid cartilage at the site of insertion of the sternothyroideus muscle when tension was applied to the suture (Figure 2-6).

Uniaxial Biomechanical Testing

Laryngeal constructs were tested in a single cycle-to-failure test using an electromechanical testing system with a 5-kN maximum load cell$_C$. The larynges were mounted to the machine as previously described (25). Briefly, a 3.2-cm diameter cylinder of polyvinyl chloride (PVC) was passed into the lumen of the larynx, and two 3.5-mm diameter, 40-cm long Steinmann pins were placed through the larynx and cylinder perpendicular to the long axis of the cylinder and to each other. One pin was placed through the cricoid cartilage, and a second pin through the center of the thyroid cartilage, securing both cartilages firmly to the PVC cylinder, avoiding interference with the cricothyroid ligament.

After mounting the cylinder and larynx on the loading frame of the electromechanical testing machine with the rostral portion of the larynx uppermost, (Figure 2-2), the ends of the suture were tied together around a 5-mm diameter steel bar attached to a custom-made holding grip, with a surgeon’s knot, and secured with 7 throws (Figure 2-2). The suture loop resided in the center of the steel bar during the testing of each specimen, to mimic the direction of the suture in-vivo and to maintain the repeatability of the testing conditions between the specimens. The pullout tests were performed at a distraction rate of 300 mm/min (25). The variables recorded for each construct included maximum load (N), stiffness (N/mm), extension at maximum load (mm), extension at the break (mm), extension at yield (mm), load at yield (N), tensile stress at yield (N/mm$_2$), and tensile stress at maximum load (N/mm$_2$). The maximum load was defined as the maximum force loaded to the point of failure of any part of the construct, and the stiffness was calculated from a load-displacement curve. Displacement was defined as a change in distance between the thyroid cartilage and steel bar, and

the tensile stress was defined as the force applied to the area of the thyroid cartilage.

Three different modes of construct failure were observed and recorded, including tearing of the thyroid cartilage, tearing of the cricothyroid ligament, and breaking of the suture. The thyroid cartilage tore when the implant pulled through the cartilage. The cricothyroid ligament tore when the implant caused the thyroid cartilage to elevate and separate from the cricoid cartilage by tearing the cricothyroid ligament, resulting in little or no damage to the thyroid cartilage. Breaking of the suture, the third mode of failure, occurred at the knot of the loop around the steel bar.

Biaxial Biomechanical Testing

The constructs tested in biaxial loading mimicked one of two clinical constructs, LTF and LTFC. Both constructs were anchored and mounted on the Instron machine[c] in the manner described above. After removing the hyoid apparatus, the larynx was mounted on the upper loading cell of the electromechanical testing machine. For the LTF construct, the free end of the ipsilateral dorsal arm of the suture and contralateral ventral arm of the suture inserted through one lamina of the thyroid cartilage were advanced rostrally and dorsally to the detached basihyoid bone, which was mounted on the loading frame of the MTS testing machine[c]. The same procedure was performed on the contralateral side. The ventral arms of the right and left sutures were tied to each other around the ventral aspect of the lingual process, with a surgeon's knot, and secured with 7 throws. The dorsal arms of the right and left sutures were tied together in a similar fashion (Figure 2-3).

To create the LTFC construct, both ends of each suture were advanced rostrally and dorsally to the ipsilateral side of the basihyoid bone (Figure 2-3). The four arms of the sutures were tied together around the ventral aspect of the lingual process of the basihyoid bone, with a surgeon’s knot, and secured with 7 throws. The pullout test was performed in a manner similar to that performed for uniaxial testing at a distraction rate of 300 mm/min. Three different modes of construct failure were observed and recorded and were the same as those observed during uniaxial testing.

Statistical Analyses

Statistical analyses were performed by using IBM SPSS Statistics 25[e]. Descriptive statistics were calculated for all variables for all treatment groups and included minimum, maximum, mean, and standard deviation. The normality of data distribution for each variable was performed by using the Kolmogorov-Smirnov test of normality.

The thickness of the 3 sites measured on laminae of the thyroid cartilage of the larynges used for uniaxial testing was compared by using a two-tailed independent

samples T-test. The thickness of the 10 sites measured on the right lamina of the thyroid cartilage of the larynges used for biaxial testing was compared to the thickness of the left lamina by using a two-tailed independent samples T-test. The results were examined for homogeneity of variance, and each site was compared by using ANOVA and the Tukey's Post-hoc test. The thickness was also correlated with the age, breed, and weight of donors by using a two-tailed Pearson correlation.

For uniaxial tests, the differences in maximum load, stiffness, extension at maximum load, extension at break, extension at yield, load at yield, tensile stress at yield, and tensile stress at maximum load between the left and right testing side of the thyroid cartilage were examined for homogeneity of variance. The differences between each testing group were then analyzed by using ANOVA and Tukey's Post-hoc test. The correlation between the construct and method of failure was examined by using Fisher's exact tests.

For biaxial tests, the differences between two constructs were compared by using a two-tailed independent samples T-test, and the correlation between the construct and method of failure was tested by using the Fisher's exact test. The level of statistical significance was established at $p < 0.05$ and the power of the experiment design and test combination was calculated using PS software[f] in the reference to the results of maximum load during mechanical testing.

Results

Study Population

The weight of the horses from which the 35 larynges were harvested ranged from 450 to 650 kg (mean 570 ± 70.7 kg), and the ages of these horses ranged from 2 to 29 years old (mean 14.8 ± 8.1 years). Information about the breed and sex of the donors was obtained only for the 20 larynges used in biaxial tests. The breeds of these 20 horses included Thoroughbred (11), American Quarter Horse (3), Tennessee walking horse (1), Warmblood (2), American Standardbred (1), Hanoverian (1), and Clydesdale (1). Ten donors were female, and 10 were geldings.

Sample Measurements Collection

The Kolmogorov-Smirnov test of normality of distribution showed the measurements of cartilage thickness to be normally distributed in all tested positions ($p > 0.05$). The Levene's test for equality of variances revealed that equal variances in all variables could be assumed ($p > 0.05$). The descriptive statistics of the thickness measurements of the thyroid cartilage of the 15 larynges used in the single-side testing (i.e., uniaxial tests) revealed that the mean thickness of the caudoventral edge of the left thyroid cartilage lamina was 4.58 ± 0.7 mm. The mean thickness of the caudoventral edge of the right thyroid cartilage lamina was 4.70 ± 0.7 mm (Table 2-3). The measurements of the caudoventral edge of the thyroid

cartilage of the 10 larynges used in biaxial testing revealed that the mean thickness of the caudoventral edge of the left thyroid cartilage lamina was 4.48 ± 1.3 mm. The mean thickness of the caudoventral edge of the right thyroid cartilage lamina was 4.50 ± 1.2 mm. The differences in the average thickness between the left and right laminae of the thyroid cartilage in the study population were not statistically significant ($p > 0.05$) (Tables 2-2 and 2-3).

Significant differences were found in the thickness of the laminae of the thyroid cartilage among the different anatomical positions ($p < 0.05$). The position numbers 7 (L – 6.01 ± 1.2 mm; R – 5.89 ± 1.2 mm), 8 (L – 4.95 ± 0.8 mm; R – 4.99 ± 0.8 mm), and 10 (L – 6.47 ± 1.4 mm; R – 6.18 ± 1.6 mm) were significantly thicker than the rest of the anatomical positions ($p < 0.05$) (Table 2-1). These sites were at the caudal margin of the thyroid cartilage at the site of insertion of each sternothyroideus muscle (Figure 2-1). No significant correlation was found between the mean thickness of the caudoventral aspect of the margin of the laminae of the thyroid cartilage and the age and breed of the donors for any sites examined ($p > 0.05$). There was, however, a significant positive correlation between the mean thickness of the laminae and the weight of the donors ($r = 0.78$, $p < 0.05$)

Uniaxial Biomechanical Testing

Data was normally distributed and homogeneous for all variables ($p > 0.05$). The two-tailed independent samples T-test did not reveal significant differences in the results of biomechanical testing between the left and right side of the lamina ($p > 0.05$) (Table 2-3). The yield on the load-displacement curve corresponded to the tearing of the thyroid cartilage ($n = 22$) or to the tearing of the cricothyroid ligament ($n = 7$).

Uniaxial testing of the constructs revealed that the mean pullout strengths of the LTFC (207 ± 43 N) and LTF (199 ± 19 N) constructs were significantly greater than the mean pullout strength of the LTFB construct (176 ± 43 N) ($p<0.05$) and that the difference in the mean pullout strength of the LTFC construct did not differ significantly from that of the LTF constructs ($p>0.05$). Similarly, the mean load at yield point was significantly greater for the LTFC (161 ± 45 N) and LTF (168 ± 23 N) constructs than that for the LTFB construct (139 ± 51 N) ($p<0.05$), but the mean load at yield point for the LTFC construct did not differ significantly from that the of the LTF construct. The results of the rest of the uniaxial mechanical testing were not significantly different between the treatment groups ($p>0.05$) (Table 2-4, Figure 2-8).

Fisher's exact test revealed a significant correlation between the construct and method of failure ($p < 0.05$). Of the constructs modified with a laryngeal clamp, 70% failed by tearing the cricothyroid ligament, and 30% failed by tearing the thyroid cartilage adjacent to the clamp. None of these constructs failed from the break of the suture. All (100%) of the LTF constructs failed from tearing the thyroid

cartilage. Constructs modified with a suture button failed from tearing the thyroid cartilage (90%) or from breaking of the suture (10%).

Biaxial Biomechanical Testing

All variables, including biomechanical values, were normally distributed ($p > 0.05$). Tests for equality of variances revealed that equal variances in all variables could be assumed ($p > 0.05$).

As occurred in the uniaxial testing, the yield on the load-displacement curve corresponded to tearing of the thyroid cartilage ($n = 8$) or to tearing of the cricothyroid ligament ($n = 3$). The LTF construct compared to the LTFC in the biaxial testing had a significantly higher mean maximum load (430.3 ± 64.84 N and 367.9 ± 55N respectively), lower mean extension at yield (33.38 ± 8.9 mm and 42.54 ± 7.81 mm respectively), higher mean extension at maximum load (64.9 ± 9.5 mm and 52.4 ± 8.4 mm respectively), higher mean extension at failure (65.4 ± 9.5 mm and 52.6 ± 8.5mm respectively), higher mean extension at maximum load (64.9 ± 9.5 mm and 52.4 ±8.4 mm respectively) and higher mean tensile stress at maximum load (43.13 ± 6.87 N/mm2 and 36.8 ± 9.1 N/mm2) ($p<0.05$) (Table 2-5). The results of the rest of the biaxial mechanical testing were not significantly different between the treatment groups ($p>0.05$) (Table 2-5, Figure 2-9).

There was a significant correlation between the construct and method of failure ($p < 0.05$). Of constructs modified with clamps, 80% failed because the suture broke, and 20% failed because the cricothyroid ligament tore (Figure 2-7). Standard LTF constructs failed because the thyroid cartilage tore (80%) or because the cricothyroid ligament tore (20%).

Discussion

The mode of failure of the construct modified with laryngeal clamps differed from the mode of failure of the LTF construct. The mode of failure of the constructs correlated with the type of implant used, regardless of whether one side of the larynx or both sides of the larynx were tested. The LTF construct and the LTFB construct failed in uniaxial testing most commonly by pulling of the implant through the thyroid cartilage. Less commonly, the construct failed when the cricothyroid ligament tore. The LTF construct failed in biaxial testing when the suture pulled through the thyroid cartilage. The construct with the laryngeal clamps failed in uniaxial testing when the thyroid cartilage elevated and separated from the cricoid cartilage at the cricothyroid ligament. All constructs with the laryngeal clamps failed in biaxial testing when the suture broke close to one of the laryngeal clamps. The laryngeal clamps, therefore, protected the thyroid cartilage from tearing during uniaxial and biaxial testing.

The mode of failure of the biaxial construct modified with clamps may have perhaps been different, and the pullout force higher, if polyethylene suture, rather

than polyester suture, had been used. Polyethylene suture has been shown to provide greater resistance to fraying, higher tensile strength, and more elasticity than the polyester suture used in both trials in our study (26,33). Although polyethylene sutures performed better than polyester sutures in another similar study, the difference in the performance of the entire construct was not statistically significant, because the failure of the construct was due to failure of the thyroid cartilage, rather than a failure of the suture (25). A study examining the mechanical properties of various suture materials found polyethylene sutures to have a 500-fold greater resistance to fraying than polyester sutures (33). This makes polyethylene sutures particularly advantageous for attaching to metallic anchors or to absorbable anchor eyelets (32). Comparing the mechanical performance of various types of sutures used with the laryngeal clamp was beyond the scope of this study.

The force required to disrupt the LTFC constructs was similar to that of the LTF and LTFB constructs in uniaxial mechanical testing. The differences in the properties of biological samples, including a difference in viscoelasticity, may explain the high variability of force required to disrupt the constructs within each group. In biaxial construct testing, however, the pullout force for the LTF constructs was greater than the pullout force for the LTFC constructs. The LTFB construct was not included in biaxial testing because it performed more poorly in the single-side testing than the LTF construct. In a recent biomechanical study, LTF constructs had a higher pullout force in biaxial testing than did constructs modified with suture buttons, regardless of whether the suture was polyethylene or polyester (25).

The types of constructs failed at different forces and displacement at yield, because of the different modes at which they failed. The yield point in the mechanical testing corresponded with the force and displacement at which the cartilage or the cricothyroid ligament started to fail. Interestingly, the extension at which the construct failed differed distinctly among the types of constructs. The force and displacement at yield was highest for the LTF construct in the uniaxial testing followed next by the LTFC construct and then by the LTFB construct. The load at yield was higher for the LTFC construct than for the LTF construct in the biaxial testing. The higher load at yield resulted in a greater displacement at yield for the LTFC construct than for the LTF construct but not significantly so. The yield point of the LTFC constructs was rarely observed, because the entire construct moved in the Instron machine until the suture failed, whereas the yield point of the LTF construct was easily observed, because the suture, rather than the entire construct, moved until the yield point of the construct was reached, which was that point at which the thyroid cartilage began to tear.

The lower tensile force required to tear the cartilage in the LTF construct was related to the higher shear stress applied directly to the thyroid cartilage by the suture. The laryngeal clamp reduced stress by distributing the tensile force over a

larger area of the thyroid cartilage. Yield points have not been reported in previous mechanical studies examining LTF constructs (25-27). The study performed by Santos et al. (2014) examined the force at 20- and 30-mm extensions (25). We found the yield point to be about 34 mm for the LTF construct and about 42 mm for the LTFC construct, but the wide standard deviation for the LTFC construct suggests that the yield point was not constant for all tested constructs.

The stiffness of the LTFB construct was higher than that of the LTF and LTFC constructs in the single-side testing, causing the LTFB to construct to have the shortest extension when the suture broke. The LTF and LTFC constructs had a similar extension at failure in the uniaxial testing. The extension at failure for the LTFB construct, however, was higher than that reported by Santos et al. (2015), though the trend in their study was similar (25). The LTFC constructs were stiffer than the LTF constructs in biaxial testing, resulting in a lower extension when the suture broke. The results of our tests showed that the LTFC constructs were stiffer than the LTF constructs in the single-side testing and the biaxial testing, and therefore, more force was required to disrupt the construct modified with clamps. The higher stiffness of the LTF constructs modified with the laryngeal clamps is likely to be associated with less laryngeal displacement under in-vivo conditions.

Clinical failure of the LTF construct is reported to occur most commonly during recovery from general anesthesia when the horse rapidly and forcefully extends its head (25). In our study, the constructs modified with the laryngeal clamps had a pullout force of approximately 5.5 times that estimated to occur during maximal head extension (25). The tensile stress at maximum load was significantly lower for the LTFC construct than for the LTF construct, but the tensile stress at yield was higher for the LTFC constructs than for the LTF constructs. This may suggest that the tensile strength of the LTFC construct was greater at the moment when the cartilage or cricothyroid ligament began to fail. In the majority of the LTFC constructs, the suture, rather than the cartilage or the ligament, failed, resulting in a short yield phase just before failure. The tensile stress applied to the constructs under in-vivo conditions is not known, and therefore, the minimal stress the constructs must withstand is not known.

The focus of this study was to evaluate the biomechanical performance of the LTF construct modified with a novel laryngeal clamp and to compare it to currently used constructs. One of the concerns with the novel design of the laryngeal clamps is the tension applied to the sutures, which results in shear stress between the sutures and metallic clamps during cyclical loading. The design tried to address these concerns and apply modifications aimed at reducing the shear stress between the suture and implant. Future research should examine additional modifications to reduce the shear stress on the suture to improve the performance of the LTFC construct. Also, the use of different sutures, such as polyethylene sutures, to anchor the clamps should be examined. The limitation of this study was the underpowered ($\beta<0.8$) design and test combination to detect hypothetical

differences in mechanical properties between the constructs. Accounting for the difference in the mean values of maximum loads between the constructs and the standard deviations within the treatment groups, the study would necessitate 237 samples per treatment group to achieve study power $\beta>0.8$. Furthermore, this is an ex-vivo study in which each of the larynges had to undergo one freeze-thaw cycle which could have influenced the mechanical performance of the thyroid cartilage or the cricothyroid ligament. The results of this study might differ from the physiologic conditions and should be therefore interpreted with caution.

Conclusions

The prototype of the laryngeal clamp may offer an alternative to suture anchoring in the thyroid cartilage in LTF constructs. The unique design of the laryngeal clamp protected the cartilage by reducing the shear stress of the suture applied to the cartilage, which resulted in the higher force and tensile strength at the failure of the cartilage or ligament. This was associated with the increase in stiffness of the construct. Increasing the stiffness of the construct could result in the lower displacement of the construct over time in-vivo. The increased stiffness of the construct modified with the clamps resulted in the sutures failing at lower maximum force and displacement.

Tables

Table 2-1. Measurements of larynx thickness.

Thickness measurements (mm)

Position	**Mean**	**Std. Deviation**
1.00	3.8872	.84690
2.00	3.9444	.76652
3.00	3.9336	.72256
4.00	3.5096	.56269
5.00	3.7696	.60627
6.00	3.9156	.67555
7.00	6.0163	1.22410
8.00	4.9548	.81034
9.00	4.4984	.67038
10.00	6.4740	1.43194

Table 2-2. Thickness comparison between laminae of thyroid cartilage.

2-tailed independent samples T-test between left and right thyroid cartilage

Measurement	Side	Mean	Std. Deviation	Sig. (2-tailed)
Position_1	L	3.8872	.84690	.278
	R	4.1456	.81930	.278
Position_2	L	3.9444	.76652	.372
	R	3.7652	.63383	.372
Position_3	L	3.9336	.72256	.563
	R	4.0536	.73439	.563
Position_4	L	3.5096	.56269	.332
	R	3.6696	.59214	.332
Position_5	L	3.7696	.60627	.910
	R	3.7496	.64440	.910
Position_6	L	3.9156	.67555	.791
	R	3.9692	.74584	.791
Position_7	L	6.0163	1.22410	.716
	R	5.8872	1.23921	.716
Position_8	L	4.9548	.81034	.856
	R	4.9972	.82942	.856
Position_9	L	4.4984	.67038	.535
	R	4.6244	.75340	.535
Position_10	L	6.4740	1.43194	.495
	R	6.1808	1.57979	.495

Comparison of thickness between the left and right laminae of the thyroid cartilage. There were no significant differences between the left and right laminae at any of the measured positions.

Table 2-3. Side comparison in uniaxial testing.

2-tailed independent samples T-test between left and right thyroid cartilage

Variable	Side	Mean	Std. Deviation	Sig. (2-tailed)
Average Thickness	L	4.5833	.73626	.670
	R	4.6987	.73201	
Maximum Load (N)	L	190.4900	34.96656	.614
	R	197.6793	41.82675	
Stiffness (N/mm)	L	4.0580	1.40277	.884
	R	4.1240	1.03332	
Extension at Failure (mm)	L	56.1173	17.44167	.627
	R	52.9907	17.37226	
Extension at Max Load (mm)	L	55.7880	17.60501	.461
	R	51.1160	16.65160	
Extension at Yield (mm)	L	38.8507	14.03225	.637
	R	41.1693	12.53842	
Load at Yield (N)	L	151.7260	45.32798	.604
	R	159.9007	39.84170	
Tensile Stress at Yield (N/mm^2)	L	15.1747	4.53286	.605
	R	15.9900	3.98632	
Tensile Stress at Max Load (N/mm^2)	L	18.8954	3.20007	.535
	R	19.7723	3.86754	

Comparison of average biomechanical results obtained during uniaxial testing involving the left or right laminae of the thyroid cartilage (2-tailed independent samples T-test). The data obtained from the left side of the larynges did not differ significantly from that obtained from the right side of the larynges.

Table 2-4. Comparison of biomechanical results during uniaxial testing.

ANOVA of three different constructs

Variable	Construct	Mean	Std. Deviation	Sig.
Maximum Load (N)	LTF	199.0180	19.27660	.024
	LTFB	176.3040	43.18806	
	LTFC	206.9320	43.21904	
Stiffness (N/mm)	LTF	3.8600	.93406	.177
	LTFB	4.7650	1.36203	
	LTFC	3.6480	1.10265	
Extension at Failure (mm)	LTF	55.6220	12.66911	.087
	LTFB	46.2630	14.58875	
	LTFC	61.7770	21.02075	
Extension at Max Load (mm)	LTF	53.0860	11.89288	.125
	LTFB	45.9100	14.71806	
	LTFC	61.3600	20.99364	
Extension at Yield (mm)	LTF	46.0220	12.83827	.125
	LTFB	29.2360	8.72437	
	LTFC	44.7720	10.95712	
Load at Yield (N)	LTF	167.5140	23.34335	.003
	LTFB	138.5570	51.10873	
	LTFC	161.3690	45.24054	
Tensile Stress at Yield (N/mm$_2$)	LTF	16.7520	2.33487	.278
	LTFB	13.8570	5.11180	
	LTFC	16.1380	4.52568	
Tensile Stress at Max Load (N/mm$_2$)	LTF	19.8430	1.86375	.279
	LTFB	18.1510	4.24579	
	LTFC	20.4567	4.23621	

This table shows the mean values and standard deviations of the results of biomechanical testing of 3 constructs. The results differed significantly in maximum load (N) and load at yield (N) between the LTFC, LTF and LTFB constructs.

Table 2-5. Comparison of biomechanical results during construct testing.

2-tailed independent samples T-test between two constructs

Variable	Construct	Mean	Std. Deviation	Sig. (2-tailed)
Average Thickness (mm)	LTF	4.6010	.33834	.500
	LTFC	4.7880	.79014	
Maximum Load (N)	LTF	430.2940	64.84309	.032
	LTFC	367.8790	55.19138	
Extension at Failure (mm)	LTF	65.3910	9.47112	.005
	LTFC	52.5820	8.49355	
Extension at Max Load (mm)	LTF	64.8970	9.52261	.006
	LTFC	52.4210	8.44992	
Extension at Yield (mm)	LTF	33.3780	8.98399	.026
	LTFC	42.5410	7.81333	
Load at Yield (N)	LTF	264.6490	65.42587	.257
	LTFC	306.2130	91.09641	
Tensile Stress at Max Load (N/mm$_2$)	LTF	43.1300	6.86934	.040
	LTFC	36.8210	9.10953	
Tensile Stress at Yield (N/mm$_2$)	LTF	26.4660	6.54315	.257
	LTFC	30.6210	5.51279	
Stiffness (N/mm)	LTF	6.7250	1.12806	.640
	LTFC	7.0420	1.78153	

The LTFC construct was inferior to the LTF construct in maximum load ($p < 0.05$), extension at failure ($p < 0.05$), extension at maximum load ($p < 0.05$), and tensile stress at maximum load ($p < 0.05$). The LTFC construct showed, however, a superior trend compared to the LTF construct in extension at yield ($p < 0.05$). The difference between the constructs in the remaining results were not significant ($p>0.05$).

Figures

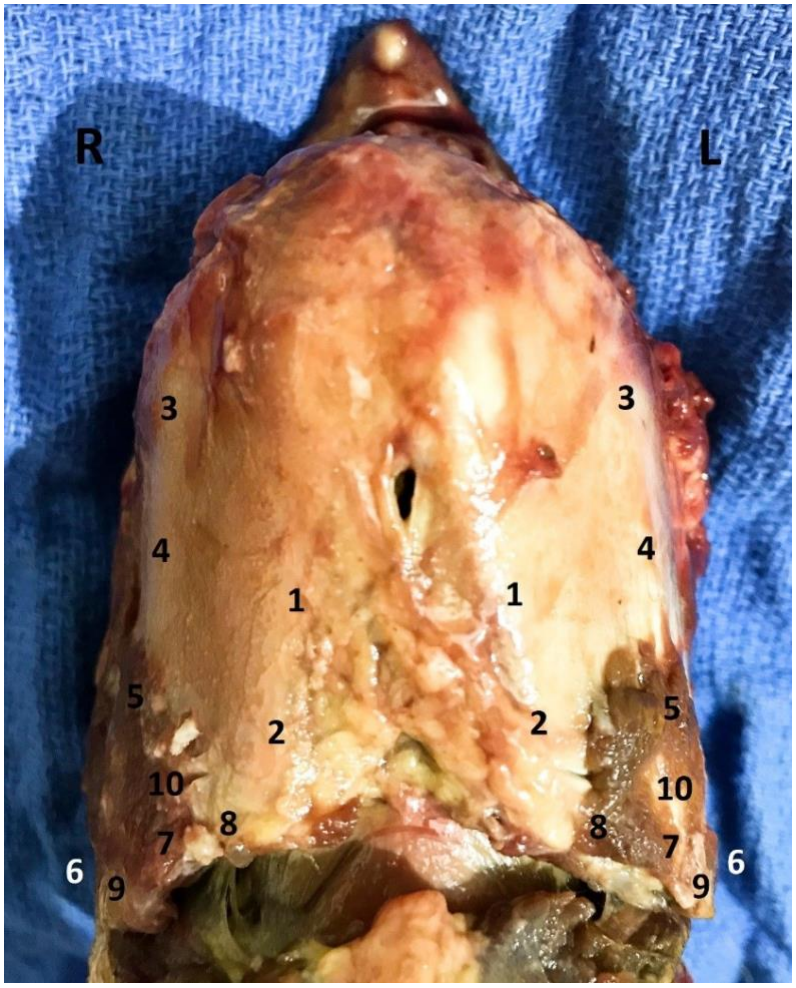


Figure 2-1. Thickness at 10 different anatomical positions.

The thickest portion of the thyroid cartilage was found in positions 7-10, at the attachment of previously removed sternothyroideus muscle.

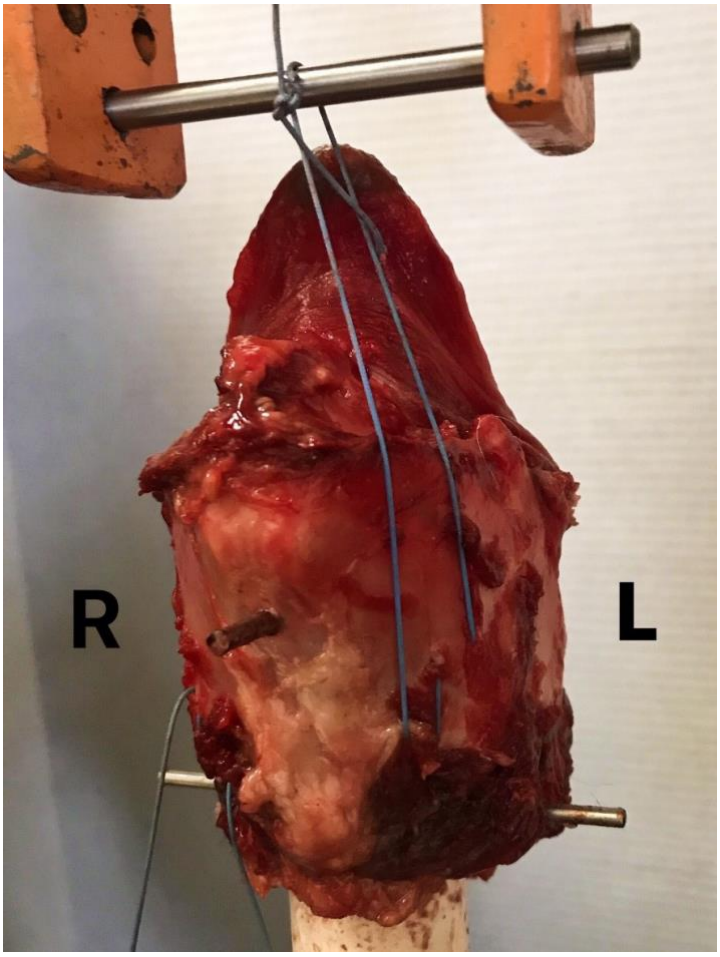


Figure 2-2. Single-side LTF mechanical testing.

This figure presents the experimental arrangement of a larynx in the MTS testing machine. The larynx was attached to the 3.2-cm PVC cylinder, which was attached to the holding grip of the MTS machine. A custom-made holding grip with a stainless-steel bar was attached to the loading cell. Each larynx was in the same treatment group, but each side of the construct was tested separately. The ends of the suture were tightened and tied around the stainless-steel bar.

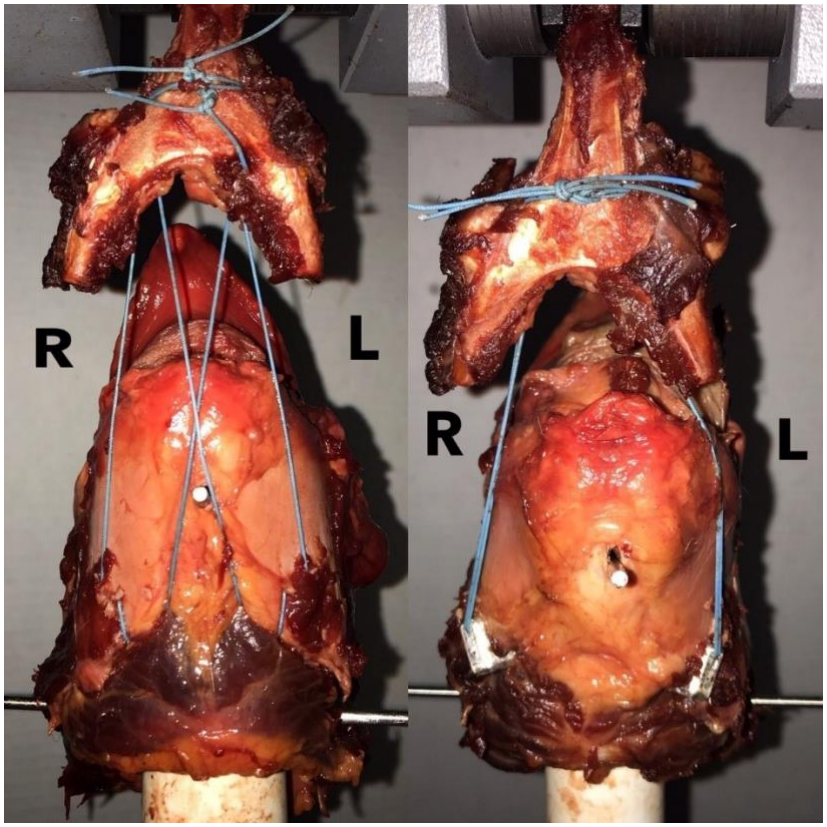


Figure 2-3. Biomechanical constructs testing.

This figure shows the arrangement of the LTF and LTFC constructs in the MTS machine. Larynges were mounted on a PVC cylinder, as in the single-side testing, and the basihyoid bone was attached to the holding grip of the loading cell. In the standard LTF construct, on the left side, the free ends of the ipsilateral dorsal suture and contralateral ventral suture were advanced rostrally and dorsally to the basihyoid bone. The same procedure was performed on the right side. The ventral and dorsal sutures were tightened and tied together around the ventral aspect of the lingual process of the basihyoid bone. In the LTF construct modified with the laryngeal clamps, both ends of the sutures were advanced rostrally and dorsal to the bone and tied together around the ventral aspect of the lingual process.



Figure 2-4. Suture Button.

The commercially available suture button used for this study was a part of the kit for the human cruciate ligament repair. The surgical technique used to anchor the thyroid cartilage was performed as described by Rossignol et al. (2012)



Figure 2-5. Views on laryngeal clamps.

The design of laryngeal clamps aimed at creating an anchor that wrapped around the caudal border of the thyroid cartilage to distribute the tensile forces applied to the suture. The laryngeal clamps were U-shaped, 5 mm wide, and 1cm long. The short arm was placed on the dorsal surface of the thyroid cartilage, and the long arm was placed on the ventral surface of the cartilage. The part connecting the bottom and top parts was responsible for distributing the tensile force. The short, dorsal arm had two holes, creating an eyelet for the suture, and the longer ventral arm had a slit, though which suture could easily be passed.

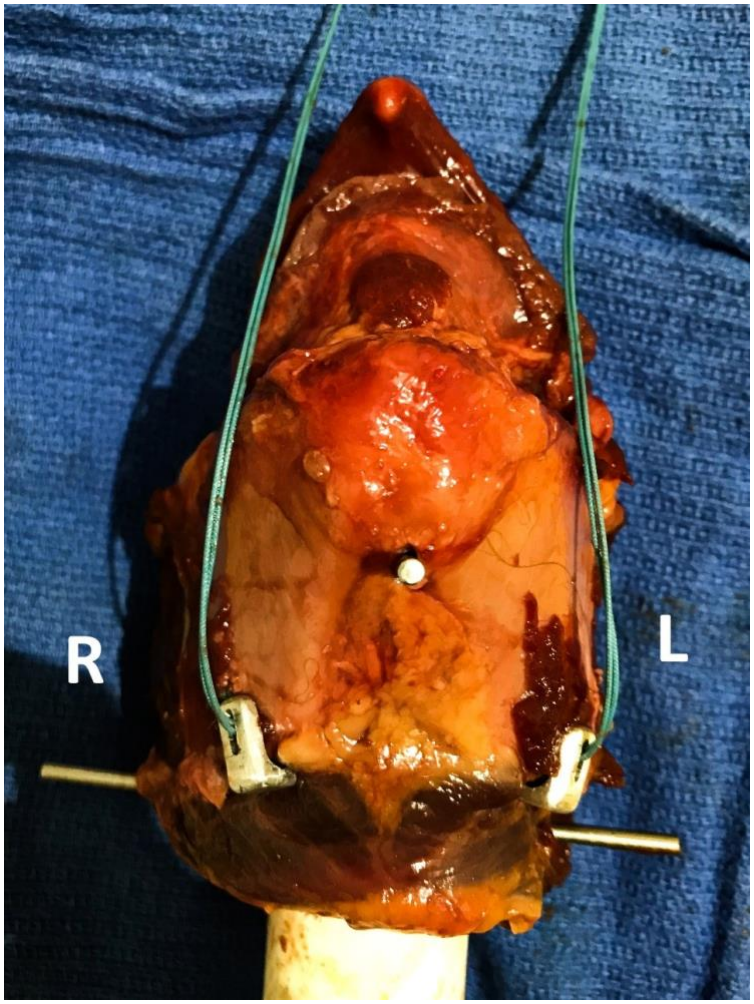


Figure 2-6. Laryngeal clamps on the thyroid cartilage.

The figure shows the arrangement of the laryngeal clamp around the caudoventral border of the thyroid cartilage. The dorsal arm had an eyelet with the relief between two holes, through which the suture was threaded before the clamp was placed. The ends of the suture were threaded through the eye of a ½-circle needle, which was passed through the caudal margin of the thyroid cartilage. After the needle was passed, the ends of the suture were threaded through the slit on the dorsal arm of the clamp. Tension applied to the suture caused the clamp to engage the caudal margin of the lamina of the thyroid cartilage. The suture of this construct had no dorsal and ventral arms, because both arms were inserted through the one hole in the lamina of the thyroid cartilage.

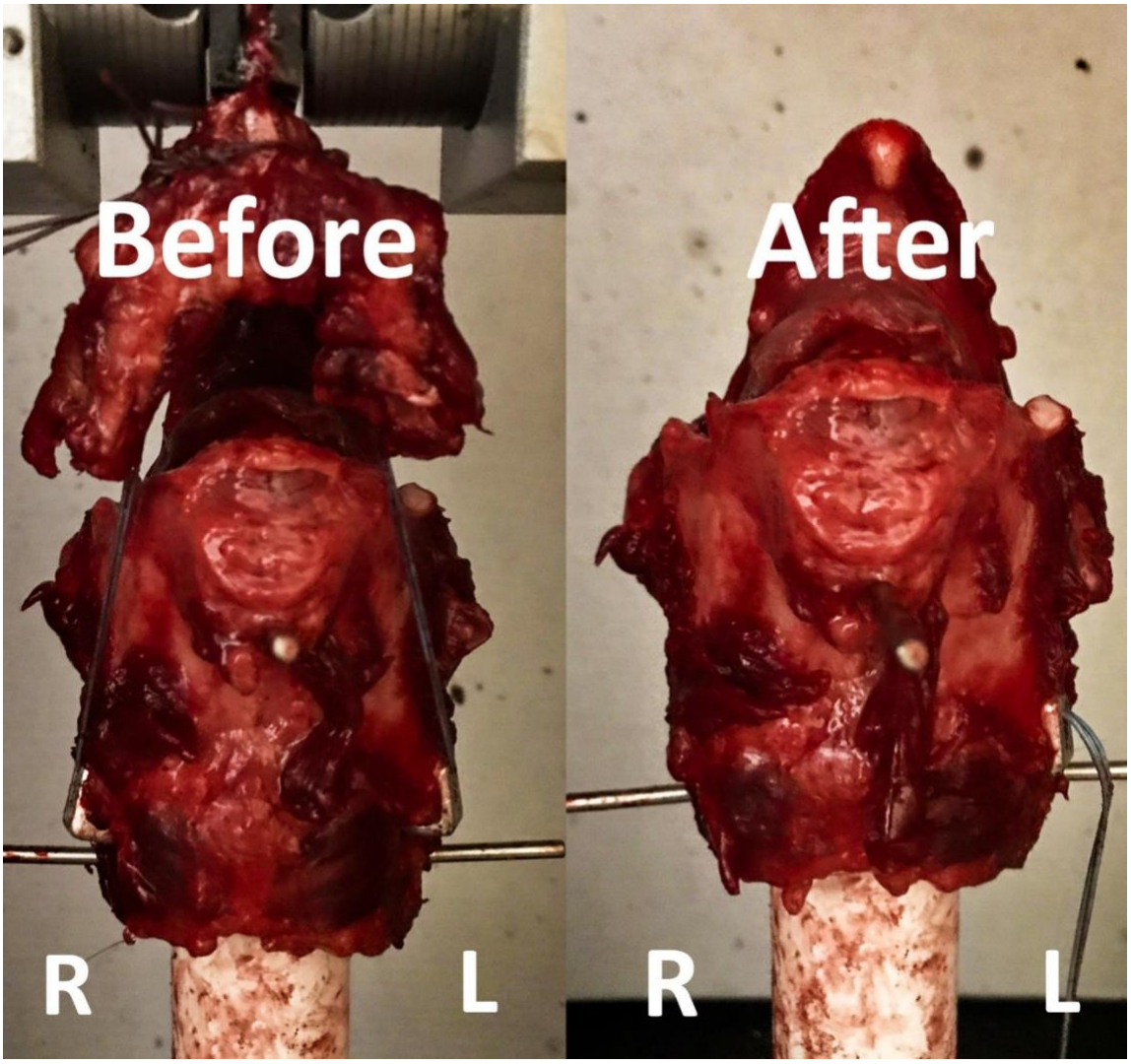


Figure 2-7. Before and after constructs testing.

The image on the left shows the construct before the testing, and the image on the right shows the construct after the testing. The left and right laminae of the thyroid cartilage are labeled. Notice that the appearance of the thyroid cartilage on the right looks similar the appearance of the thyroid cartilage before the test. In this case, the right laryngeal clamp pulled out from the thyroid cartilage without inducing severe disruption of the crico-thyroid ligament and alteration of the geometry of the thyroid cartilage.

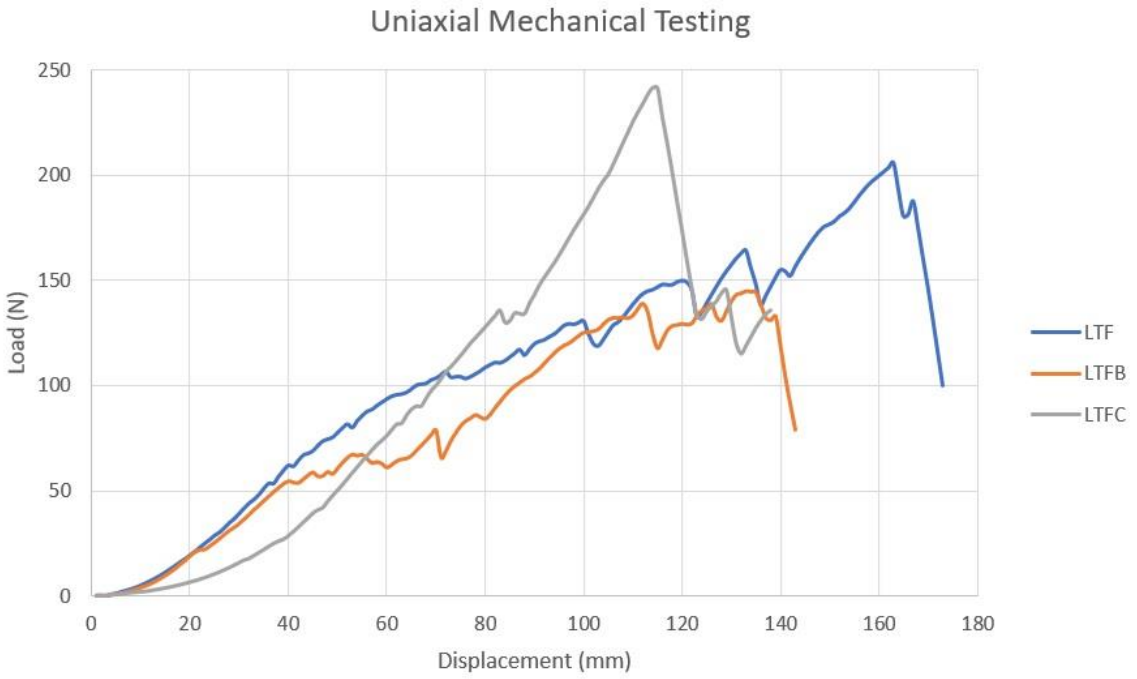


Figure 2-8. Comparison of biomechanical performance of uniaxial constructs.

The uniaxial LTFC construct (gray line) attained the highest maximum load followed first by the LTF and then LTFB construct. The method of failure associated with LTFC construct was tearing of the cricothyroid ligament, whereas the LTF and LTFB constructs failed because the thyroid cartilage tore. The LTFC construct protected the cartilage.

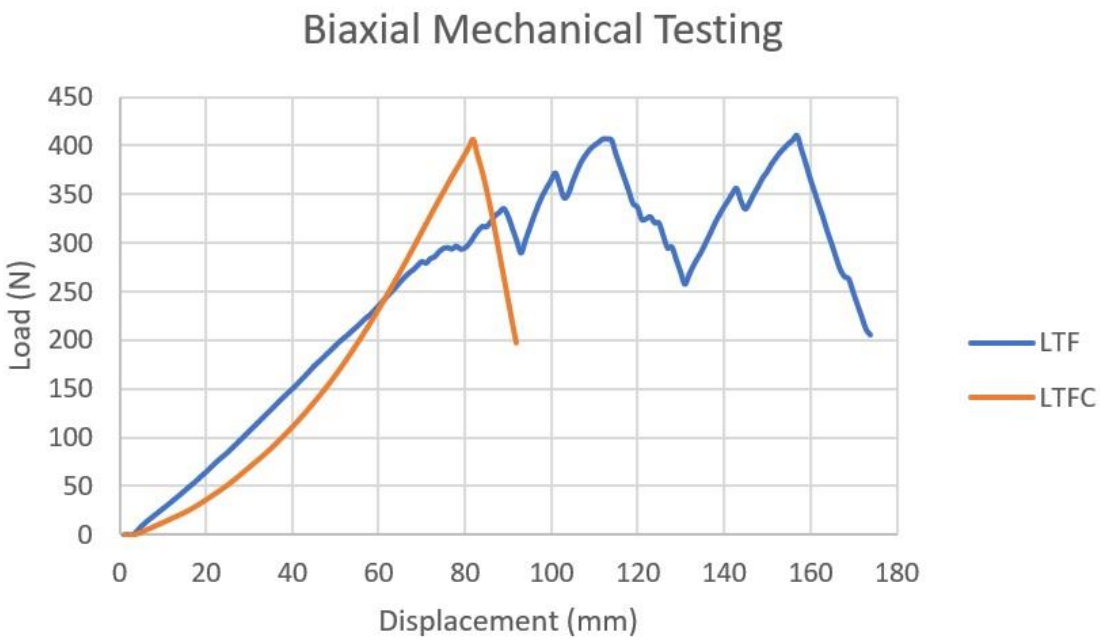


Figure 2-9. Comparison of biomechanical performance of the constructs.

The yield point of the LTF construct corresponded to the moment at which the construct started to tear the thyroid cartilage. The first peak in this graph represents tearing of the thyroid cartilage, and the second peak represents tearing of the cricothyroid ligament. The LTFC construct failed when the suture failed its attachment to the laryngeal clamp; no damage to thyroid cartilage was noticed at the point of failure. The laryngeal clamp provided higher stiffness, force, and tensile stress at yield point and a different method of failure, which was significantly associated with the suture breaking.

Abbreviations

IDDSP – Intermittent Displacement of the Soft Palate
LTF – Laryngeal Tie-forward
LTFB – Laryngeal Tie-forward modified with suture buttons
LTFC – Laryngeal Tie-forward modified with laryngeal clamps
PVC – Polyvinyl Chloride

Footnotes

a. Husky Digital Caliper, The Home Depot, Atlanta, GA
b. Covidien, 710 Medtronic Parkway, Minneapolis, MN
c. Instron 5900, Instron, Norwood, MA
d. Richard-Allan, cat. no. 217001, Aspen Surgical, Caledonia, MI
e. SPSS ver. 25, IBM, 1 New Orchard Road Armonk, NY
f. PS Power and Sample Size Calculations ver 3.0, Vanderbilt University, Department of Biostatistics

Bibliography

References

1. Parente EJ, Martin BB, Tulleners EP, Ross MW. Dorsal Displacement of the Soft Palate in 92 Horses During High-Speed Treadmill Examination (1993-1998). Vet Surg (2002) 31:507-512.
2. Dart AJ, Dowling BA, Hodgson DR, Rose RJ. Evaluation of high-speed treadmill video endoscopy for diagnosis of upper respiratory tract dysfunction in horses. Aust Vet J (2001) 79:109-112.
3. Tan RH, Dowling BA, Dart AJ. High-speed treadmill video endoscopic examination of the upper respiratory tract in the horse: The results of 291 clinical cases. Vet J (2005) 170:243-248.
4. Lane JG, Bladon B, Little DR, Naylor JR, Franklin SH. Dynamic obstructions of the equine upper respiratory tract. Part 1: Observations during high-speed treadmill endoscopy of 600 thoroughbred racehorses. Equine Vet J (2006) 38:393-399.
5. Ducharme NG. "Pharynx," In: Auer JA, Stick JA, editors. Equine Surgery. 4th Edition. Philadelphia, PA: Sounders Elsevier (2012). p. 561-590.
6. Davison JA, Lumsden JM, Boston RC, Ahern BJ. Overground endoscopy in 311 Thoroughbred racehorses: findings and correlation to resting laryngeal function. Aust Vet J (2017) 95:338-342.
7. Stick JA, Peloso JG, Morehead JP. Endoscopic assessment of airway function as a predictor of racing performance in Thoroughbred yearlings: 427 cases (1997–2000). J Am Vet Med Assoc (2001) 219: 962-966.
8. Hackett ES, Leise BS. Exercising upper respiratory video endoscopic findings of 50 competition draught horses with abnormal respiratory noise and/or poor performance. Equine Vet J (2019) 51:370-374.
9. Cheetham J. "Dorsal Displacement of the Soft Palate: Pathophysiology and New Diagnostic Techniques," In: Hawkins J, editor. Advances in Equine Upper Respiratory Surgery. 1st Edition. Indianapolis, IN: John Wiley & Sons (2015). p. 89-95.
10. Ducharme NG, Hackett RP, Woodie JB. The investigation into the role of the thyrohyoid muscles in the pathogenesis of dorsal displacement of the soft palate. Equine Vet J (2003) 35:258-263.
11. Woodie JB, Ducharme NG, Kanter P, Hackett RP, Erb NH. Surgical advancement of the larynx (laryngeal tie-forward) as a treatment for the dorsal displacement of the soft palate in horses: a prospective study 2001-2004. Equine Vet J (2005) 37:418-423.
12. Cheetham J, Pigott JH, Thorson LM, Mohammed HO, Ducharme NG. Racing performance following the laryngeal tie-forward procedure: A case-controlled study. Equine Vet J (2008) Suppl 40:501.
13. Holcombe SJ, Derksen FJ, Stick JA. Bilateral nerve blockade of the pharyngeal branch of the vagus nerve produces persistent soft palate dysfunction in horses. Am J Vet Res (1998) 59:504-508.

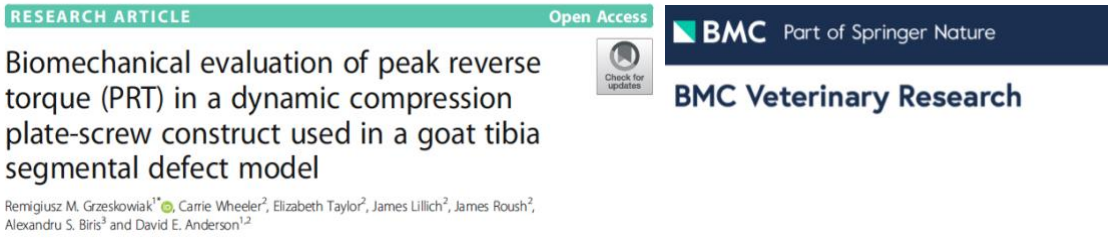
14. Cheetham J, Pigott JH, Hermanson JW, Campoy L, Soderholm LV, Thorson LM, et al. Role of the hypoglossal nerve in equine nasopharyngeal stability. J Appl Physiol (2009) 107:471-477.
15. Gille D, Lavoie JP. Review of seven cases of ulcers of the soft palate. Equine Pract (1996) 18:9-13.
16. Blythe LL, Cardinet GH, Meagher DM. Palatal myositis in horses with dorsal displacement of the soft palate. J Am Vet Med Assoc (1983) 183:781-785.
17. Holcombe SJ, Derksen FJ, Stick JA, et al. Effects of bilateral hypoglossal and glossopharyngeal nerve blocks on epiglottic and soft palate position in exercising horses. Am J Vet Res (1997) 58:1022-1026.
18. Duncan DW. Retrospective study of 50 Thoroughbred racehorses subjected to radical myectomy surgery for treatment of displacement of the soft palate. Proc Am Assoc Equine Pract (1997) 43:237-238.
19. Llewellyn HR, Petrowitz AB. Sternothyroideus myotomy for the treatment of dorsal displacement of the soft palate. Proc Am Assoc Equine Pract (1997) 43:239-243.
20. Harrison IW, Raker CW. Sternothyrohyoideus myectomy in horses: 17 cases (1984-1985). J Am Vet Med Assoc (1988) 193:1299-1302.
21. Anderson JD, Tulleners EP, Johnston JK, et al. Sternothyrohyoideus myectomy or staphylectomy for treatment of intermittent dorsal displacement of the soft palate in racehorses: 209 cases (1986-1991). J Am Vet Med Assoc (1995) 206:1909-1912.
22. Ahern TJ. Oral palatopharyngoplasty. J Equine Vet Sci (1993) 13:185-188.
23. Ducharme NG. Update on the laryngeal tie-forward operation. In: Proceedings of the Equine Upper Airway Symposium; Lexington, KY. Rood and Riddle Foundation (2013). p.1-3.
24. Ahern BJ, Parente EJ. Surgical complications of the equine upper respiratory tract. Vet Clin North Am: Equine Pract (2008) 24:465-484.
25. Santos MP, Gutierrez-Nibeyro SD, Horn GP, Hicke JD, Stewart MC, Schaeffer DJ. In vitro mechanical evaluation of equine laryngeal tie-forward constructs prepared with different suture materials and placement patterns. Am J Vet Res (2015) 76: 373-383.
26. Santos MP, Gutierrez-Nibeyro SD, Horn GP, Wagoner Johnson AJ, Stewart MC, Schaeffer DJ. Mechanical properties of various suture materials and placement patterns tested with surrogate in vitro model constructs simulating laryngeal advancement tie-forward procedures in horses. Am J Vet Res (2014) 75: 500-506.
27. Rossignol F, Ouachee E, Boening KJ. A modified laryngeal Tie-forward procedure using metallic implants for the treatment of dorsal displacement of the soft palate. Vet Surg (2012) 41:685-688.
28. Ahern BJ, Boston RC, Parente EJ. In Vitro Mechanical Testing of an Alternate Laryngoplasty System (ALPS) for Horses. Vet Surg (2012) 41:918-923.

29. Secor EJ, Gutierrez-Nibeyro S, Horn GP. Biomechanical evaluation of modified laryngoplasty by use of a toggle technique for stabilization of arytenoid cartilage in specimens obtained from equine cadavers. Am J Vet Res (2018) 79:226-232.
30. Chan RW, Titze IR. Effect of Postmortem Changes and Freezing on the Viscoelastic Properties of Vocal Fold Tissues. Ann Biomed Eng (2003) 31:482-491.
31. Changoor A, Fereydoonzad L, Yaroshinsky A, Bushmann MD. Effects of Refrigeration and Freezing on the Electromechanical and Biomechanical Properties of Articular Cartilage. J Biomech Eng (2010) 132:1-6.
32. Szarko M, Muldrew K, Bertram JEA. Freeze-thaw treatment effects on the dynamic mechanical properties of articular cartilage. BMC Musculoskelet Disord (2010) 11:1-8.
33. Wuest DM, Meyer DC, Favre P, Gerber C. Mechanical and handling properties of braided polyblend polyethylene sutures in comparison to braided polyester and monofilament polydioxanone sutures. Arthroscopy (2006) 22:1146-1153.

CHAPTER THREE
BIOMECHANICAL EVALUATION OF PEAK REVERSE TORQUE (PRT) IN A DYNAMIC COMPRESSION PLATE - SCREW CONSTRUCT USED IN A GOAT TIBIA SEGMENTAL DEFECT MODEL

The manuscript has been published in peer-reviewed journal, BMC Veterinary Research in September 2019. Utilization of the manuscript in dissertation was granted by the publisher. Student is the primary author on the manuscript, meaning that student conducted the research project as well as wrote the manuscript.

Grzeskowiak RM, Wheeler C, Taylor E, Lillich J, Roush J, Biris AS, Anderson DE. Biomechanical Evaluation of Peak Reverse Torque (PRT) in a Dynamic Compression Plate - Screw Construct Used in a Goat Tibia Segmental Defect Model. BMC Veterinary Research 2019; 15:321.
doi: 10.1186/s12917-019-2058-7


RESEARCH ARTICLE Open Access

Biomechanical evaluation of peak reverse torque (PRT) in a dynamic compression plate-screw construct used in a goat tibia segmental defect model

Remigiusz M. Grzeskowiak[1*], Carrie Wheeler[2], Elizabeth Taylor[2], James Lillich[2], James Roush[2], Alexandru S. Biris[3] and David E. Anderson[1,2]

BMC Part of Springer Nature

BMC Veterinary Research

The strength of the bone and implant interface has been significantly correlated with the primary and secondary stability of the implant. Primary stability is achieved by the implant immediately after placement and it leads ultimately to secondary stability, through the osseointegration process. Osseointegration has been found to be influenced by several factors, from which the most important are loading conditions applied to the implant and associated micromotion. The loading stresses are not evenly distributed between the screws placed in orthopedic plate and plate axial stability has been attributed to the stability of the weakest screw. The purpose of the conducted in-vivo study was to evaluate the osseointegration of the screws placed in dynamic compression plate (DCP) in tibial segmental defects in goats. Further objective included the comparison of osseointegration between the non-self-tapping and self-tapping screws after 60 days of in-vivo loading.

Abstract

Background

Peak reverse torque (PRT) is a valid method to evaluate implants' secondary stability in the healing bone. The secondary stability is achieved by the implant over time and it has been positively correlated with the implants' osseointegration level. In other words, peak reverse torque is the force required to break the bone-implant interface. The purpose of this study was to compare the peak reverse torque for the self-tapping and non-self-tapping screws used in a dynamic compression plate–screw–bone construct after 60 days of loading when used to stabilize 2.5-cm defects in the tibia of goats. The second objective was to compare the peak removal torque of the screws placed in the different positions to evaluate the impact of construct biomechanics on implants osseointegration.

Results

In total, 176 non-self-tapping screws and 66 self-tapping screws were used to fix the 8-holes dynamic compression plates to the bones. The screws were placed in the tibiae from proximal (position sites 1,2, 3) to distal (position sites 4,5,6) and were removed 60 days post-implantation. The goats remained weight-bearing throughout the study period. The screws placed in the proximal diaphysis had significantly less peak reverse torque than screws placed in the distal diaphysis in both groups ($p < 0.05$). The peak reverse torque resistance was also significantly less for the non-self-tapping screws as compared with the self-tapping screws ($p < 0.05$). The intracortical fractures in the trans-cortex occurred significantly more frequently during the placement of non-self-tapping screws ($p < 0.05$) as compared with self-tapping screws ($p < 0.05$).

Conclusions

Based on these results, we concluded that self-tapping screws may be expected to maintain a more stable bone-implant interface during the first 60 days of loading as compared with non-self-tapping screws. This should be a consideration for

orthopedic surgeons and scientists using bone plates to stabilize non-load sharing fractures when a stable plate-screw-bone interface is needed to ensure prolonged stability.

Introduction

Maintenance of the interface between screws and bone is important to ensure adequate stabilization of fractures and to maintain mechanical support for the healing tissue (1,2). The screw is a critical linkage to secure bone plates to bone. Assuming that, the plate is sufficiently stiff and resilient under cyclical loading conditions, and then the integrity of the screw-bone interface determines the overall stability of the construct. The bone-screw interface is defined by its primary and secondary stability. Primary stability is obtained by the screw immediately after placing it into the bone and has been associated with several factors: surgical technique, implant design, surface properties, loading, and quality of the bone (1,3-6). Secondary stability refers to the long-term stability of the screw-bone interface and is directly related to the osseointegration between the bone and the implant's surface (3,7). Several factors have been described to be of importance in this process: biocompatibility, surface texture, surgical technique, the status of the host tissue, and loading conditions (3,7). Secondary stability can be measured using resonance frequency (RF) or peak reverse torque (PRT) (3,8). Several studies, mostly on orthodontic implants, have used PRT (3-7,9-15) showing that peak reverse torque has been positively correlated with the osseointegration process (3,5-6,13-16) and bone density (3,6,11,14).

Various fixation techniques have been described and used to stabilize tibia defects using large animal models (17-21). These techniques include a single dynamic compression plate fixation (17-19), locking intramedullary nail (20), and double plate fixation (21) resulting in the different mechanical environments for the regenerating bone. The studies that have used a single DCP concluded that this fixation technique provides adequate stabilization for most large animal tibia defect models (17-19).

Dynamic Compression Plate (DCP) is a type of conventional plate commonly used in the fracture repairs (22). The plate mechanics rely on a transfer of the axial loading forces from the bone to the proximal screws, which transfer the load into the plate; this load is then transferred from the plate back to the distal bone segment via the distal screws. Ground reaction forces are controlled in the same manner but in a reverse direction. The resulting shear (frictional) forces across the plate-bone interface concentrate stress at the plate-screw-bone unit (2,22). The plate-screw-bone unit exerts shear forces along the bone-screw thread interface as a result of the torque applied to the screws during insertion when fixing the plate to the bone (approximately 3–5 Nm for 3.5 mm cortical screws placed into human femur) (23,24). The mechanical stability of the plate is affected by how well it is fitted against the surface of the bone (2). With the use of DCP, as the screw is being tightened, the screw head slides down on the decline slope within the screw

hole, converting the descending movement of the screw into a gliding movement of the plate (2). Therefore, during the implant placement, the screw torque generates relative compressional strain on the bone surface and tension in the cortical bone around the screw threads (2). Each screw in this construct is loaded individually at the screw-bone interface and the farthest screws at each end of the plate tend to experience the largest interface loads (25).

Although the entire construct can be tested via compression, bending, and torsion of the plate-screw-bone construct, those tests do not assess individually the integrity of each screw-bone interface. Peak reversal torque is a valid method to evaluate the implants interface as an indicator of osseointegration. Osseointegration has been positively correlated with the loading conditions around the implant. The axial strength of the plate may be predicated on the axial strength of the weakest screw in the plate-screw-bone construct because this weakening results in transference of loading forces to adjacent screws. The evaluation of each screws' osseointegration provides insight into this aspect of the plate-screw-bone construct stability. Although the PRT of the various screws has been studied, to our knowledge, studies on reverse torques of screws used in plate-screw-bone constructs after periods of loading are lacking.

The objectives of this study were to measure the peak reverse torque (PRT) of each screw used in a plate-screw-bone construct at the time of its removal after 60 days of in-vivo loading in a non-load sharing, 2.5 cm segmental defect in goats. We hypothesized that the PRT would vary among the screw positions as a result of the cyclical loading construct biomechanics. Secondly, we hypothesized that the ST screws used to fix the plate would have superior PRT compared with that of NST screws after 60 days of cyclical loading.

Materials and Methods

Animal study: The goats in the study were participating in a research project studying bone healing of a non-load sharing, mid-diaphysis segmental defect (2.5-cm length) of the tibia under an approved protocol (KSU IACUC # 2947) (Figure 3-1, all figures and tables are placed in the appendix). The goats participating in the study were mix bred adult (>2 years old) female goats weighing 35 to 65 kgs purchased from the local vendors for the research purpose and owned by the university. The goats were healthy and without evidence of lameness or bone abnormalities. Briefly, the defect creation procedure was performed under general anesthesia which was maintained with the Isoflurane[a] gas inhalant (2.5% - 4% MAC at the beginning of anesthesia and 1.5% MAC – 1.0% MAC during the procedure). The goats were sedated with 0.05 mg/kg, IV Xylazine[b] (20 mg/ml) and induced with 5mg/kg IV Ketamine[c] (100 mg/ml) and 0.25 mg/kg IV Midazolam[d] (5 mg/ml). During the defect creation procedure an 8 - hole 4.5 mm 316L stainless steel DCP[e] and 3.5 mm 316L stainless steel cortical bone screws[e] were used to stabilize the bone. Each bone segment (proximal, distal) received 3 screws. For statistical analysis, screw positions in the proximal bone segment were assigned

positions 1, 2 and 3 from proximal to distal. Screws placed in the distal bone segment were assigned positions 4, 5 and 6 from proximal to distal. Goats were monitored for lameness daily during the study periods to assess the use of the operated limb.

In each goat, the DCP were fixed with only one type of screw, either NST cortical screws or ST cortical screws. All the screws used for this study were placed in standard AO/ASIF fashion and all were bi-cortical screws (near and far cortex). Briefly, the thread hole (2.4 mm diameter) was drilled with 12 V battery operated performance drill[f] (maximum torque 19.21 Nm) and in the NST screws group it was tapped manually prior to the screw placement. Both screw types (NST and ST) were placed manually, using a handheld screwdriver. The screw lengths ranged between 18 mm to 24 mm, the core diameter equaled 2.4 mm, the thread diameter equaled 3.5 mm, and the thread pitch equaled 1.25 mm. The screws were inserted by three of the surgeons (DEA, JR, and JL) and the method was uniformly used by all surgeons. It has been recommended that the tapered tip and cutting flutes extend beyond the far cortex, therefore a care was taken that at least 3 threads of the screw were anchored in the far cortex to maintain rigid fixation (35). All DC plates were fixed with 6 screws in total; 3 proximal to the osteotomy and 3 distal to the osteotomy (Figure 3-1). The screws remained in place for 60 days (40) and were removed at the termination of the study period. Radiographic images were obtained for all goats on days 7, 14, 30, and 60 of the study periods, and they were evaluated to document the occurrence of transcortical diaphyseal tibial fractures in the cortices evident on radiographs and any change in screw-plate-bone interface, position, and fracture gap.

After 60 days of the study period the goats were euthanized with overdose of pentobarbital administered intravenously. Euthanasia was induced by rapid intravenous injection into the jugular vein using pentobarbital (100 mg/kg body weight, IV) in accordance with the AVMA guidelines on the euthanasia of goats (41). Pentobarbital rapidly induces unconsciousness without excitation. Death was confirmed by cessation of any detectable heartbeat and breathing, and loss of corneal reflexes. All implants were removed in the same manner, starting from the most proximal position (1) and following the order (from 1 to 6) until the most distal screw (6). The plate was stabilized manually and therefore prevented from its movement during implant removal. The peak reverse torque for each screw was measured using a handheld torque driver[g]. The pressure was applied gradually increasing, until the screw turned and then stopped. The torque driver did not require calibration and zeroing prior to the test. The handheld torque driver measured torque in the range between 0 – 22.6 Nm. After the implants had been removed and the tissues had been harvested for histopathology within the study on the bone regeneration, the cadavers were disposed at the Kansas State University.

Data was analyzed using a mixed-effects multinomial logistic regression model with the reverse torque categories as the multinomial outcome variable and the screw type (non-self-tapping and self-tapping) as well as screw position in the plate (proximal to distal with the increasing numbers from 1 to 6) as the fixed independent effects (multinomial exposure variable). The Odds Ratios, as well as 95 % Confidence Intervals (95% CI) for fixed effects (screw type and screw position), were estimated with the reference to the screw position no. 6 and self-tapping screw type while holding other effects constant. Statistical significance was identified at the level of $p < 0.05$. The statistical analysis of the association between the transcortical diaphyseal tibial fractures and the screw type as well the fractures and PRT was done using two-sided Fisher's exact test. Statistical Analysis was performed using PROC GLIMMIX in SAS9.4 TS1M4 for Windows 64x$_h$.

Results

All goats remained weight-bearing throughout the study period. A total of 318 screws were used for the study, of which the PRT data for 76 screws were not included in the PRT study due to the following factors: large callous formation around the plate and screw heads (3 plates), plate bending (4 plates), goat removal from the study prior to 60 days (3 plates) and device reading errors (16 screws). The plate bending observed in 4 constructs occurred in goats which showed subjectively evaluated higher level of activity as compared to the other goats. There was no relationship between the weight of the goat and bending of the construct. The remaining 3 goats were removed from the study approximately 1 month after the procedure due to the pullout and displacement of the three most proximal screws resulting in the plate displacement more than 1 cm away from the tibia. The peak reverse torques of 242 screws were included in this study, of which 176 were NST screws and 66 were ST screws (Table 3-1).

Based on evaluation of the initial results of the PRT measurements, PRT data was categorized into four reverse torque ranges: low ($t = 0$ Nm), medium (0 Nm$< t <0.66$ Nm), high (0.66 Nm$< t <2.60$ Nm) and maximal PRT ($t > 2.60$ Nm). After 60 days of loading, 9.09% of all NST screws, as well as 4.55 % of all ST screws, were placed in the low PRT category ($t = 0$ Nm). The 38 ST screws and 44 NST screws (58% of all ST screws and 25% of all NST screws respectively) exceeded 22.6 Nm, the maximum range of the torque driver.

The two-sided Fisher's Exact Test revealed that the transcortical diaphyseal tibial fractures occurred significantly more frequently in the NST screws group ($p < 0.05$). The fractures however did not influence the PRT after 60 days ($p > 0.05$). During the placement of the screws, the transcortical diaphyseal tibial fractures occurred in 37 NST screws and in 5 ST screws (21% of all NST screws and 8% of all ST screws, respectively). The transcortical fractures were most often observed in the screw position no. 4 and no. 5 (41.4% and 31.03% of all transcortical fractures in NST screws group, respectively) (Table 3-2). The pattern was not observed in the

ST screws where the fractures were equally distributed between each position, from 1 through 5 (20% of all fractures in each position in ST screw group) (Table 3-2).

Statistical analysis revealed significant differences between the NST screw PRT and the ST screw PRT ($p < 0.05$). NST screws were significantly more likely to result in PRT less than 0.66 Nm (Table 3-1). ST screws were significantly more likely to have PRT greater than 0.66 Nm (Table 3-1). Significant differences in PRT were found based on the screw insertion position. Screws placed in the proximal tibia (positions 1, 2, and 3) had significantly lower PRT as compared with those placed in the distal tibiae (position 4, 5, and 6) (Table 3-1). The relationship of screw position and PRT was similar among ST and NST screws (Table 3-1).

Discussion

To our knowledge, measurement of PRT has not been reported after a sustained period of loading in-vivo. The model used herein is a non-load sharing model resulting in significant cyclical forces being applied to the bone-screw-plate construct and especially at the bone-screw interface. Similar to previous studies, the DCP provided adequate fixation with satisfactory stability for the non-load sharing tibia defect during this 60-day period of study (17-19).

Screws placed proximal to the ostectomy tended to exhibit lower PRT than the screws placed distal to it. Lower torsional forces needed to break the bone-implant interface have been related to less implant osseointegration (3,5-6,13-16). There are several factors which are of importance in the osseointegration process: biocompatibility, surface quality, surgical technique, the status of the host tissue, and loading conditions (3,7). In the DCP-screw-bone construct, the screws on each end of the plate tend to be exposed to higher loads (2,22) and this has been negatively associated with implant osseointegration (3,7). Bottland et al showed that screws placed remotely to the fracture or osteotomy sustain greater loads than the screws adjacent to the fracture (26). The reduced exposure to mechanical forces may allow for improved osseointegration resulting in greater extraction torques (26). Repeated loading delays bone on-growth around the implant lessening osseointegration (1,11,26). In this study, proximal screws exhibited lower PRT which was most likely due to higher absorption of repeated load than the distal screws. This phenomenon was less clearly observed in the ST screw group. This may be related to the already proven increased insertional torque and primary stability of the ST screws (27-31). PRT has been shown to have a positive correlation to the surrounding bone quality (3,6,11). Several studies have shown that the tibiae have lower BMD in the proximal-mid part of the bone and greater in the distal portion (32-34). The goats used for our study were adult, healthy, and free of lameness or pathologic bone condition. Thus, we would expect that BMD likely influenced some of the PRT results.

ST screws exhibited greater peak reverse torques (PRT) than NST screws after a period of 60 days of loading in a screw-plate-bone construct. The ST screw threads placed into the bone are expected to more closely contact the bone surface with compression as compared with NST screws due to the lack of the tapping process prior to the screw placement (1,35). The tap device designed for use with NST screws has been shown to have longer threads than the screws and this discrepancy creates a micro space between the screw thread and cut bone (35). This incongruity can result in implant micromotion (35) which can reduce the primary stability of the screws. Several studies have shown that the ST screws exhibit greater peak insertional torque (PIT) than the NST screws (1,5,16,36). According to these studies, ST screws obtain greater primary stability than the NST screws (3) and show better interfacial stiffness at the implant-bone interface (4). Micromotion causes filling of the space between the bone and the implant with fibrous tissue or encapsulation of the implant (5). Moreover, this process can lead to excessive bone resorption and inflammation around the implant (peri-implantitis) (4,5,35). These processes will result in reduced implant secondary stability which will negatively influence the longevity of the implant as reflected by decreased PRT. In contrast, the ST screws due to their greater insertional stress have been associated with increased incidence of bone damage promoting bone failure (1) and transcortical diaphyseal tibial fractures (35). These incidences may reduce primary as well as secondary stability. In contrast, the number of transcortical diaphyseal tibial fractures in our study was greater within the NST screws than in ST screws.

The length of the NST and ST screws ranged between 18 and 24 mm in our study and all of the screws were placed bicortical. Previous research on a different length of the orthodontic implants (1.4 – 3.8 mm) did not show any significant correlation between the length of the implant and PRT as long as the implant was longer than 1.4 mm, which was considered as implants' minimal length (37). The minimal length of the cortical screw is considered when at least 3 threads of the implant can be placed through the far cortex in order to achieve the rigid fixation (1). In this study in all cases at least 3 threads of the screw were anchored in the far cortex. The mean PRT of ST and NST screws in this study are comparable with the previous studies on PRT of screw implants. PRT values vary between studies due to factors affecting the osseointegration process and different materials used for the biomechanical tests (3,14,38).

Reverse torque can be a valid method to assess the biomechanical properties of orthodontic implants. This method has been used to reach a better understanding of the osseointegration process (3-7,10-16). The term 'integration strength' refers to the force required to break the bond between the implant and the bone, and this can be measured with the PRT (4). Okazaki et al. showed that insertional torque positively influenced PRT immediately after implant placement. However, the PRT decreased with healing time and showed no difference between the screws at weeks 6, 9, and 12 after insertion (4). Biomechanical interlocking decreases over

time but may increase again as remodeling of the surrounding bone takes place (5). Histological examination of the bone healing process around titanium implants has shown that the existing bone initially resorbs at the bone-implant surface and is replaced by newly formed bone (5). The screws in our study were used in a non-load sharing segmental defect of the tibiae model in goats for approximately 8 weeks resulting in varied reverse torques between ST and NST screws. Some investigators have observed a positive correlation between the bone-implant contact (BIC) and PRT (13,15) while others claimed that the bone quality formed around the implant is more important than the amount (3,6,11,14).

The main limitation of this study is the lack of measured peak insertional torque (PIT) during the screw placement. Even though the PIT defines implants primary stability (1,26,39) not their secondary stability (3) which was measured in this study, it could have been used to standardize the screw placement within the plate. In this study however, limitations of equipment and study design prevented measurement of insertion torque, therefore the variability of insertion torque may have contributed to differences in PRT. Next, the torque unit was limited in a range which resulted in the inability to measure low and high range torques. The torque cell had been selected based on expectations derived from previous studies. Finally, hence this in-vivo study was a part of another research project, introducing the control group was not possible. The control group would have consisted of the screws on which the primary stability would have been measured. The screws would have been placed in the same fashion as described above and they would have been removed immediately after their placement. The PRT would have been measured right before the implant removal. These are the weaknesses that may be addressed in future work.

Conclusions

The DCP-screw-bone construct is an adequate fixation method providing a sufficient stabilization in this 2.5 cm tibial defect model. The construct stabilization can be assessed by measuring implants osseointegration. The ST screws were shown to have a stronger bone-implant interface based on better PRT as compared with NST screws after 60 days post-implantation. Screws placed in the proximal tibia exhibited significantly lower peak reverse torque than those placed in the distal tibia. The lower reverse torque in the proximal tibia may be influenced by load distribution in the goats' tibiae-plate assembly or because of different bone density between the proximal and distal parts of the bone. This phenomenon was less evident in the self-tapping screws presumably because of the greater primary stability as compared with non-self-tapping screws.

Tables

Table 3-1. Peak Reverse Torque categories for NST and ST screws.

Peak Reverse Torque Groups

	NST Screws (Number)					**ST Screws (Number)**				
Prox to Dist	Max	High	Med	Low	Total	Max	High	Med	Low	Total
1	5	8	13	4	30	3	3	3	2	11
2	5	13	9	2	29	4	4	3	0	11
3	4	2	14	9	29	5	4	2	0	11
4	9	12	8	0	29	9	1	0	1	11
5	16	8	5	0	29	9	2	0	0	11
6	9	11	9	1	30	8	3	0	0	11
Total	48	54	58	16	176	38	17	8	3	66
% of total	27%	31%	33%	9%	100%	57%	26%	12%	5%	100%

Most of the NST screws PRT were categorized as High and Medium, whereas the ST screws PRT were mostly categorized as Maximal and High. Overall screws in the position 1-3 were categorized as Medium and Low, whereas the distal screws in positions 4-6 in the majority were categorized as Maximal and High in both screw types (ST and NST). The last line of the table presents the percentage of overall screws placed in the different categories.

Table 3-2. Prevalence of cortical fractures within each screw type.

	Screw Type					
	NST			**ST**		
Position	Total (n)	Intracortical Fracture (n)	Intracortical Fracture (%)	Total (n)	Intracortical Fracture (n)	Intracortical Fracture (%)
1	30	2	6.7	11	1	9.1
2	29	6	20.7	11	1	9.1
3	29	5	17.2	11	1	9.1
4	29	12	41.4	11	1	9.1
5	29	9	31.0	11	1	9.1
6	30	3	10.0	11	0	0

The intracortical fractures occurred in the trans cortex more frequently during the placement of the non-self-tapping screws (37) as compared with the self-tapping screws (5). The position most commonly associated with the fractures were position no. 4 and position no. 5 in the NST screws group. In the ST screws group the fractures were more equally distributed between the positions.

Figures

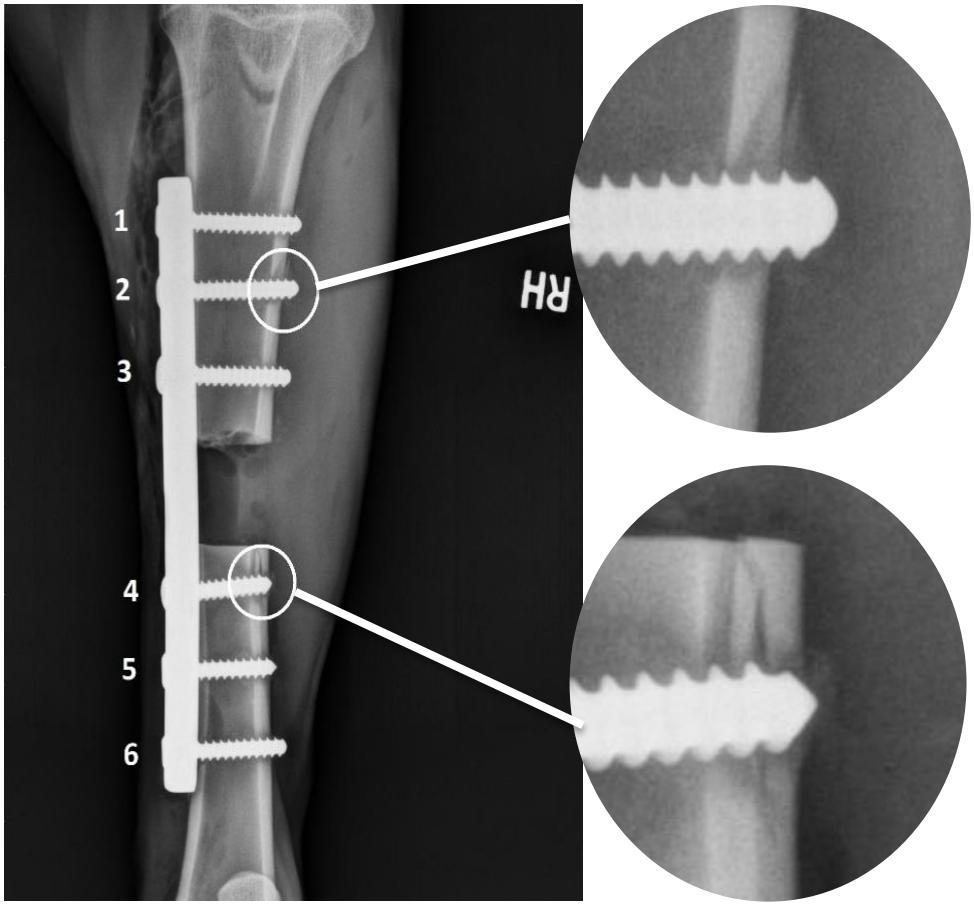


Figure 3-1. Goat tibial defect ostectomy.

Goat tibial ostectomy model supported with an 8 – hole dynamic compression plate (DCP). The 2.5 cm defect was created in the mid-tibia and the plate was fixed with 6 ST or NST screws placed proximally to the ostectomy (pos. 1 – 3) and distally (pos. 4 - 6). The two white circles are labeling the transcortical diaphyseal tibial fractures.

Abreviations

BMD – Bone Mineral Density
BIC – Bone Implant Contact
DCP – Dynamic Compression Plate
IV – Intravenous
MAC – Minimal alveolar concentration
NST – Non-self-tapping
PRT – Peak Reverse Torque
PIT – Peak Insertional Torque
RF – Resonance Frequency
ST – Self-tapping

Footnotes

a. Isoflurane, Abbott Laboratories Inc., 100 Abbott Park Road, Abbott Park, IL60064, USA
b. AnaSed, Lloyd Laboratories Inc., #10 Lloyd Avenue, First Bulacan Industrial City Brgy Tikay, City of Malolos, Bulacan, Philippines
c. Ketamine, Pfizer Inc., 235 East 42nd Street NY, NY 10017, USA
d. Midazolam, AmerisourceBergen Inc., 1300 Morris Drive, Chesterbrook, PA 19087, USA
e. Dynamic Compression Plate, Self-tapping and Non-self-tapping screws, DePuy Synthes Inc., 325 Paramount Dr. Raynham, MA 02767, USA
f. Performax 12 V 3/8” cordless drill, 5101 Menard Drive, Eau Claire, WI 54703, USA
g. Electrotorque System TQJE1500, Snap-on Inc, 2801 80th Streer Kenosha, WI 53143, USA
h. SAS Institute Inc. 100 SAS Campus Drive, Cary, NC 27513 – 2414, USA

Bibliography

References

1. Andrea C.R., Stover S.M., Galuppo L.D., Taylor K.T., Rakestraw P.C. Comparison of Insertion Time and Pullout Strength Between Self-Tapping and Non–Self-Tapping AO 4.5-mm Cortical Bone Screws in Adult Equine Third Metacarpal Bone. Vet Surg 2002;21:189-194
2. Augat P., Von Rueden Ch. Evolution of fracture treatment with bone plates. Injury, Int. J. Care Injured 49S1 (2018):S2-S7
3. Stenlund P., Murase K., Stalhandske C., Lausmaa J., Palmquist A. Understanding mechanisms and factors related to implant fixation a model study of removal torque. Journal of the mechanical behavior of biomedical materials 2014;34:83-92
4. Okazaki J., Komasa J., Sakai D., Kamada A., Ikeo T., Toda L., Suwa F., Inoue M., Etoh T. A torque removal study on the primary stability of orthodontic titanium screw mini-implants in the cortical bone of dog femurs. Int. J. Oral Maxillofac. Surg. 2008;37:647–650
5. Chowdhary R., Jimbo R., Thomsen C., Carlsson L., Wennerberg A. Biomechanical evaluation of macro and micro-designed screw-type implants: an insertional torque and removal torque study in rabbits. Clin. Oral. Impl. Res.2013;24:342-346
6. Ryken T.C., Clausen J.D., Traynelis V.C. Biomechanical analysis of bone-mineral density, insertion technique, screw torque, and holding strength of anterior cervical plate screws. Journal of Neurosurgery 1995;83(2):324-329
7. Cho S.A., Park K.T. A removal torque of titanium screw inserted in rabbit tibia treated by dual acid etching. Biomaterials 2003;24:3611-3617
8. Tseng Y.C., Ting C.C., Du J.K., Chen C.M., Wu J.H., Chen H.S. Insertion torque, resonance frequency, and removal torque analysis of microimplants. Kaohsiung Journal of Medical Sciences 2016;32:469-474
9. Yovich JV, Turner AS, Smith FW, et al: Holding power of orthopedic screws, comparison of self-tapped and pre-tapped screws in foal bone. Vet Surg 15:55-59, 1986
10. Carlsson L, Rostlund T, Alberktsson B, Alberktsson T. Removal torques for polished and rough titanium implants. Int J Oral Maxillofac Implants 1988: 3:21–24
11. White A.A., Kubacki M.R., Samona J., Telehowski P., Atkinson P.J. Removal torque of nail interlocking screw is related to screw proximity to the fracture and screw breakage. J Engineering in Medicine 2016;230(6):599-603
12. Morberg R., Albrektsson T. A histomorphometric and removal torque analysis of c.p. titanium implants inserted in reamed bone beds with and without acrylic cement. J Mater Sci: Mater M 1992;3(3):170–174
13. Johansson C.B., Gretzer C., Jimbo R., Mattison I., Ahlberg E. Enhanced implant integration with hierarchically structured implants: a pilot study in rabbits. Clin. Oral. Implants Res. 2012;23:943-953

14. Wen B., Zhu F., Li Z., Zhang P., Lin X., Dard M., The osseointegration behavior of titanium-zirconium implants in ovariectomized rabbits. Clin. Oral. Implants Res. 2013;25(7):819-825
15. Cho, S. A., Lee, B. K., Park, S. H., Ahn, J. J. The bone integration effects of platelet-rich fibrin by removal torque of titanium screw in the rabbit tibia. Platelets 2014;25(8):562-566
16. Bahr W: Pretapped and self-tapped screws in the human midface: Torque measurements and bone screw interface. Int J Oral Maxillofac Surg 19:51-53, 1990
17. Reichert J.C., Cipitria A., Epari D.R., Saifzadeh S., Krishnakanth P., Berner A., Woodruff M.A., Schell H., Mehta M., Schuetz M.A., Duda G.N., Hutmacher D.W. A Tissue Engineering Solution for Segmental Defect Regeneration in Load-Bearing Long Bones. Sci Transl Med 2012; 4(141):1-10
18. Berner A., Reichert J.C., Woodruff M.A., Saifzadeh S., Morris A.J., Epari D.R., Nerlich M., Schuetz M.A., Hutmacher D.W. Autologous vs. allogenic mesenchymal progenitor cells for the reconstruction of critical-sized segmental tibial bone defects in aged sheep. Acta Biomaterialia 2013; 9:7874–7884
19. Cipitria A., Reichert J.C., Epari D.R., Saifzadeh S., Berner A., Schell H., Mehta M., Schuetz M.A., Duda G.N., Hutmacher D.W. Polycaprolactone scaffold and reduced rhBMP-7 dose for the regeneration of critical-sized defects in sheep tibiae. Biomaterials 2013; 34:9960-9968
20. Field JR, McGee M, Stanley R, Ruthenbeck G, Papadimitrakis T, Zannettino A, et al. The efficacy of allogeneic mesenchymal precursor cells for the repair of an ovine tibial segmental defect. Vet Comp Orthop Traumatol 2011; 24:113–21.
21. Niemeyer P, Schonberger TS, Hahn J, Kasten P, Fellenberg J, Suedkamp N, et al. Xenogenic transplantation of human mesenchymal stem cells in a critical size defect of the sheep tibia for bone regeneration. Tissue Eng Part A 2010; 16:33–43.
22. Egol K.A., Kubiak E.N., Fulkerson E., Kummer F.J., Koval K.J. Biomechanics of Locked Plates and Screws. J Orthop Trauma 2004; 18(8):488-493
23. Perren S.M. Evolution of the internal fixation of long bone fractures. The scientific basis of biological internal fixation: choosing a new balance between stability and biology. J Bone Joint Surg Br. 2002; 84:1093–1110.
24. Borgeaud M., Cordey J., Leyvraz P.E., et al. Mechanical analysis of the bone to plate interface of the LC-DCP and of the PC-FIX on human femora. Injury. 2000; 31(suppl3):C29–C36.
25. Cordey J., Borgeaud M., Perren S.M. Force transfer between the plate and the bone: relative importance of the bending stiffness of the screws friction between plate and bone. Injury 2000;31 Suppl 3:C21–8

26. Bottlang M., Doornink J., Lujan T.J., Fitzpatrick D.C., Marsh J. L., Augat P., von Rechenberg B., Lesser M., Madey S. Effects of construct stiffness on healing of fractures stabilized with locking plates. Journal of Bone and Joint Surgery 2010;(92):12-22
27. Yovich JV, Turner AS, Smith FW, et al: Holding power of orthopedic screws, comparison of self-tapped and pre-tapped screws in foal bone. Vet Surg 15:55-59, 1986
28. Xu XX, Rahn BA, Cordey J: Photoelastic model and morphological changes of bone following insertion of self-tapped and non–self-tapped screws. J Biomechanics 1990; 23:389-392
29. Foley WL, Frost DE, Tucker MR: The effect of repetitive screw hole use on the retentive strength of pretapped and self-tapped screws. J Oral Maxillofac Surg 48:264-267, 1990
30. Koranyi E, Bowman CE, Knecht CD, et al: Holding power of orthopedic screws in bone. Clin Orthop 72:283-286, 1970
31. Schatzker J, Sanderson R, Murnaghan JP: The holding power of orthopedic screws in-vivo. Clin Orthop 108:115-126, 1975
32. Alho A., Hoeiseth A. Bone mass distribution in the lower leg: A quantitative computed tomographic study of 36 individuals. Acta Orthop Scand1991; 62(5):465-470
33. Leung K.S., Siu W.S., Cheung N.M., Lui P.Y., Chow D.H.K., James A., Qin L. Goats as an Osteopenic Animal Model. Journal of Bone and Mineral Research 2001;16(12):2348-2355
34. Karl M., Grobecker – Karl T. Effect of bone quality, implant design, and surgical technique on primary implant stability. Quintessence Int. 2018 Jan 22:189-198
35. Phillips J.H., Rahn B.A. Comparison of Compression and Torque Measurements of Self-Tapping and Pretapped Screws. Plast and Reconstr Surg. 1989;83(3):447-58
36. Boyle III JM, Frost DE, Foley WL, et al: Torque and pullout analysis of six currently available self-tapping and emergency screws. J Oral Maxillofac Surg 51:45-50, 1993
37. Lee J.H., Cha H.S. Screw loosening and changes in removal torque relative to abutment screw length in a dental implant with external abutment connection after oblique cyclic loading. J Adv Prosthodont. 2018; 10(6):415-421
38. Johansson C, Albrektsson T. Integration of screw implants in the rabbit: A 1-year follow-up of removal torque of titanium implants. Int J Oral Maxillofac Implants 1987; 2:69–75.
39. Murphy T.D., Hill C.M., Kapatkin A.S., Radin A., Shofer F.S., Smith G.K. Pullout Properties of 3.5-mm AO/ASIF Self-Tapping and Cortex Screws in a Uniform Synthetic Material and in Canine Bone. Vet Surg 2001; 30:253-260

40. Raghavendra S., Wood M.C., Taylor T.D. Early wound healing around endosseous implants: a review of the literature. Int J Oral Maxillo fac Implants 2005;20(3):425-431
41. Leary S., Underwood W., Anthony R., Cartner S., Corey D., Grandin T., Greenacre C., Gwaltney-Brant S., McCrackin M.A., Meyer R., Miller D., Shearer J., Yanong R. AVMA Guidelines for the Euthanasia of Animals: 2013 Edition. Version 2013.0.1. AVMA, Schaumburg, IL 60173

CHAPTER FOUR
ASSESSMENT OF A 3D HYDROPHILIC POLYURETHANE SCAFFOLD CONTAINING NANO-HA AND BONE PARTICLES, WITH OR WITHOUT BMP2 OR MESENCHYMAL STEM CELLS, ON BONE REGENERATION AND NEOVASCULARIZATION OF MASSIVE (> 5CM) SEGMENTAL DEFECTS

Abstract

Background

Large segmental bone defects (>5cm) result from a traumatic injury and are often associated with extremity amputation. This research provides a valuable alternative to restore such defects with novel nano-based bone scaffolds (PU-nHA-DBP). 61 female and mature goats were included in this study. The goats were randomly assigned to 4 treatment groups with average of n=8, including control, bone scaffold only, bone scaffold soaked in rhBMP-2 and bone scaffold coated with cMSC (n=7) as well as to 2 different study time points, including 2 months (n=31) and 6 months (n=30). Bone healing was evaluated using HD IR Thermography, Radiography, Dual X-ray Absorptiometry (DXA), Dual-phase quantitative Computed Tomography – Angiography as well as Histology. Peripheral blood was collected for the VEGF and BMP-2 measurements.

Results

The results of the bone healing assessment methods revealed significantly more dynamic bone regeneration within the bone scaffold with the cMSC treatment group. The defect healing within the bone scaffold rhBMP-2 and bone scaffold were comparable and significantly higher when compared to the controls. Neither the bone scaffolds nor the bioactive agents significantly stimulated the macroscopic neovascularization process. The peripheral blood BMP-2 concentration increased in a linear manner in all treatment groups and the highest increase was observed in the scaffold rhBMP-2 group.

Conclusions

The bone scaffolds showed promising results in the restoration of large segmental tibial defects (>5 cm) in a goat animal model. None of the implants presented adverse defects in the body associated with implant rejection.

Introduction

The injuries of the musculoskeletal system are a significant problem in human orthopedics. Although the bone has extremely high potential to regenerate itself after damage (1-3) the efficacious repair of large bone defects resulting from resections, traumas, large defects or non-union fractures still requires the implantation of bone grafts (4-5). To date, the optimal bone grafts include the grafts from autologous bone harvested from the donor site of the individual. The significant disadvantage of those grafts is however associated with the increase of morbidity after the implantation and with the necessity of a second surgery (6). Therefore, the orthopedic research seeks to create the synthetic allografts which would reduce the morbidity and eliminate the requirement for additional surgery. The three-dimensional porous bone scaffolds with interconnected channels aim to provide an appropriate base for tissue growth and cell proliferation (7) as well as stimulate bone regeneration with incorporated cells and or growth factors (8).

An ideal bone scaffold should have enough porosity to accommodate osteoblasts or osteoprogenitor cells, to support cell proliferation and differentiation, and to enhance bone tissue formation (9). The early cellular ingrowth, as well as rapid microvascular network formation, has been found to be optimal in the implants with the pore size ranging from 50 to 300 μm diameter (9-11). The larger channels of 500 to 800 μm diameter support ingrowth or larger vessels which directly influence the bone regeneration (9-11). The neovascularization is one of the most important processes in the newly regenerated bone, as it provides oxygen and nutrients to the regenerating bone tissue (12-16). The process occurs most dynamically during the early stages of bone healing (14). The aim of the synthetic biomaterials is to enhance the bone healing and a variety of them have been tested. Polyurethanes are frequently employed in the biomaterials due to mechanical and biological advantages and recently they have gained interest as the platform used for the bone scaffolds (11,17-24). Furthermore, depending on the synthesis method the porosity in the material can be controlled in a feasible way (11).

This study utilizes a novel technology bone scaffold technology that consists of the unique combination of three-dimensional and completely resorbable polyurethane platform (PU) coated with a nanophase Hydroxyapatite (nHA) and decellularized bone particles (DBPs) (25,26). The pore size varied between 50 and 800 μm. The scaffold technology utilized in this research differs from those utilized in previous reports on polyurethane implants coated with nano-Hydroxyapatite in patented manufacturing methods as well as in the polyurethane platform (25-30). The novel technology implants are evaluated in the large animal (goat) model with a large (>5 cm) full-thickness segmental tibial defect. The study evaluates implants' influence on the neovascularization process during a short postoperative period and within the newly formed bone throughout the healing process.

The first objective of this study (O1) was to assess scaffolds bone regenerative properties, specifically its ability to enhance the neovascularization process within 2 and 6 months after the surgery. The bone scaffold was compared to the bone void (negative control) as well as to the scaffold coated with the recombinant human bone morphogenetic protein-2 (BMP-2) and scaffold seeded with caprine mesenchymal stem cells (cMSC). Both bioactive agents have been already proven to have a positive influence on bone regeneration, and BMP-2 furthermore has been described to mediate proangiogenic effects (31-34). The second objective of this study (O2) was to evaluate the recombinant human bone morphogenetic protein – 2 (rhBMP-2) and caprine mesenchymal stem cells (cMSC) influence on the bone regeneration and neovascularization process. The third objective (O3) was to evaluate the vascular endothelial growth factor (VEGF) and bone morphogenetic protein-2 (BMP-2) concentration within the peripheral blood. The first hypothesis (H1) was that the bone scaffold will be osteoinductive, osteoconductive and osseointegrated and will therefore stimulate bone

regeneration of the large tibial defect. The second hypothesis (H2) was that it will further enhance the early neovascularization process. The third (H3) and fourth hypothesis (H4) were that the bone regeneration and neovascularization will be different between the treatment groups including scaffolds, scaffolds coated with BMP-2 and scaffolds seeded with cMSC. The fifth hypothesis (H5) was that there will be a difference in the peripheral blood VEGF and BMP-2 concentration between the treatment groups depending on the pace of bone regeneration. The bone regeneration was defined by tissue ingrowth and on growth caused by implants osteoinductive, osteoconductive and osseointegrative properties (35).

Materials and Methods

Study Population

The study included 61 mix-bred adult (>2 years old) female goats weighing between 35 and 65 kgs. The goats underwent a routine screening process before the acquisition which consisted of general clinical health assessment and orthopedic evaluation. Any goat which showed clinical signs of a chronic disease, bad body condition score (1-2/5), signs of lameness due to an underlying disease or was positive for pregnancy screening was not included in the study. The length of the right tibiae varied between 22 and 25 cm. 61 goats were included in the study and randomly assigned to 4 treatment groups (n=7-8 goats per group) and 2 study termination time points. The treatment groups involved negative control with the bone defect left unfilled, and the scaffold containing treatment groups, including bone scaffold, bone scaffold coated with e-coli derived recombinant human bone morphogenetic protein – 2 (rhBMP-2)[a] and bone scaffold seeded with the bone marrow-derived caprine mesenchymal stem cells (cMSC). The goats were humanely sacrificed at 2 study termination time points, including 60 days after the surgery and 180 days after the surgery. The study was performed under a protocol that was approved by the University of Tennessee Institutional Animal Care and Use Committee under protocol number 2606-0518.

Nano-HA polyurethane scaffold preparation

The nano-HA polyurethane scaffolds with demineralized bone particles were prepared as previously described (25,26). Each of the Nano-scaffolds assigned to the rhBMP-2[a] treatment group was soaked in 2 mg of rhBMP-2[a] (1mg/ml) 15 minutes before implantation into the defect. The rhBMP-2[a] was applied on the scaffold surface during the surgery by the surgeon in sterile manner. Each of the bone scaffolds assigned to the cMSC treatment group was sterilely loaded with the low passage (P2-4) 5 x 10^6 cMSC/cm diameter 24 hours before implantation.

Caprine Mesenchymal Stem Cell Collection and Culture

The bone marrow was harvested from the goats' sternum in the presence of 1 ml of 1,000 USP units/ml heparin per 10 ml of harvested bone marrow, using a previously described technique (36-38). The collected bone marrow was added to a T175 tissue culture flask[b] and incubated at 37°C with 5% CO2 for 48 hours.

Adhered cells were washed with addition of HBSS[c] to remove extraneous blood agents and growth media, Dulbecco's Modified Eagle Medium with glutamine, 4-(2-hydroxyethyl)-1-piperazineethanesulfonic acid (HEPES buffer), and sodium pyruvate added (DMEM/F-12 1:1 modified)[d] containing 10% fetal bovine serum[e] (fetal bovine serum) and a 1% solution of 10,000 units/ml of penicillin[f] and 10,000 µg/ml streptomycin[g] (penicillin-streptomycin solution) was added. Cell cultures were expanded by regular media changes every 3 days until the cells reached 80% confluency, at which point cells were harvested using 0.25% trypsin[h]. Harvesting and seeding cycles were repeated to generate a stock of cells passage 2-4. For storage, aliquots of 10 million bone marrow-derived cMSCs were resuspended in 1.5mL freezing medium, comprised of 50% fetal bovine serum, 5% dimethyl sulfoxide (Hybri-Max)[i], and 45% of DMEM/F-12 1:1 modified media, and cryopreserved in liquid nitrogen[j]. For application, cells were thawed at 37°C, and re-suspended gently with DMEM/F-12 1:1 modified media and were carefully seeded to scaffolds 24 hours prior to implantation at a concentration of $5x10^6$ cMSC/cm of scaffold length.

Surgical Procedure and Postoperative care

The goats received antibiotics including ceftiofur sodium[k] 2.2 mg/kg IV and anti-inflammatories including flunixin meglumine[l] 1 mg/kg for 3 days around the surgery time. Before the anesthesia, they were sedated with xylazine hydrochloride[m] (0.05 mg/kg IV) and induced under general anesthesia using ketamine hydrochloride[n] (5mg/kg IV) and midazolam[o] (0.05 mg/kg IV). General anesthesia was maintained in dorsal recumbency using Isoflurane[p] and oxygen. The right hind limb was clipped, aseptically prepped and draped accordingly to the surgery. A 20 cm skin incision was made over the dorsal and medial aspect of the right tibia to expose the bone and 5-7 cm full-thickness defect was created in the mid tibia with the oscillating bone saw[q]. The defect was stabilized with a 4.5 mm 8 holes – locking plate[r] which was applied to the dorsomedial surface of the tibia. The plate was fixed to the bone with eight bi-cortical screws[s], four in the distal and four in the proximal aspect of the tibia. The created void in the bone was thoroughly washed with a 10% gentamicin[t] solution and the defect was filled either with the scaffold accordingly to previous treatment group assignment or left unfilled in the control group. The subcutaneous tissue was closed using absorbable taper suture[u] in the simple continuous manner and the skin incision was closed using a simple continuous pattern with non-absorbable cutting suture[v]. A sterile bandage with the full limb splint support was applied to the right hind limb and the goat was recovered on the mat. During the postoperative care, the goats were housed individually for up to 30 days after the surgery and following that in the group pens containing 5-6 goats. The sutures were removed 30 days after the surgery and the full support bandages were removed 60 days after surgery. The fiberglass cast was applied to the limbs which required additional stabilization, including limbs with the locking plate constructs bending or limbs with the excessive periosteal reaction around the proximal bone due to the construct instability. During the postoperative

period, the bone healing assessment data was acquired, including thermography, radiography, dual X-ray absorptiometry (DXA), dual-phase Computed Tomography (CT) Angiography as well as histology. The peripheral blood was collected over several time points to evaluate the VEGF and BMP-2 concentration.

High Definition Infrared Thermography (HD IR Thermography)

Thermography was performed on the operated right hind limb to evaluate the blood flow in the local tissues associated with the inflammatory process using the high definition infrared thermometer camera[w]. The camera was adjusted to the surrounding environment including the temperature and humidity each time before the data acquisition process was started. The acquisition process was standardized, and it was performed by two investigators (RG and RR). The scans were acquired 10 minutes after the bandage was removed. The scans were obtained 1 m away from the operated limb with the device directed perpendicularly to the limb and aimed at the area of interest in the center of the right tibia. Two projections obtained every time included the anterior-posterior projection as well as the latero-medial projection. The temperature was measured in both projections in degrees of Celsius and the average value was recorded.

Radiography

The new bone formation within the defects was assessed with the radiographic examination. The radiography was performed by two investigators (RG and RR) using the portable radiographic machine[x], digital radiography plates[y] and a clinical radiographic digital system[z]. The radiography involved two projections, the dorso-plantar and latero-medial projection of the right tibia. The radiographs were obtained immediately after the procedure, 24 hours after the procedure, followed by monthly examinations until the end of the study. Obtained radiographs were exported in digital imaging and communications (DICOM) format to the picture archival and communication system (PACS)[aa] for the further analysis by the board-certified radiologist (SH). The monthly radiographs were evaluated and the gap-filling with new bone (range of scores from 0 to 4) (Table 4-1), opacity of newly formed bone (range of scores from 0 to 2) (Table 4-2) as well as opacity increase within the scaffold (0 – no and 1 – yes) were scored. The median scores were compared between the treatment groups. Next, the defects were monthly measured in three different locations. The first location consisted of the line drawn adjacent to the locking plate construct, the second location consisted of the line drawn in the center of the defect and the third location consisted of the line drawn in the far cortex. The defects showing evidence of collapse due to the locking plate bending were excluded from this analysis.

Defect densitometry - Dual X-ray Absorptiometry (DXA)

The bone density of the defects was measured with the dual x-ray absorptiometry (DXA)[bb]. The DXA system was calibrated based on two materials of defined composition, one mineral (hydroxyapatite) and a homogeneous soft tissue of a set

area adjacent to the bone area. DXA scans were obtained 24 hours after the surgery followed by monthly examinations until the end of the study. The goats were sedated with Xylazine hydrochloride[m] (0.05mg/kg IV) and placed in sternal recumbency. The hind limbs were extended caudally and the scans of the entire length of the tibiae parallel to the long axis of the bone were performed. The scanner was set for the lumbar spine using a single beam and the bone mineral density (BMD) calculations were performed. The region of interest (ROI) was drawn between the most distal screw in the proximal bone segment and the most proximal screw in the distal bone segment. The ROI was subsequently divided into three segments (L1-L3), including the distal aspect of the proximal bone segment (L1), the defect (L2) and the proximal aspect of the distal bone segment (L3). All segments were analyzed in a DXA software[bb] and the report was generated. The bone area was defined and expressed in cm^2 and BMD was calculated and expressed in g/cm^2.

Dual-Phase Computed Tomography (CT) Angiography

The vascular integrity following large defect creation in the tibiae was assessed with the dual-phase computed tomography (CT) angiography. The CT was performed using a 40-slice helical CT scanner[cc]. Obtained CT images were sent to the PACS system[aa] for further evaluation by the board-certified radiologist (SH). The scans were performed before the goat was sacrificed under general anesthesia at two study termination time points (60 and 180 days). During the scans, the transverse images of the tibia from the distal aspect of the femur to the tarsus were obtained prior to contrast medium administration. The images were acquired as a multi-slice helical data set and were reconstructed into 0.67- and 5-mm slices using soft tissue and bone algorithms. The dual-phase CT angiography consisted of two contrast injection phases, including test bolus of a contrast medium[dd] (185 mg I/kg) administration and a full dose of contrast medium[dd] (814 mg I/kg) administration. The number of visible vessels surrounding the defect as well as their branches were recorded. The contrast enhancement was also measured as an indicator of vascularity of the tissues within the osteotomy gap. Attenuation values before contrasting medium administration and during peak arterial and venous enhancement were determined, and a contrast enhancement ratio between post- and pre-contrast measurements was calculated. The defect density was measured using Hounsfield Units (HU).

Histology

The goats received intravenous oxytetracycline[ee] (20 mg/kg IV) one time, 24 hours before euthanasia to label the metabolically active bone. After the euthanasia, the tibia segments were harvested and fixed in 95% Ethanol fixative until sectioned. The specimens with insufficient healing and tissue integrity to perform whole segment histology were divided into proximal, middle and distal segments. The proximal segment included 1-cm of the proximal bone and the transition zone between bone and the scaffold. The middle segment included 2 cm of the center

of the scaffold, and the distal segment included 1 cm of the distal bone and the transition zone between bone and the scaffold. Those samples underwent routine protocol decalcification process which included preservation in 10% neutral buffered formalin[ff] for 5 days after tissue biopsy followed by a short, up to 5 days decalcification with hydrochloric acid[gg] (39). The specimens were subsequently stained with hematoxylin-eosin and Masson's trichrome according to the routine staining protocols (40-42). Tissues with sufficient bone healing and integrity were harvested in their entirety and ultimately embedded in methyl methacrylate[hh] for staining and analysis (40). The embedding process included tissue dehydration using an automated tissue processor[ii] and placing the tissues in the infiltration solution (methyl methacrylate and dibutyl phthalate) for a period of 1.5 - 2 weeks. Infiltrated tissues underwent following staining, including von Kossa, Goldner's Trichrome, Tartrate-resistant acid phosphatase (TRAP) and Verhoeff-Van Gieson (VVG) accordingly to the routine protocols previously described in the literature (43-45). For fluorescence microscopy, slides were coverslipped and left unstained due to the fluorochrome labeling to determine bone formation. Descriptive analysis and quantitative assessment of the stained specimens were performed. The quantitative assessment of new bone formation (mineralized tissue) in the proximal and distal segment as well as the osteoid (unmineralized tissue) formation in the middle sections was conducted using NIH Fiji[jj] (46,47). The quantification was carried out through the generation of binary masks for images, permitting measurement of the mineralized and non-mineralized area relative to the total image area. Bone and osteoid areas expressed as a percentage of the total area of images were averaged, and statistical relations among groups obtained.

VEGF and BMP-2 concentration measurement

The peripheral blood was collected from the goats to evaluate the vascular endothelial growth factor (VEGF) and bone morphogenetic protein-2 (BMP2) concentration up to 30 days after surgery. The timeline was established according to the previous reports, which found the most dynamic changes in the concentration of those growth factors within the first month of the healing (48). The collected blood was centrifuged to obtain plasma which was stored in -80°C freezer until analysis. The analysis was performed using commercially available BMP2[kk] and VEGF ELISA kits[ll] which allowed for the measurements of the concentration of each growth factor.

Statistical Analysis

The statistical analysis was performed using IBM SPSS Statistics 25®[mm]. The treatment groups assigned to the 2-month time point and 6-month time point were analyzed separately. The descriptive statistics including mean values as well as standard deviations of each variable were performed. The continuous variables were tested for the normality of distribution using the Kolmogorov - Smirnov test and for the homogeneity of variance using Levene's test.

The differences between the treatment groups at each data collection time points were analyzed using one-way analysis of variance (ANOVA) test with Tukey's Post-hoc test with the treatment group as the factor. The changes within each treatment group over time were evaluated with the bivariate 2 – tailed Pearson's correlation test and multivariate regression analysis with the treatment groups as the dependent variables and time as the covariate. The adjusted R squared as well as beta coefficients for each dependent variable were obtained and the significance of each beta coefficient was evaluated. The categorical data were compared between the treatment groups using the Kruskal – Wallis nonparametric test. The survival rate of the study population due to a complication occurrence was calculated using the Kaplan-Meier survival curve. The statistical significance of the tests was established at alpha equaled 0.05 and the power of the study was calculated to be $\beta = 0.8$.

Results

Study Population

The study included 61 out of 67 mature female goats (> 2 years old). The goats were assigned to 2 study terminal time points, including 2-month (n = 30) and 6-month (n=31). The average size of the defect created in the study was 6.63 ± 1.4 cm in both time points. The average weight of the goats was 51.49 ± 8.0 kg and 55.59 ± 7.9 kg in the 2- and 6-month treatment groups respectively. The calculated Kaplan-Meier survival curve revealed no statistical difference in the survival rate between all the treatment groups due to an event that was defined as a complication ($p > 0.05$) (Figure 4-1, all figures and tables are placed in the appendix).

High Definition Infrared Thermography (HD IR Thermography)

The statistical analysis confirmed the normality of data distribution and homogeneity of variance within all analyzed variables ($p > 0.05$). The analysis of data obtained from the goats assigned to the 2-month time point did not reveal statistically significant differences in the temperature yielded by the local tissues surrounding the surgery site between all treatment groups at any of the data collection time points. A statistically significant reduction of local tissue temperature over 2 months after surgery in all treatment groups was observed ($p < 0.05$). This was confirmed with the multivariate regression which was significant for all treatment groups and yielded following *beta coefficients,* -0.54, -0.47, -0.41, -0.58 and R^2 values, 0.356, 0.219,0.132,0.090 for the control, scaffold, scaffold rhBMP-2 and scaffold cMSC treatment group respectively ($p < 0.05$).

The analysis of data obtained from the goats assigned to the 6-month time point showed a similar trend, revealing no statistically significant differences in the temperature of the local tissues at any of the data collection time points ($p > 0.05$). A statistically significant reduction of local tissue temperature overtime after surgery in all treatment groups was confirmed ($p < 0.05$). Similarly, this was

confirmed with the multivariate regression which was significant for all treatment groups and yielded following *beta coefficients,* -0.74, -0.77, -0.75, -0.80 and R_2 values, 0.663,0.710,0.728,0.706 for the control, scaffold, scaffold rhBMP-2, and scaffold cMSC treatment group respectively ($p < 0.05$) (Figure 4-2).

Radiography

The subjective radiographic assessment revealed that in the 2- and 6-month time points treatment groups, the scores of osteotomy gap filling, the scores of newly formed bone opacity as well as in the scaffold containing treatment groups - the scores of the opacity increase within the graft did not differ significantly between all treatment groups ($p > 0.05$) (Figures 4-3,4-9,4-10, and 4-11*)*. The objective analysis involved the defect measurement results collected from 40 out of 61 goats (Figure 4-3). The results from 21 goats were excluded from this analysis due to the defect collapse during the postoperative period. The statistical analysis confirmed the normality of data distribution and homogeneity of variance within all analyzed variables ($p > 0.05$). The statistical analysis of the results obtained from the 2-months treatment groups did not reveal significant differences between the treatment groups in general reduction of the defect at any of the measurement time points ($p > 0.05$) (Table 4-3). Similarly, the detailed analysis of 3 different defect measurement locations (lines 1,2 and 3) did not reveal significant differences between the treatment groups in the defect reduction at any of the measurement time points ($p > 0.05$) (Table 4-3). This was confirmed with the multivariate analysis which revealed no significant defect reduction over 2 months after the surgery ($p > 0.05$), except for the scaffold only treatment group for which the analysis showed a significant reduction in the size of the defect measured at the line no. 1 and 2 (*beta coefficient* = - 0.161, R_2 = 0.421 and – 0.113, R_2 = 0.610 respectively) ($p < 0.05$).

The differences between the treatment groups in defect reduction were more noticeable in the goats assigned to the 6-month time point (Table 4-3). The calculated defect reduction slope was more dynamic within the first 3 months after surgery yielding -0.093 mm/day, -0.099 mm/day, -0.126 mm/day, -0.338 mm/day for the control, scaffold, scaffold rhBMP-2 and scaffold cMSC treatment group respectively. The slope plateaued after 3 months post-surgery, resulting in -0.028 mm/day, -0.073 mm/day, -0.060 mm/day, -0.125 mm/day in the control, scaffold, scaffold rhBMP-2 and scaffold cMSC treatment group respectively (Figure 4-4). The statistical analysis of the general defect reduction revealed significant differences from the 3rd month after the surgery in the size of the defect between the scaffold cMSC and the remaining treatment groups ($p < 0.05$) (Table 4-3). The detailed analysis revealed that the defect reduction in scaffold cMSC differed significantly from the control treatment group 4-, 5- and 6-months after surgery in the line no. 3 as well as from the scaffold in the line no.1, 4 months after surgery and in the line no. 3, 4-, 5- and 6-months after surgery ($p < 0.05$) (Table 4-3). The analysis of the measurements in the remaining line no.2 did not reveal significant

differences in the defect size between the treatment groups at any of the data collection time points ($p > 0.05$) (Table 4-3). The results of the multivariate regression analysis of the measurements taken in line no.1 were statistically significant for all treatment groups and yielded following *beta coefficients,* -0.121, -0.098, -0.151, -0.311 and R^2 values, 0.155, 0.087, 0.286, 0.376 for the control, scaffold, scaffold rhBMP-2, and scaffold cMSC treatment group respectively (Figure 4-4). The multivariate regression analysis of the measurements taken in line no.2 was statistically significant only for the scaffold containing treatment groups and yielded following *beta coefficients,* -0.093,-0.076, -0.301 and R^2 values, 0.097, 0.128, 0.335 for the scaffold, scaffold rhBMP-2 and scaffold cMSC treatment group respectively (Figure 4-4). The multivariate regression analysis of the measurements taken in line no.3 was statistically significant only for the scaffold cMSC treatment group and the *beta coefficient* equaled -0.273, as well as R^2 value, equaled 0.309 (Figure 4-4).

Densitometry - Dual X-ray Absorptiometry (DXA)

The statistical analysis of the DXA results confirmed the normality of data distribution and homogeneity of variance within all analyzed variables ($p > 0.05$). The bone mineral density (BMD) recorded on the tibiae in the goats assigned to the 2-month time point varied between the treatment groups. At the 2-months data collection time point, the statistical analysis revealed significant differences in BMD between the treatment groups containing the scaffold and the controls ($p < 0.05$) (Table 4-4, Figure 4-5). The differences were however not statistically relevant between the scaffolds containing treatment groups ($p > 0.05$) (Table 4-4). The calculated BMD slopes varied between the treatment groups revealing 0.001 g/cm^2/day, 0.004 g/cm^2/day, 0.005 g/cm^2/day for the control, scaffold as well as scaffold rhBMP-2 and scaffolds cMSC treatment group respectively. The multivariate analysis confirmed the trend yielding following *beta coefficients*, 0.001, 0.04, 0.001, 0.005 and R^2 values, 0.077, 0.711, 0.665, 0.537 for the control, scaffold, scaffold rhBMP-2 and scaffold cMSC treatment group respectively ($p < 0.05$).

At 6-months data collection time point, the statistical analysis revealed significant differences in BMD between the treatment groups at all data collection time points ($p < 0.05$) (Table 4-4, Figure 4-5). The differences in BMD were found between the groups containing the scaffolds and the control ($p < 0.05$) (Table 4-4). Further analysis found statistically significant differences between the scaffold cMSC and the scaffold treatment group revealing lower BMD in the scaffold cMSC, 24 hours after the surgery and higher BMD in the scaffold cMSC, 4 and 5 months after the surgery ($p < 0.05$) (Table 4-4). The BMD was also significantly higher in the scaffold cMSC as compared with the scaffold rhBMP-2 at 4, 5 and 6 months after the surgery ($p < 0.05$) (Table 4-4). The differences between the scaffold and the scaffold rhBMP-2 were not statistically significant ($p > 0.05$) (Table 4-4). The calculated BMD slope showed its most dynamic increase during the first 3 months

revealing 0.0005 g/cm$_2$/day, 0.0023 g/cm$_2$/day, 0.0024 g/cm$_2$/day, and 0.0048 g/cm$_2$/day increase within the control, scaffold, scaffold rhBMP-2, and scaffold cMSC respectively (Figure 4-6). After 2- and 3-months post-surgery, the BMD slopes gradually plateaued in all treatment groups, resulting in 0.0013 g/cm$_2$/day, -0.0014 g/cm$_2$/day, -0.0014 g/cm$_2$/day, and 0.0021 g/cm$_2$/day increase in the control, scaffold, scaffold rhBMP-2 and scaffold cMSC treatment group respectively (Figure 4-6). The multivariate regression confirmed the trend and it was significant in all treatment groups yielding following *beta coefficients*, 0.000, 0.001, 0.001, 0.004 and R_2 values, 0.075, 0.126, 0.126, 0.351 for the control, scaffold, scaffold rhBMP-2 and scaffold cMSC treatment group respectively ($p < 0.05$) (Figure 4-6).

Dual-Phase CT Angiography

The statistical analysis of results obtained from the computed tomography (CT) with angiography confirmed the normality of data distribution and homogeneity of variance within all analyzed variables ($p > 0.05$). Further analysis of the results obtained from 2-month treatment groups revealed that defect density was significantly different between the scaffold containing treatment groups and the control ($p < 0.05$). The results were however not significantly different between the treatment groups containing scaffolds ($p > 0.05$) (Table 4-5). The density of newly formed bone and the number of newly formed vessel branches within the defect did not differ significantly between the treatment groups ($p > 0.05$) (Table 4-5). The number of vessels contacting the implant did not differ significantly between the treatment groups containing scaffolds ($p > 0.05$) (Table 4-5). The contrast enhancement ratio was significantly higher in the scaffold as compared with the scaffold cMSC treatment group ($p < 0.05$) (Table 4-5). Further analysis revealed that the cortical density of the proximal and distal bone fragment was significantly different between the operated limb and non-operated limb in control, scaffold rhBMP-2 and scaffold cMSC treatment group ($p < 0.05$). The difference was not statistically relevant in the scaffold treatment group ($p > 0.05$). The muscle mass of the gluteal muscle group was significantly different in the non-operated limb as compared with the operated limb in the scaffold and scaffold cMSC treatment group ($p < 0.05$). The difference was not statistically relevant in the control and scaffold rhBMP-2 treatment group ($p > 0.05$).

The statistical analysis of results obtained from the computed tomography (CT) with angiography of the 6-month treatment groups revealed that defect density measured differed significantly between the scaffold containing treatment groups and the control ($p < 0.05$). The results were however not significantly different between the treatment groups containing scaffolds ($p > 0.05$) (Figure 4-12, Table 4-5). The density of the newly formed bone and the number of newly formed vessel branches within the defect did not differ significantly between the treatment groups ($p > 0.05$) (Figure 4-4, Table 4-5). The number of vessels contacting the implant did not differ significantly between the scaffold containing treatment groups

containing ($p > 0.05$) (Table 4-5). The contrast enhancement ratio did not differ significantly between the treatment groups ($p > 0.05$) (Table 4-5). Further analysis revealed that the cortical density of the proximal and distal bone fragment was significantly different between the operated limbs and non-operated in all treatment groups ($p < 0.05$). The muscle mass of the gluteal muscle group was significantly different in the non-operated limb as compared with the operated limb in the scaffold and scaffold cMSC treatment group ($p < 0.05$). The difference was not statistically relevant in the control and scaffold rhBMP-2 treatment group ($p > 0.05$).

Histology

The specimens harvested from the controls differed significantly in the macroscopic as well as the microscopic view from the scaffold containing treatment groups, similarly, among decalcified and undecalcified specimens. The controls involved only the proximal and distal bone segment as the newly formed bone did not bridge the defect in the controls (Figure 4-13). Furthermore, the medullar cavities of the proximal and distal sections were enclosed with the cortical bone consistent with early non-union changes. Bone segments treated with scaffolds had osseointegration of the scaffold ends within the medullary cavity. The ends of the bone segment remained open with new bone formation extending within the scaffold and growing on the surface of the implants. New bone on-growth along the surface of the scaffolds had extensive non-mineralized tissue containing high concentrations of collagen (osteoid) (Figures 4-13 and 4-14). The osteoid was well-formed within the pores and channels of the scaffolds, and it was equally distributed within all the sections of the implant. In the tissues harvested from 2-month goats, the osteoid appeared more mineralized in the proximal and distal third of the scaffold and less within the center of the scaffold. This trend was less noticeable, as the osteoid mineralization was equally distributed across the specimen (Figure 4-14). The cortical bone was well integrated with the osteoid and newly synthesized cortical bone surrounding the implant. The periosteum presented a continuous extension from the proximal and distal bone segment to the newly formed bone and osteoid surrounding the implant. The unstained slides revealed a higher level of fluorescence which corresponded with higher bone metabolic rate in the specimens with lower mineralization, confirming that the bone formation in those specimens was more active as compared with the tissues already containing higher mineralization (Figure 4-15). The medullar cavity in all the specimens was filled with adipose tissue. The large polynuclear cells were not found in the transition zones between the bone segments and the scaffolds. Quantitative assessment of the scaffold treated specimens, harvested at 2 and 6 months after surgery, did not reveal statistically significant differences between the treatment groups in the bone content in the proximal and distal sections as well as in the osteoid content in the middle sections ($p > 0.05$) (Table 4-6). There were no statistically relevant differences in the bone content and in the osteoid content between the 2- and 6-months goat treatment groups. ($p > 0.05$).

VEGF and BMP-2 concentration measurement

The results of the VEGF concentration analysis were not significantly different between treatment groups at any of the blood collection time points. Furthermore, the analysis did not reveal a significant linear change in the VEGF concentration within the treatment groups (Figure 4-7). The VEGF concentration increased from the baseline concentration over 10 days after surgery and then gradually decreased to the values before surgery, except in the control group (Figrue 4-7). The results of the rhBMP-2 concentration analysis revealed a significant linear increase of the rhBMP-2 concentration within the first month after the surgery among all treatment groups (Figure 4-8). The increase was noticed to be most dynamic in the treatment group containing the scaffold soaked in rhBMP-2 (2-fold of the baseline), followed by the treatment group with the scaffold coated with cMSC, scaffold only and the negative control. The rhBMP-2 concentration was significantly higher in the treatment group containing the scaffold soaked with rhBMP-2 10 and 30 days after the surgery as compared to the control and control and scaffold coated with cMSC respectively (Figure 4-8).

Discussion

The study showed promising results in bone regeneration using a novel technology 3D nHA-PU-DBP bone scaffold, and therefore the first hypothesis (H1) of the study was accepted. The bone regeneration was however not associated with the macroscopic appearance of the neovascularization process. The second hypothesis (H2) that the bone scaffold will stimulate the neovascularization was therefore rejected. Similarly, the third (H3) and fourth hypothesis (H4) that there will be a significant difference in the bone regeneration and neovascularization between the treatment groups containing scaffolds were rejected. Another outcome of this study revealed that the concentration of the bone morphogenetic protein – 2 increased in the linear fashion among all treatment groups. Furthermore, the highest increase of this growth factor was noticed in the scaffold rhBMP-2 treatment group which was associated with the gradual release of rhBMP-2 from the scaffold.

The bone scaffold significantly enhanced tissue regeneration in the scaffold containing treatment groups. This was constant among the outcomes of all assessment tools used in this study. The intervals of radiographs and DXA scans performed in the study were established accordingly to the previous reports using similar bone healing models, to most accurately detect the changes in the defect filling with the new bone (40,49-53). The bone healing was found to be significantly more dynamic within the scaffold cMSC treatment group. 2 goats assigned to this treatment group bridged the defect completely with a new bone. The defects healed in all goats in the same manner showing the most dynamic bone healing adjacent to the stainless-steel locking plate implant which has been already shown to be osteoconductive (35,54). Only the scaffold containing treatment groups showed significant bone formation in the center of the defect as well as between

the far cortices, surrounding the scaffold and justifying the osteoconductive properties of the utilized implant (35). The bone and osteoid formation occurred in the same manner among all the treatment groups growing within the implant equally from the proximal and distal segment of the bone towards the center. The radiography and DXA showed the most dynamic bone formation within the second and third month after surgery. Interestingly, the DXA revealed the most dynamic increase in BMD in the defect during the second month after surgery and the radiography showed the most dynamic defect reduction within the third month after surgery and thus one month after the BMD increase. In other words, the healing process started with the osteoid formation within the pores and interconnected channels of the implant and this was followed by the bone on growth on its surface what relates to the osteoinductive properties of the implant (35). The defect reduction plateaued gradually within the fourth, fifth and sixth months after surgery.

The neovascularization is one of the most important processes in bone regeneration, as it provides oxygen and nutrients to the regenerating bone tissue (12-16). The angiogenesis in the regenerating bone occurs due to the enhanced mobilization of the bone marrow-derived endothelial progenitor cells (EPCs) and the new vasculature determines the architecture and quality of newly formed bone (15,16,55). The study did not find statistically significant differences in the number of newly formed vessel branches and branches contacting the scaffold between all the treatment groups. A trend was noticed however that the numbers were higher 2 months after the surgery as compared with the scans taken 6 months after the surgery. This can be explained by the fact that the neovascularization process has been found to be most dynamic during the early phases of bone regeneration (14). The lack of the statistically and clinically significant differences may be associated with the fact that the used CT machine was not sensitive enough to detect the microvasculature (50 µm – 500 µm) around the scaffold as well as within the scaffold. Because of the size of a goat limb, the utilization of a micro-CT to detect the microvessels was not possible. This study addressed this issue estimating the contrast enhancement ratio which was directly associated with the contrast concentration within the defect vasculature. In brief, the analysis of the contrast enhancement ratio, however, did not show a difference between the treatment groups. Summarizing, even though neither the scaffold nor the cMSC nor the BMP-2 significantly influenced the macro vasculature and the contrast concentration within the defect, they still could have had an influence on the microvasculature formation and architecture. Because of the above-mentioned limitations, the study findings regarding the neovascularization should be interpreted with caution.

The bone marrow-derived allogeneic caprine mesenchymal stem cells (cMSCs) had a significant positive impact on bone healing. The defects in 2 goats (6.5 cm and 7.2 cm) which were assigned to the scaffold cMSC treatment group bridged the defect entirely over 6 months after surgery. The mesenchymal stem cells have

been already proven to have bone regenerative capacity (31,32,46,52), however, because of the relatively small number of the goats with such outstanding results, the bone regeneration in those 2 cases was rather due to the cMSCs interaction with the host progenitor cells and not due to the pure benefit of the allogeneic cMSCs. The bone regeneration occurred in the scaffold rhBMP-2 treatment group was on the other hand not significantly different than that which occurred in the scaffold only treatment group, even though the rhBMP-2 has been also already proven to have a stimulative effect on osteogenic differentiation of both mesenchymal stem cells and osteoblasts (33,56,57). This may be related to the dose of E-BMP-2 used in this study which was 3 mg per scaffold (approximately in the concentration of 0.5 mg/cm3) or to the other factors influencing bone regeneration in such large segmental defects (51,58-60). Furthermore, the stimulative effect of BMP2 on angiogenesis has been already described in the literature as well (61-63).BMP2 is known to stimulate migration and tube formation of human endothelial cells (61-63).

The peripheral blood vascular endothelial growth factor (VEGF) concentration analysis revealed no differences between treatment groups and no significant linear changes within 30 days after surgery. There was however an increase in VEGF concentration from the baseline concentration within the immediate postoperative period. The positive association between the VEGF concentration in the local tissues and bone regeneration has been already established in the literature (48,63-66). Increased secretion of VEGF has been found in osteoblasts during bone repair as well as in peripheral blood lymphocytes and platelets in patients with colorectal cancer (48,67). This study, however, did not find significant differences between the treatment groups in the peripheral blood VEGF concentration. This may be associated with the fact that the concentration oscillations correlated with a different pace of bone healing were very low in peripheral blood and hard to detect or that the size of defect influenced the concentration more than the pace of tissue regeneration. The analysis of peripheral blood BMP-2 concentration, on the other hand, revealed a significant linear increase in this growth factor in the peripheral blood within the 30 days of defect healing in all treatment groups. The increase was significantly higher in the scaffold BMP-2 treatment group as compared with the remaining groups, which was associated with the gradual release of BMP-2 from the implant.

The bone scaffolds were made from biocompatible polyurethane (D3 PU) platform which was coated with nano-hydroxyapatite (nHA) (25,26). The scaffold architecture consisted of multiple PU-nHA platforms that were laid on each other and the decellularized bone particles (DBPs) which were placed in between the platforms. The PU used in this study is biologically stable for up to 30 days after implantation (25,26). The PU/nHA ratio is vital for optimal bone regeneration and it has been previously optimized, and it equaled 80 PU to 20 nHA (25,26). The porosity, as well as the pore size of manufactured implants, were within the optimal

range for bone regeneration. The polyurethanes have been previously employed in multiple biomedical devices (11,17-24) and recently they have gained an interest in the research due to the significant number of mechanical and biological advantages which allow them to be incorporated in the bone scaffolds. Furthermore, depending on the synthesis method, the porosity of synthetized PU can be controlled in a feasible way (11). They are an excellent candidate to serve as a platform for the bioactive nanomaterials including nano-Hydroxyapatite in the bone scaffolds (22-23). Nanostructured hydroxyapatite promotes fibroblastic cell (a model cell line) and osteoblastic cell (bone-forming cell) adhesion and proliferation, osseointegration, and the deposition of calcium-containing minerals on the surface of these materials (68-70). The rough surfaces of nHA are found to cause asymmetrical division of stem cells into osteoblasts which are also important for osteoinduction (70). The nanomaterials can alter the surface energy of materials to control initial protein adsorption and confirmation to inhibit inflammatory cell functions and promote tissue forming cell functions (71). The scaffolds coated with nano-HA have been known to improve the mechanical properties, including increased compressive strength (maximum 0.45 versus to 0.16 MPa for no coating) and elastic modulus (maximum 1.43 versus 0.79 for no coating) (11,72,73). The final advantage of nano Ha is a porous structure with a high-binding affinity makes it an excellent drug delivery device and the low solubility of nano-HA under physiologic condition contributes to its longer degradation rate and allows the drug delivery in a more controlled manner (70,74-78). Therefore, the nHAP particles have been shown to be excellent carriers of antibiotics (75), anticancer drugs (76), growth factor (77) and enzymes (77,78) for its notorious adsorption ability.

We encountered several complications while conducting this study, including orthopedic locking plate bending, excessive periosteal reaction, plate pullout from the proximal bone segment, fractures of the proximal and distal bone segments as well as surgery side infections. The scaffold migration after implantation was observed within 24 hours post-implantation and in all cases, the implant migrated caudally at its insertion into the distal segment of the tibia. The study utilized a not commonly used in the research large segmental (up to 7 cm) and full-thickness tibial defect and some amount of above-mentioned complications were to be expected. The most common complications included the orthopedic plate bending and excessive periosteal and endosteal reaction. Neither of them was associated with the weight of the goat or with the size of the defect (Table 4-7). In the authors' subjective opinion, the goats which encountered plate bending showed a higher level of activity in the postoperative period. This was however not assessed in an objective manner. The excessive periosteal and endosteal reactions occurred in both cortices around the screw implants and could have resulted from an instability in the plate-screw constructs. The further complications including fractures and infections occurred in the goats with a higher size of the defect (above 7 cm) and it can be therefore concluded that they were related to the size of the defect and the size of the remaining bone segments. The rate of infections was higher in those

goats because of a higher amount of created dead space after the segment removal. All the complications occurred within the first and second months after the surgery. The overall survival rate in this study was calculated at 91% (61/67 goats).

Conclusions

Bone scaffolds not only provided the surface for the bone on growth (osteoconduction) but also stimulated the bone ingrowth within the implant (osteoinduction) as well as around the implant (osseointegration) as compared with the negative controls. Furthermore, the tested bone scaffolds were excellent delivery devices for the bioactive agents such as the human recombinant bone morphogenetic protein-2 and caprine mesenchymal stem cells which significantly stimulated and enhanced bone regeneration. Neither the scaffolds, scaffolds with rhBMP-2, nor scaffolds with cMSC improved the macro angiogenesis in the regenerating bone. However, their influence on the microvasculature formation remains unknown. Furthermore, the bone scaffolds used in this study did not cause excessive inflammatory processes within the healing defects as compared to the control defects. The animal model with such a magnitude of the tibial segmental defect (> 6 cm) has been successful as the bone regeneration model with a high survival rate and relatively low complication rate.

Tables

Table 4-1. Radiographical ostectomy gap scoring.

Ostectomy Gap Filling

Score	**Ostectomy gap filling**
0	No interval change compared to immediate post-operative radiographs
1	New bone filling <25% of ostectomy gap
2	New bone filling 26-50% of ostectomy gap
3	New bone filling 51-99% of ostectomy gap
4	Ostectomy gap completely filled and/or bridging callus present on at least 3 cortices

Table 4-2. Radiographical opacity of new bone scoring.

Opacity of new bone

Score	**Opacity of new bone**
0	No interval change compared to immediate post-operative radiographs
1	New bone less opaque than normal cortex
2	New bone of similar or greater opacity compared to normal cortex

Table 4-3. Radiographic defect size evaluation.

Defect Reduction

Time point	**After 2 Months Post OP**				**After 6 Months Post OP**			
Tx Group	Line 1 (mm)	Line 2 (mm)	Line 3 (mm)	**Average (mm)**	Line 1 (mm)	Line 2 (mm)	Line 3 (mm)	**Average (mm)**
Control	2.8	4.9	2.1	**3.3**	19.5	8.1	2.0	**9.9**
	±5.1	±8.1	±2.8	**±5.5**	±18.6	±7.5	±4.1	**±13.4**
Scaffold	5.8	5.5	3.3	**4.9**	20.0	13.2	9.4	**14.2**
	±6.8	±2.1	±3.1	**±4.3**	±11.9	±3.8	±5.5	**±8.7**
Scaffold + rhBMP-2	2.7	2.6	-2.1	**1.1**	27.0	14.5	6.6	**16.1**
	±4.8	±2.9	±2.4	**±3.9**	±9.1	±2.5	±2.9	**±10.2**
Scaffold + cMSC	4.1	3.7	4.4	**4.1**	43.5	41.9	36.8	**40.8**
	±3.1	±1.9	±5.2	**±3.4**	±36.2	±40.6	±37.0	**±34.5**
Total	3.8	4.2	1.9	**3.3**	27.5	19.4	13.7	**20.2**

Table 4-4. BMD results comparison.

BMD (g/cm2) Comparison Table

Tx Group	**2 Months**			**6 Months**						
	D0	M1	**M2**	D0	M1	M2	M3	M4	M5	**M6**
Control	0.00	0.01	**0.07**	0.00	0.00	0.01	0.05	0.07	0.05	**0.07**
	±0.0	±0.0	**±0.1**	±0.0	±0.0	±0.0	±0.1	±0.1	±0.1	**±0.1**
Scaffold	0.29	0.42	**0.51**	0.38	0.47	0.56	0.58	0.53	0.48	**0.46**
	±0.0	±0.1	**±0.1**	±0.1	±0.0	±0.0	±0.0	±0.1	±0.1	**±0.1**
Scaffold + BMP2	0.27	0.41	**0.51**	0.31	0.45	0.52	0.53	0.49	0.45	**0.40**
	±0.0	±0.1	**±0.1**	±0.0	±0.0	±0.0	±0.1	±0.1	±0.1	**±0.1**
Scaffold + cMSC	0.27	0.42	**0.56**	0.27	0.43	0.64	0.68	0.75	0.80	**0.80**
	±0.0	±0.1	**±0.2**	±0.0	±0.1	±0.2	±0.3	±0.3	±0.4	**±0.5**

Table 4-5. CT Evaluation

	2 Months Post OP				***6 Months Post OP***		
	Treatment Group	**Mean**	**Std Dev**	**Sig**	**Mean**	**Std Dev**	**Sig**
Density of defect/graft (HU)	Control	40.71	±4.07	0.00	28.86	±21.63	
	Scaffold	857.00	±75.35		777.67	±128.47	0.00
	Scaffold + rhBMB2	803.88	±83.36		625.86	±121.84	
	Scaffold + cMSC	833.83	±73.96		812.50	±310.96	
Density of new bone (HU)	Control	930.00	±274.66	0.57	1050.80	±347.40	
	Scaffold	665.33	±229.80		1200.60	±201.09	0.53
	Scaffold + rhBMB2	809.00	±243.30		1170.17	±190.56	
	Scaffold + cMSC	790.50	±64.35		1288.20	±254.70	

Table 4-5. CT Evaluation (Continuation)

		2 Months Post OP			*6 Months Post OP*		
	Treatment Group	**Mean**	**Std Dev**	**Sig**	**Mean**	**Std Dev**	**Sig**
Number of vessel branches	Control	28.14	±11.35		14.86	±2.91	
	Scaffold	40.71	±12.51		23.56	±12.00	
	Scaffold + rhBMB2	32.50	±21.17	0.44	21.29	±7.78	0.47
	Scaffold + cMSC	30.00	±11.37		23.00	±17.44	
Number of vessels contacting the graft	Control	0.00	±0.00		0.00	±0.00	
	Scaffold	9.43	±4.16		4.56	±2.46	
	Scaffold + rhBMB2	8.13	±4.45	0.00	5.43	±2.70	0.01
	Scaffold + cMSC	8.17	±3.97		4.63	±4.34	
Defect density pre contrast (HU)	Control	222.43	±36.64		136.71	±50.39	
	Scaffold	253.00	±48.85		200.33	±62.38	
	Scaffold + rhBMB2	236.25	±43.62	0.33	215.86	±56.76	0.03
	Scaffold + cMSC	262.67	±35.88		215.25	±42.91	
Defect density post contrast (HU)	Control	255.43	±42.30		158.71	±48.84	
	Scaffold	310.57	±62.87		228.44	±47.29	
	Scaffold + rhBMB2	269.13	±51.06	0.20	248.14	±52.27	0.01
	Scaffold + cMSC	287.67	±33.97		247.75	±54.82	
Contrast Enhancement Ratio	Control	1.15	±0.10		1.19	±0.12	
	Scaffold	1.23	±0.08		1.18	±0.16	
	Scaffold + rhBMB2	1.14	±0.07	0.03	1.17	±0.09	0.91
	Scaffold + cMSC	1.10	±0.03		1.15	±0.08	

Table 4-6. Bone and osteoid formation.

	Control	Scaffold	Scaffold rhBMP-2	Scaffold cMSC
	(%) 2 - Month Treatment Groups			
Prox	50.7	46.9	47.9	50.2
	±18.9	±11.7	±15.4	±9.2
Middle	0.0	43.0	38.5	45.3
	±0.0	±10.7	±17.9	±3.8
Dist	63.2	51.0	58.2	52.4
	±10.7	±12.7	±12.0	±5.5
	(%) 6 - Month Treatment Groups			
Prox	57.1	43.8	44.8	50.3
	±15.6	±13.8	±7.9	±13.5
Middle	0.0	43.7	44.8	50.2
	±0.0	±9.7	±16.6	±12.5
Dist	58.4	40.1	50.1	48.5
	±12.1	±10.1	±18.4	±9.9

Table 4-7. Complications.

	Number of complications					
Complication	**0**	**1**	**2**	**3**	**4**	**5**
No of goats	61.0	17.0	11.0	4.0	3.0	4.0
% of goats	100.0	28.0	18.0	6.6	4.5	6.6
Average Defect Size	6.6 ±1.4	6.7 ±1.4	6.2 ±1.5	5.3 ±1.6	7.4 ±0.4	7.1 ±1.7
Average Weight	55.6 ±7.9	55.4 ±8.9	54.1 ±9.2	57.0 ±5.3	40.7 ±4.7	50.3 ±5.7

Complication description: 0 – study population, 1 – orthopedic plate bending, 2 – excessive periosteal reaction, 3 – scaffold migration, 4 – deep infection, 5 – split fracture of the bone fragment.

Figures

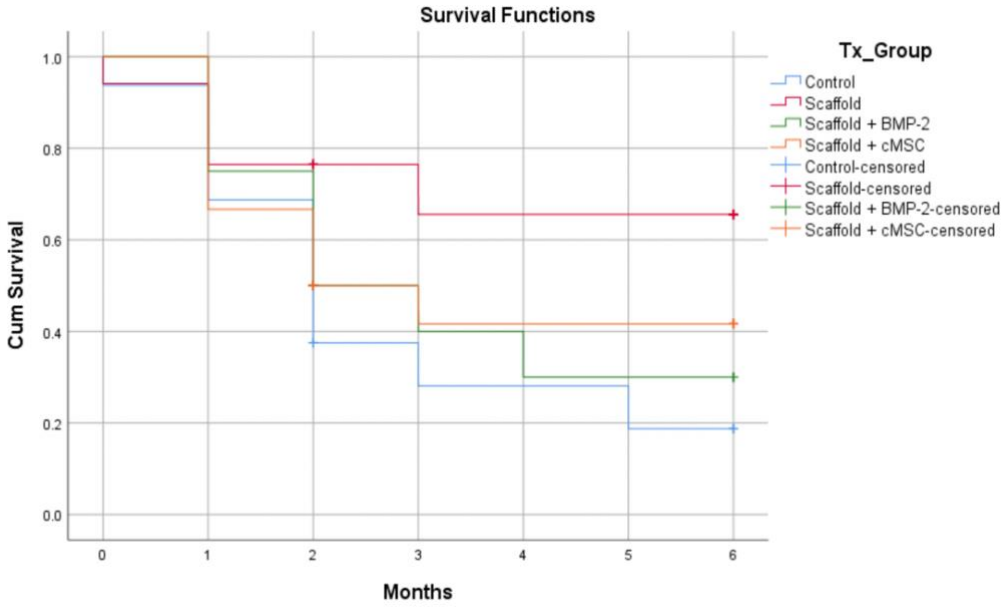


Figure 4-1. Survival Kaplan-Meier curve.

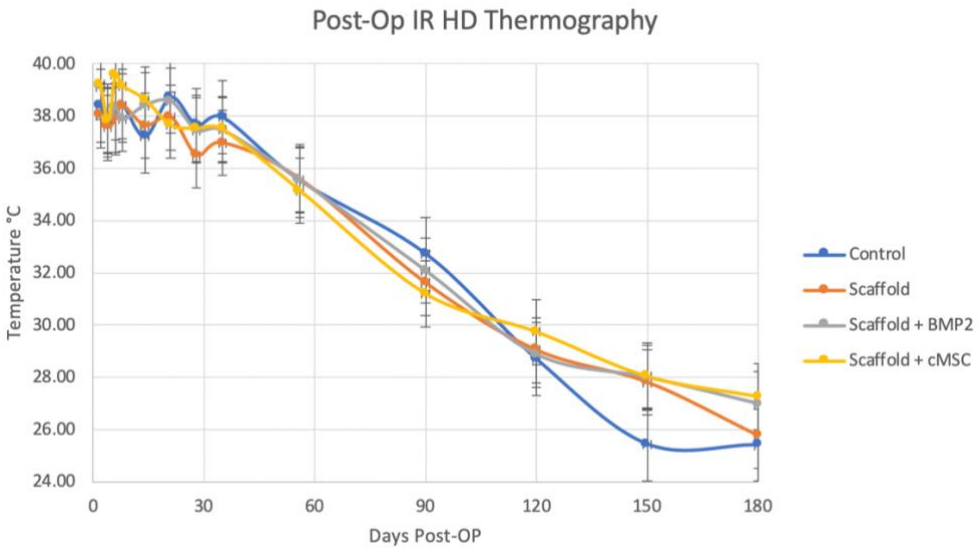


Figure 4-2. Thermography curve.

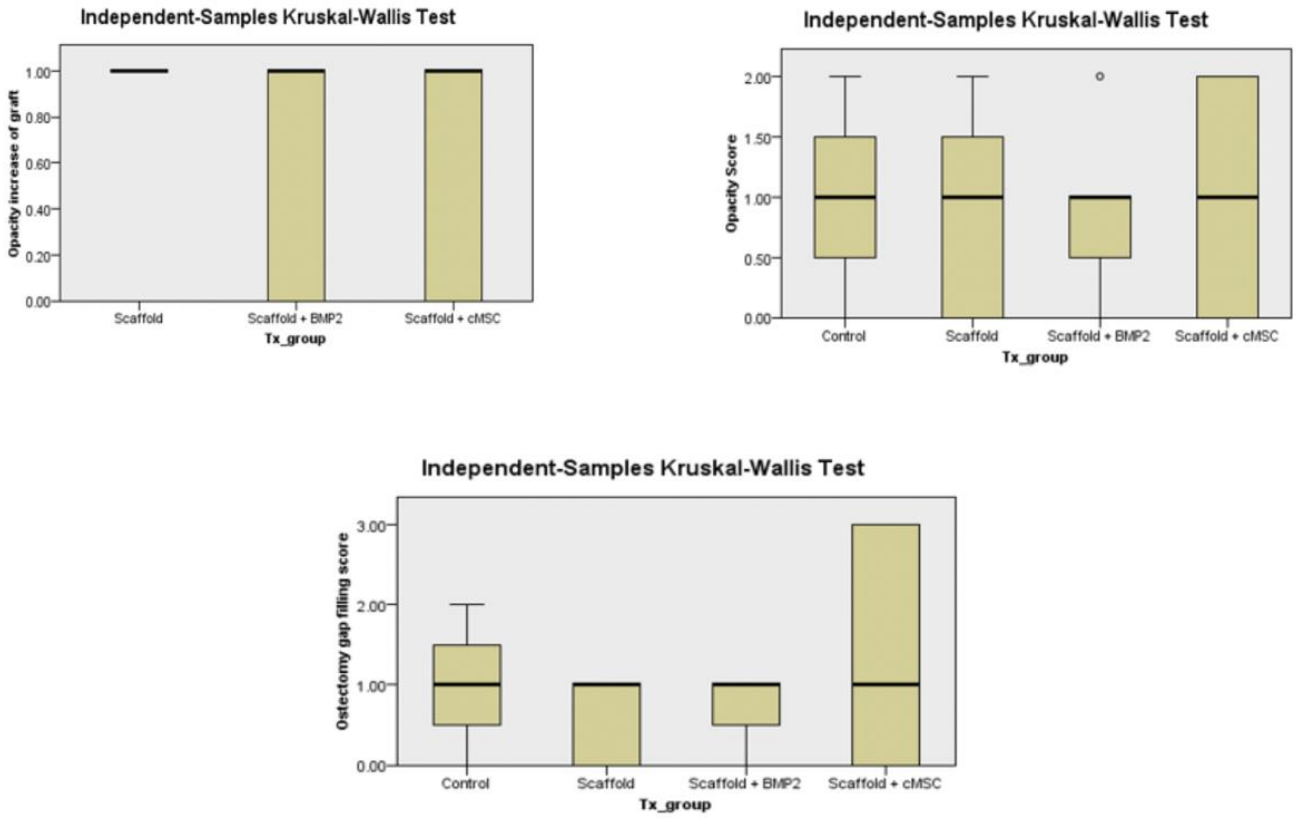


Figure 4-3. Radiographical assessment.

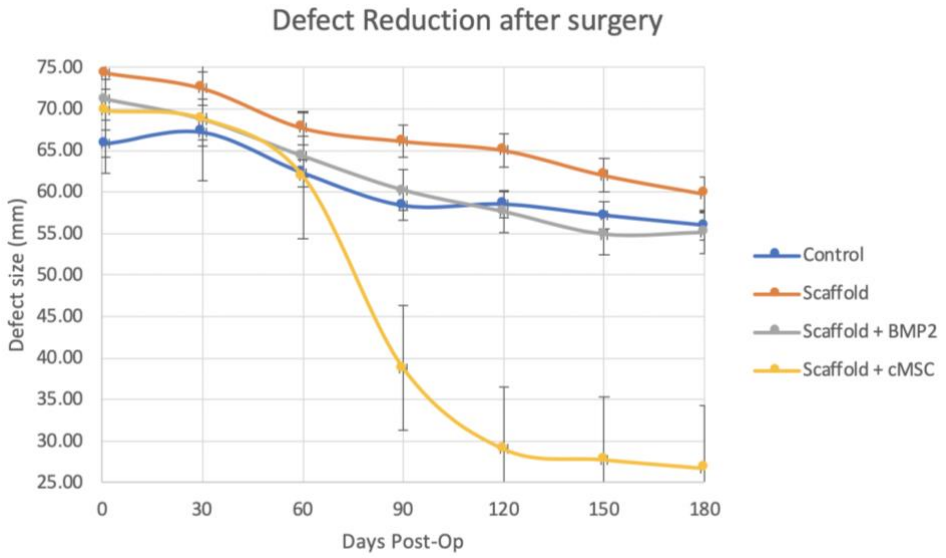


Figure 4-4. Defect reduction after surgery.

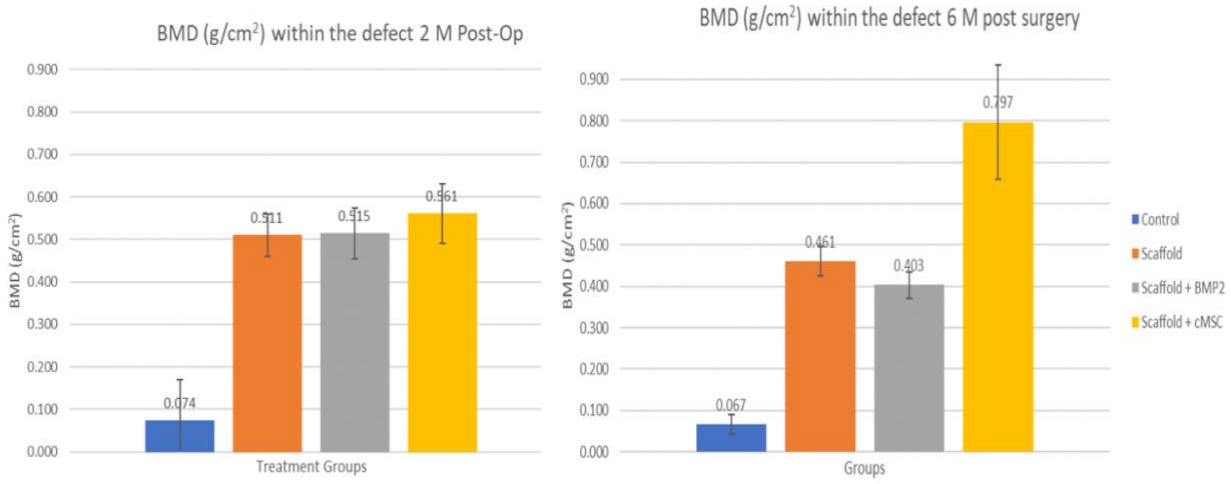


Figure 4-5. BMD comparison at termination points.

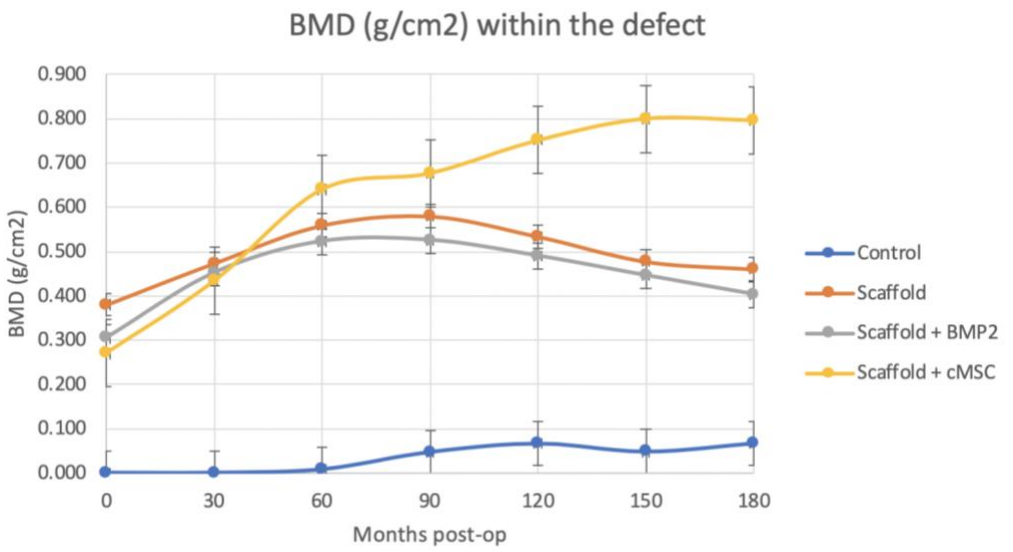


Figure 4-6. BMD curve.

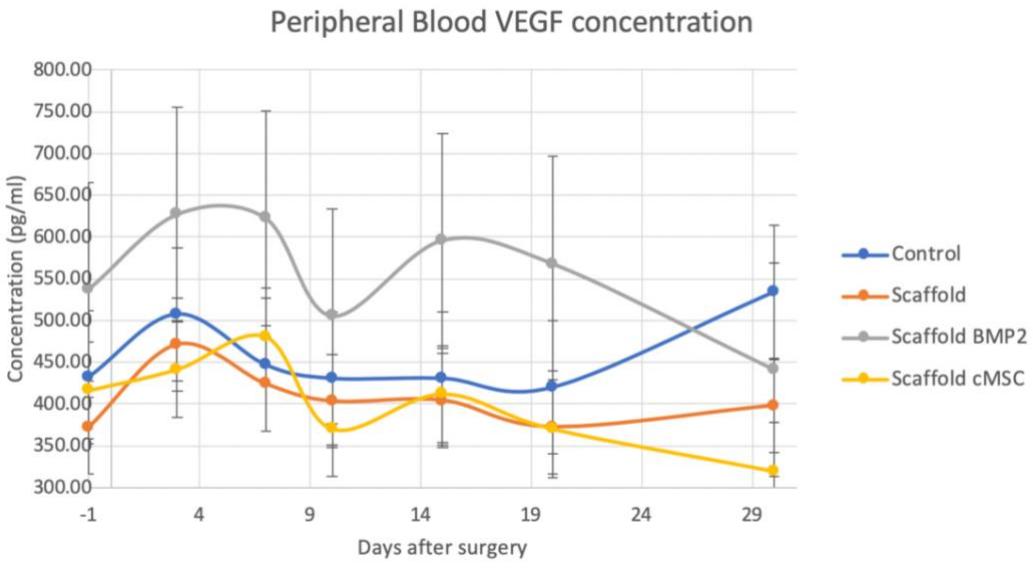


Figure 4-7. Peripheral VEGF curve.

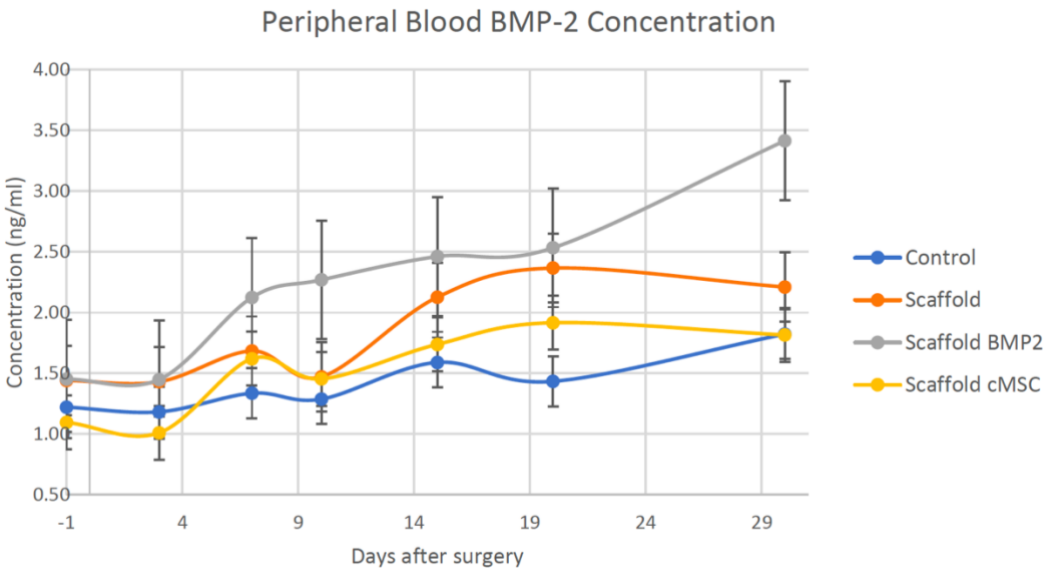


Figure 4-8. Peripheral BMP2 curve.

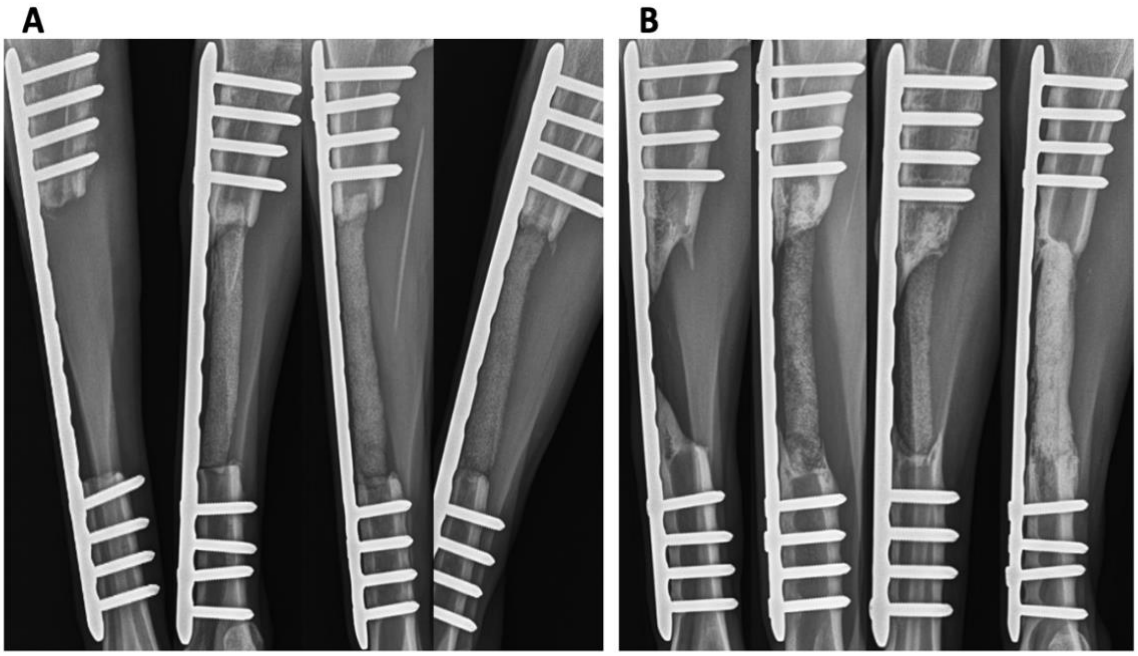


Figure 4-9. Defect Comparison.

The comparison of defects assigned to different treatment groups, 2 months after surgery (A) and 6 months after surgery (B). The treatment groups in both time points from the left side, control, scaffold, scaffold rhBMP2, and scaffold cMSC.

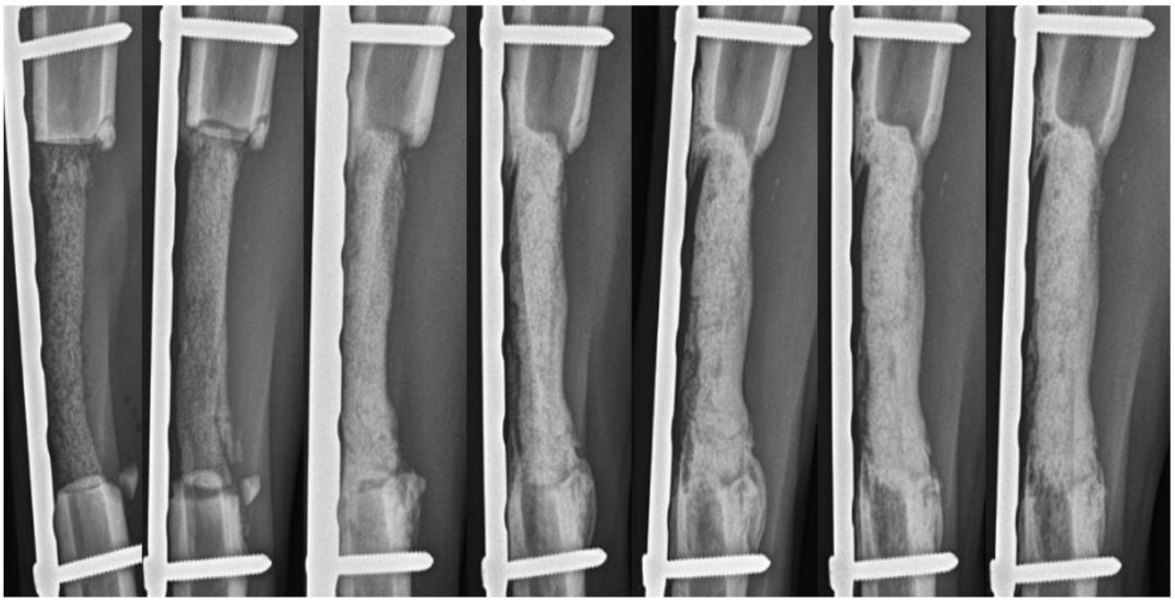


Figure 4-10. Representative defect cMSC healing.

The sequential monthly radiographic evaluation of the representative defect of ana goat assigned to the 6 months scaffold cMSC group. The images are organized from left side in following order - day 1 after the surgery, 1 month, 2 months, 3 months, 4 months, 5 months and 6 months after the surgery.

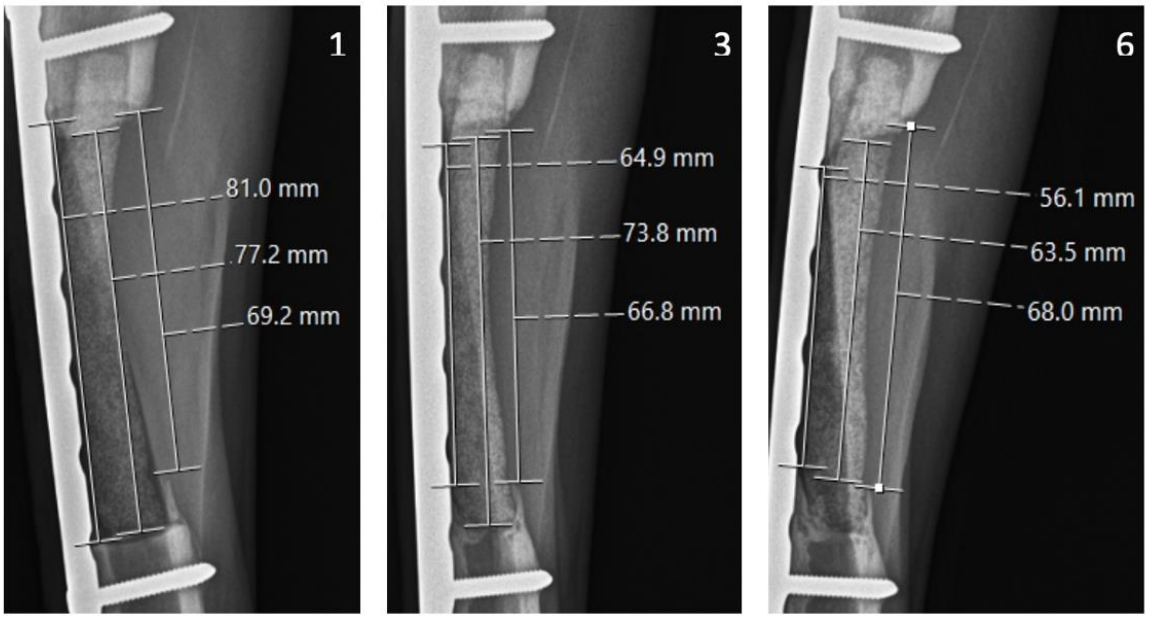


Figure 4-11. Defect measurements.

Defect measurements in goat assigned to the 6 months scaffold only treatment group. The first image on left side shows defect 1 month after surgery, image in the middle shows the defect 3 months after surgery and the last image from left side shows the defect 6 months after the surgery. The defects were measured in 3 different lines and all three different lines were analyzed separately.



Figure 4-12. 3D CT reconstruction.

Representative image of Computed Tomography – Angiography. Osteotomy limbs were directed towards outside of this image. Note, increased density of vasculature after the surgery as well as new vessel branches entering the scaffold from proximal side. This goat was assigned to the 6-month study time point, scaffold cMSC treatment group.

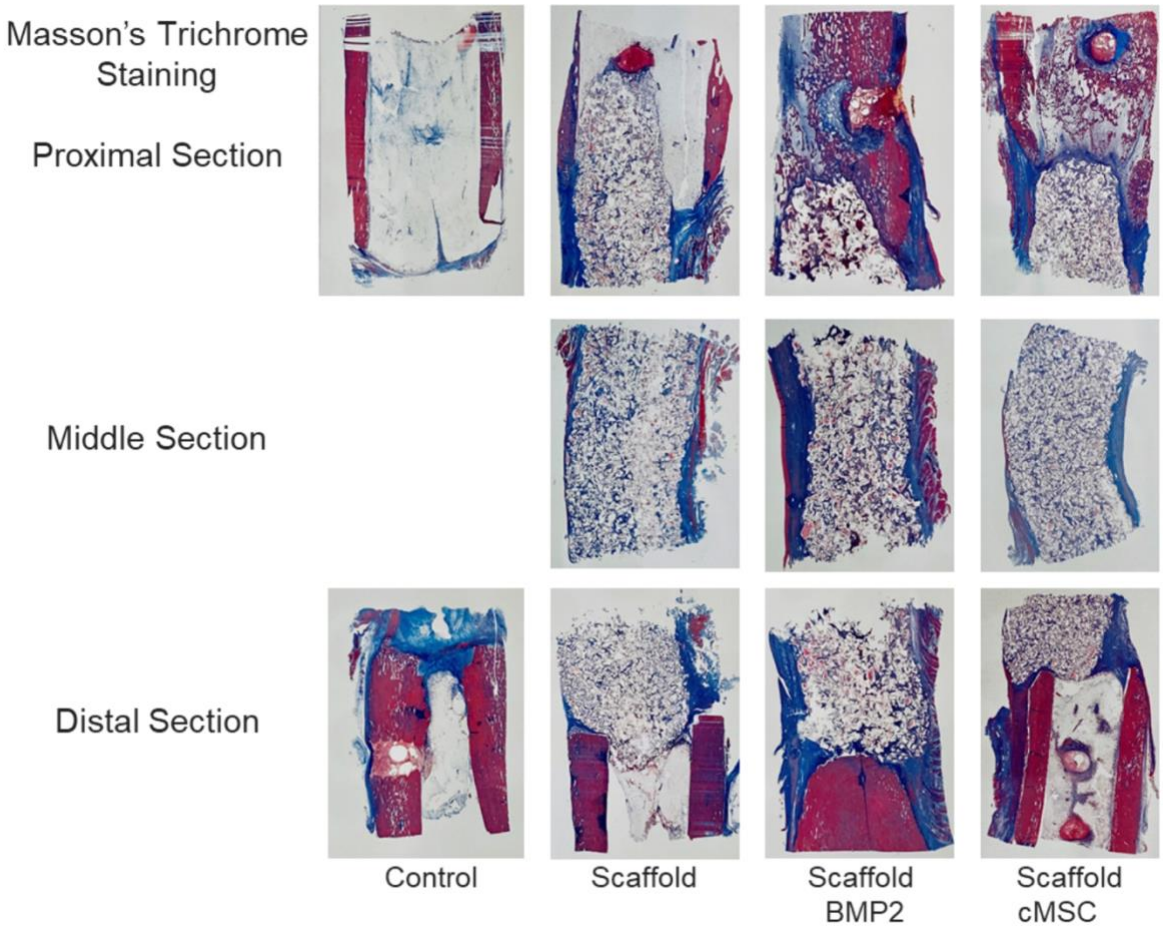


Figure 4-13. 2-month goats histology.

Tissues harvested from goats assigned to the 2-month time point. Presented specimens have been stained according to the Masson's trichrome protocol. The red color is associated with mineralized tissue whereas blue color is associated with non-mineralized tissue. Mineralized tissue has been defined as bone and non-mineralized tissue as osteoid. Tissues have been divided into proximal, middle and distal sections. The figure contains representative images of, beginning from left, control, scaffold, scaffold with rhBMP2 and scaffolds with cMSC respectively. Difference in bone content was not found to be statistically significant between treatment groups, as well as difference in osteoid within scaffold was not found to be significant between treatment groups.

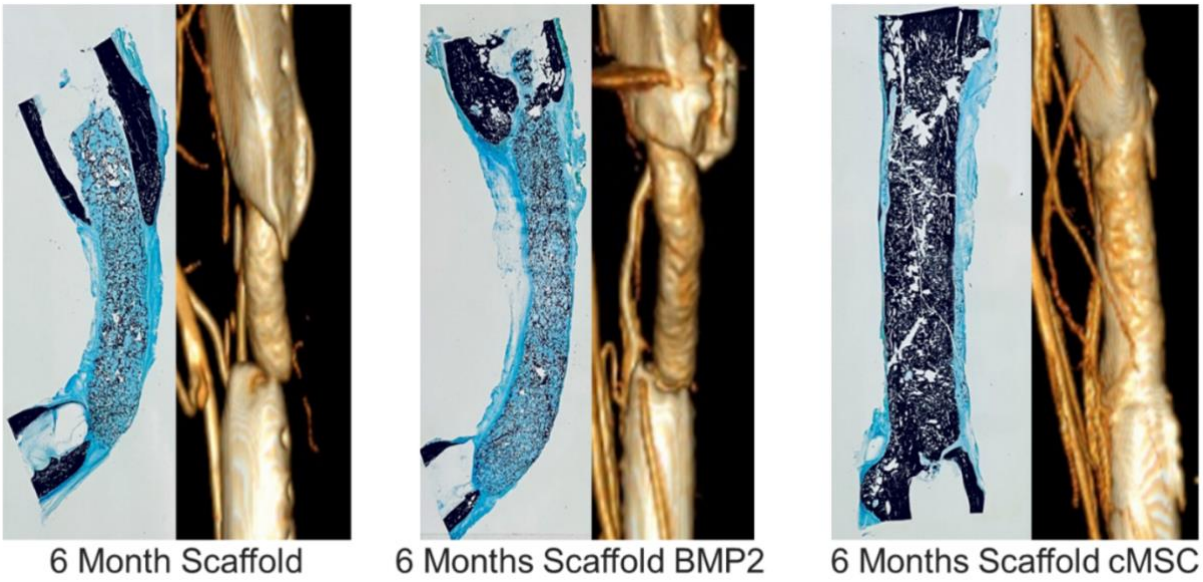


Figure 4-14. 6-month goats histology.

Tissues harvested from goats assigned to the 6-month time point. Specimens were harvested in their entirety and processed undecalcified. Presented specimens were stained accordingly to von Kossa protocol. The mineralized tissue with high calcium concentration stained black, whereas the non-mineralized tissue stained blue. The figure shows representative specimens of three treatment groups, beginning from left, scaffold, scaffold with rhBMP2, and scaffold with cMSC respectively. Histology images are directly compared with their respective CT images.

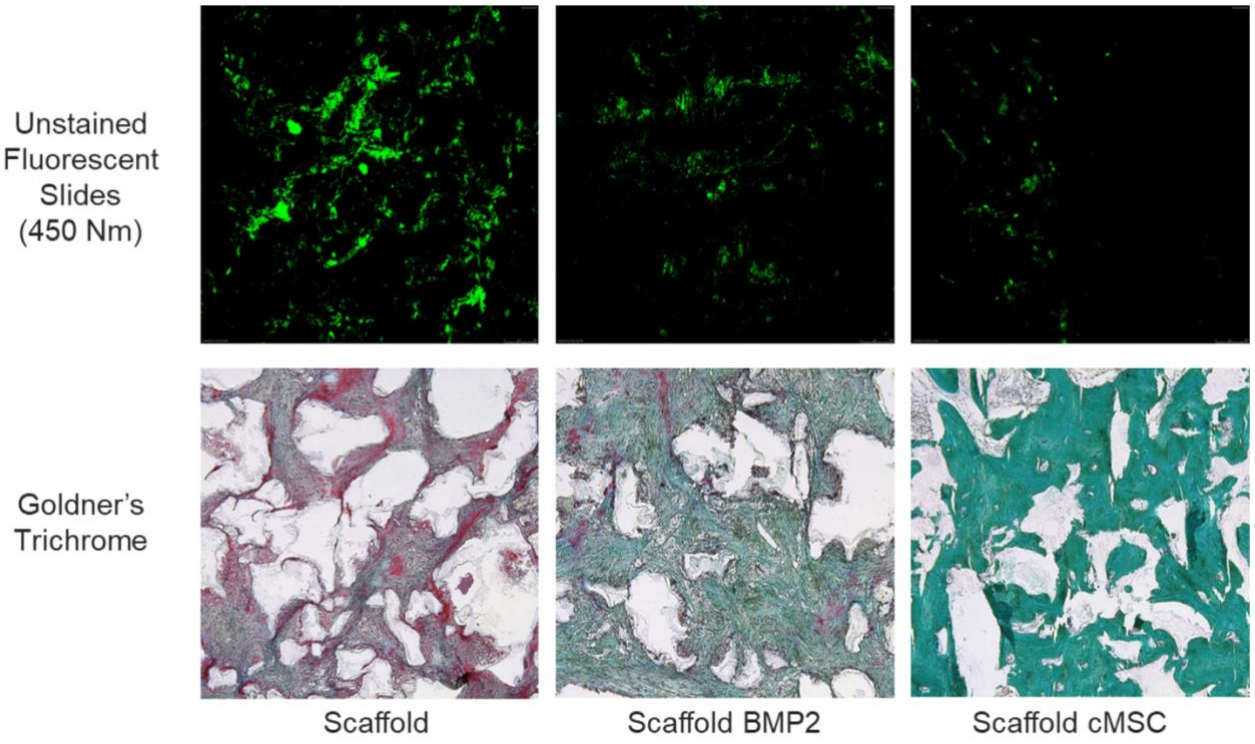


Figure 4-15. Fluorescence of 6-month specimens.

Tissues harvested from goats assigned to the 6-month time point. The images in the top row were left unstained to evaluate fluorescence associated with metabolically active bone and images in bottom row were stained accordingly to Goldner's trichrome protocol. It was noticed that the specimens with tissue containing a higher amount of non-mineralized tissue (red stain in Goldner's) presented higher fluorescence as compared with the specimens containing a higher amount of mineralized tissue (green stain in Goldner's). The figure presents unstained slides of tissues harvested from three different treatment groups, beginning from left, scaffold, scaffold with rhBMP2, and scaffold with cMSC with their respective Goldner's images.

Abbreviations

ANOVA – Analysis of Variance
BMD – Bone Mineral Density
BMP2 – Bone Morphogenetic Protein-2
rhBMP2 – human recombinant Bone Morphogenetic Protein-2
cMSC – caprine Mesenchymal Stem Cells
CT – Computed Tomography
DBP – Decellularized Bone Particles
DMEM - Dulbecco's Modified Eagle Medium
DICOM – Digital Imaging and Communications
DXA – Dual X-ray Absorptiometry
HBSS – Hanks Balanced Salt Solution
HU – Hounsfield Units
nHA – nanophase Hydroxyapatite
PACS – Picture Archival and Communication System
PU – Polyurethane
ROI – Region of Interest
TRAP – Tartrate-resistant acid phosphatase
VEGF – Vascular Endothelial Growth Factor
VVG – Verhoeff-Van Gieson

Footnotes

a. Recombinant human bone morphogenetic protein – 2, SBH Sciences Inc, Natick, MA
b. T175 tissue culture flask, Fisher Scientific, Hampton, NH
c. Hank's Balanced Salt Solution, 500 ml, HyClone Laboratories, Logan, UT
d. Dulbecco's Modified Eagle Medium with glutamine, HEPES buffer, pyruvate, HyClone Laboratories, Logan, UT
e. Fetal bovine serum, Life Technologies, Eugene, OR
f. Penicillin, HyClone Laboratories, Logan, UT
g. Streptomycin, HyClone Laboratories, Logan, UT
h. Trypsin, Trypsin 0.25% 1x, HyClone Laboratories, Logan, UT
i. Dimethyl sulfoxide, Hybri-Max, Milipore-Sigma, St. Louis, MO
j. Liquid Nitrogen, HyClone Laboratories, Logan, UT
k. Ceftiofur sodium, 1g powder, Naxcel, Zoetis, Parsippany-Troy Hills, NJ
l. Flunixin meglumine, 50mg/ml, Prevail, VetOne®, Boise, ID
m. Xylazine hydrochloride, Xylamed, 20 mg/ml, VetOne®, Boise, ID
n. Ketamine hydrochloride, Zetamine, 100 mg/ml, VetOne®, Boise, ID
o. Midazolam, 5 mg/ml, Akorn, Ann Arbor, MI
p. Isoflurane, 250 ml, VetOne®, Boise, ID
q. Oscillating bone saw,
r. 8-hole 4.5 mm locking plate, Veterinary Orthopedic Implants, St. Augustine, FL
s. 4.0 locking head screws, Veterinary Orthopedic Implants, St. Augustine, FL
t. Gentamicin sulfate,100mg/ml, VetOne®, Boise, ID
u. PDS II - Polydioxanone #2-0 (3.0 metric) suture with CT-1 36 mm 1/2c taper needle, Ethicon, Guaynabo, Puerto Rico
v. Surgipro™ – Polypropylene monofilament #0 (3.5 metric) suture with C-17 39 mm 3/8 cutting needle, Covidien, Mansfield, MA
w. Fluke VT04A Visual IR Thermometer, Fluke Corporation, Everett, WA
x. Portable radiography machine, Philips Easy Diagnost RF System, Philips International B.V., Amsterdam, Netherlands
y. Digital radiography plates (CXDI-50G), Canon USA, Inc., Melville, NY
z. NEXT Equine DR™ EDR6, Sound - Eklin®, Sound Technologies, Carlsbad, CA
aa. PACS system, Spectra PACS IDS7, Spectra AB, Linkoeping, Sweden
bb. Dual X-ray Absorptiometry system, QDR 4500 Hologic Inc.
cc. CT scanner, Philips Brilliance-40, Philips International B.V., Amsterdam, Netherlands
dd. Optiray™ 350, Mallinckrodt Inc, Hazelwood, MO
ee. Oxytetracycline, 200 mg/ml, Liquamycin®, Zoetis, Parsippany-Troy Hills, NJ
ff. Decalcifying solution protocol A, Fisher Scientific, Hampton, NH
gg. Decalcifying solution protocol B, Fisher Scientific, Hampton, NH

hh. PMMA, Sigma-Aldrich, Histological Grade, St. Louis, MO
ii. Automated tissue processor, ASP300S, Leica, Germany
jj. Fiji, ImageJ, National Institute of Mental Health, Bethesda, Maryland
kk. BMP2 ELISA kit, ABclonal, Woburn, MA
ll. VEGF ELISA kit, ABclonal, Woburn, MA
mm. IBM® SPSS Statistics™ v.25 Software, IBM, New York, NY

Bibliography

References

1. Rossi F., Santoro M., Perale G. Polymeric scaffolds as stem cell carriers in bone repair. J Tissue Eng Regen Med 2015; 9:1093–1119
2. Costa-Pinto A.R., Reis R.L., Neves N.M. Scaffolds based bone tissue engineering: the role of Chitosan. Tissue Eng B Rev 2011; 17: 331–347
3. Jones E., Yang X.B. Mesenchymal stem cells and bone regeneration: current status. Injury 2011; 42:562–568.
4. Fassina L., Saino E., Sbarra M.S., et al. In vitro electromagnetically stimulated SAOS-2 osteoblasts inside porous hydroxyapatite. J Biomed Mater Res A 2010; 93A:1272–1279.
5. Kretlow J.D., Mikos A.G. Review: Mineralization of synthetic polymer scaffolds for bone tissue engineering. Tissue Eng 2007; 13: 927–938
6. Kruyt M., Dhert W., Yuan H., Wilson C., Blitterswijk C., Verbout A., Bruijn J. Bone Tissue Engineering in a Critical Size Defect Compared to Ectopic Implantations in the Goat. J. Orthop. Res. 2004, 22 (3), 544−551.
7. Mathieu L.M., Montjovent M.O., Bourban P.E., Pioletti D.P., Manson J.A. Bioresorbable composites prepared by supercritical fluid foaming. Published online 21 July 2005. Available at: http://www.interscience.wiley.com/. J Biomed Mater Res A. 2005; 75(3): 88-97.
8. Rezwan K., Chen Q.Z., Blaker J.J., et al. Biodegradable and bioactive porous polymer/ inorganic composite scaffolds for bone tissue engineering. Biomaterials 2006; 27: 3413–3431
9. Fuentes E., Sáenz de Viteri V., Igartua A., Martinetti R., Dolcini L., Barandika G. Structural characterization and mechanical performance of calcium phosphate scaffolds and natural bones: a comparative study. J Appl Biomater Biomech 2010; 8(3):159-165
10. Karageorgiou V., Kaplan D. Porosity of 3D biomaterial scaffolds and osteogenesis. Biomaterials 2005; 26:5474-5491
11. Janik H., Marzec M. A review: Fabrication of porous polyurethane scaffolds. Materials Science and Engineering C 2015; 48:586–591
12. Xie C., Lin A.S.P., Schwarz E.M., Goldberg R.E., O'Keefe R.J., Zhang X. Assessment of neovascularization in fracture healing of COX-2-/- mice using micro-computed tomography. Journal of Bone and Mineral Research 2005; 20(9):S324-S324
13. Ma X.L., Sun X.L., Wan C.Y., Ma J.X., Tian P. Significance of circulating endothelial progenitor cells in patients with fracture healing process. Journal of Orthopedic Research 2012; 30(11): 1860-1866
14. Matsumoto T., Kuroda R., Mifune Y., Kawamoto A., Shoji T., Miwa M., Asahara T., Kurosaka M. Circulating endothelial/skeletal progenitor cells for bone regeneration and healing. Bone 2008; 43:434-439
15. Gerstenfeld LC, Cullinane DM, Barnes GL, Graves DT, Einhorn TA. Fracture healing as a post-natal developmental process: molecular, spatial, and temporal aspects of its regulation. J Cell Biochem 2003; 88:873–84.

16. Karsenty G, Wagner EF. Reaching a genetic and molecular understanding of skeletal development. Dev Cell 2002; 2:389–406
17. Gogolewski S., Pennings A.J. An artificial skin based on biodegradable mixtures of polylactides and polyurethanes for full thickness skin wound covering, Makromol. Chem. Rapid Commun. 1983; 4: 675–680.
18. Gogolewski S., Galletti G., Usia G. Polyurethane vascular prostheses in pigs, Colloid Polym. Sci. 1987; 265:774–778.
19. Chiono V., Sartori S., Rechichi A., Tonda-Turo C., Vozzi G., Vozzi F., et al. Poly(ester urethane) guides for peripheral nerve regeneration, Macromol. Biosci. 2011; 11 (2): 245–256.
20. Tetteh G., Khan A.S, Delaine-Smith R.M., Reilly G.C, Rehman I.U. Electrospun polyurethane/hydroxyapatite bioactive Scaffolds for bone tissue engineering: The role of solvent and hydroxyapatite particles, J. Mech. Behav. Biomed. Mater. 2014; 39:95–110
21. Kon E., Filardo G., Zaffagnini S., Di Martino A., Di Matteo B., Muccioli G.M.M., Busacca M., Marcacci M. Biodegradable polyurethane meniscal scaffold for isolated partial lesions or as combined procedure for knees with multiple comorbidities: clinical results at 2 years, Knee Surg. Sports Traumatol. Arthrosc. 2014; 22(1): 128–134.
22. Gibas I., Janik H. Medical polyurethane with different hard segment content obtained from polycaprolactonediol, aliphatic diisocyanates and butanediol, Pol. J. Appl. Chem. 2009; 53 (1): 9–14.
23. Chena Q., Lianga S., Thouasb G.A. Elastomeric biomaterials for tissue engineering, Prog. Polym. Sci. 2013; 38:584–671.
24. Pedicini A., Farris R.J. Mechanical behavior of electrospun polyurethane, Polymer 2003; 44:6857–6862
25. Jackson B.K., Bow A.J., Kannarpady G., Biris A.S., Anderson D.E., Dhar M.S., Bourdo S.E. Polyurethane/nano-hydroxyapatite composite films as osteogenic platforms. Journal of Biomaterials Science, Polymer Edition 2018; 29(12):1426-1443
26. Bow A., Newby S., Rifkin R., Jackson B.K., Matavosian A., Griffin C., King W., Alghazali K., Mhannawee A., Berryhill S.B., Morello R., Hecht S., Biris A.S., Anderson D.E., Bourdo S.E., Dhar M. Evaluation of a Polyurethane Platform for Delivery of Nanohydroxyapatite and Decellularized Bone Particles in a Porous Three-Dimensional Scaffold. ACS Appl. Bio. Mater. 2019; 2:1815-1829
27. Meskinfam M, Bertoldi S, Albanese N, Cerri A, Tanzi MC, Imani R, Baheiraei N, Farokhi M, Fare S. Polyurethane foam/nano-hydroxyapatite composite as a suitable scaffold for bone tissue regeneration. Mater Sci Eng C Mater Biol Appl. 2018; 82:130–140.
28. Zhang D, Liu W, Wu XD, et al. Efficacy of novel nano-hydroxyapatite/polyurethane composite scaffolds with silver phosphate particles in chronic osteomyelitis. J Mater Sci Mater Med. 2019;30(6):59

29. Yu J, Xia H, Teramoto A, Ni QQ. The effect of hydroxyapatite nanoparticles on mechanical behavior and biological performance of porous shape memory polyurethane scaffolds. J Biomed Mater Res A. 2018;106(1):244–254.
30. Mi HY, Palumbo S, Jing X, Turng LS, Li WJ, Peng XF. Thermoplastic polyurethane/hydroxyapatite electrospun scaffolds for bone tissue engineering: effects of polymer properties and particle size. J Biomed Mater Res B Appl Biomater. 2014; 102(7):1434–1444.
31. Han D.S., Chang H.K., Kim K.R., Woo S.M. Consideration of Bone Regeneration Effect of Stem Cells: Comparison of Bone Regeneration Between Bone Marrow Stem Cells and Adipose-Derived Stem Cells. Journal of Craniofacial Surgery 2014; 25(1):196-201
32. Eriksen E.F. Cellular mechanism of bone remodeling. Reviews in endocrine and metabolic disorders 2010; 11(4):219-227
33. Bostrom M.P.G. Expression of Bone Morphogenetic Proteins in Fracture Healing. Clinical Orthopaedics and Related Research 1998; 355: S116-S123
34. García de Vinuesa A, Abdelilah-Seyfried S, Knaus P, Zwijsen A, Bailly S. BMP signaling in vascular biology and dysfunction. Cytokine Growth Factor Rev. 2016 Feb; 27:65-79.
35. Albrektsson T., Johansson C. Osteoinduction, osteoconduction and osseointegration. European Spine Journal 2001; 10:S96-S101
36. Ursini T.L., Amelse L.L., Elkhenany H.A., Odoi A., Carter-Arnold J.L., Adair H.S., Dhar M.S. Retrospective analysis of local injection site adverse reactions associated with 230 allogenic administrations of bone marrow-derived mesenchymal stem cells in 164 horses. Equine Vet J. 2019;51(2):198-205
37. Carter-Arnold J.L., Neilsen N.L., Amelse L.L., Odoi A., Dhar M.S. In vitro analysis of equine, bone marrow-derived mesenchymal stem cells demonstrates differences within age- and gender-matched horses. Equine Vet. J. 2014; 46: 589-595
38. Villagrán C.C., Amelse L., Neilsen N., Dunlap J. Dhar M.S. Differentiation of equine mesenchymal stromal cells into cells of neural lineage: potential for clinical applications. Stem Cells Int. 2014;
39. Callis G., Sterchi D. Decalcification of Bone: Literature Review and Practical Study of Various Decalcifying Agents. Methods, and Their Effects on Bone Histology. Journal of Histolotechnology 1998; 21(1):49-58
40. Varela A., Jolette J. Bone Toolbox: Biomarkers, Imaging Tools, Biomechanics and Histomorphometry. Toxicologic Pathology 2018; 46(5):511-529
41. Titford M. Progress in the Development of Microscopical Techniques for Diagnostic Pathology. Journal of Histotechnology 2009; 32(1):9-19
42. Foot C.N. The Masson Trichrome Staining Methods in Routine Laboratory Use. Stain Technology 1933; 8:101-110

43. Dahl L.K. A Simple and Sensitive Histochemical Method for Calcium. Proceedings of the Society for Experimental Biology and Medicine 1952; 80(3):474-479
44. Filgueira L. Fluorescence-based Staining for Tartrate-resistant Acidic Phosphatase (TRAP) in Osteoclasts Combined with Other Fluorescent Dyes and Protocols. Journal of Histochemistry & Cytochemistry 2004; 52(3): 411-414
45. Puchtler H., Waldrop F.S. On the mechanism of Verhoeff's elastica stain: a convenient stain for myelin sheaths. Histochemistry 1979; 62(3):233-47
46. Dempster D.W., Compston J.E., Drezner M.K., Glorieux F.H., Kanis J.A., Malluche H., Meunier P.J., Ott S.M., Recker R.R., and Parfitt A.M. Standardized Nomenclature, Symbols, and Units for Bone Histomorphometry: A 2012 Update of the Report of the ASBMR Histomorphometry Nomenclature Committee. J Bone Miner Res 2013; 28(1):2-17
47. Schindelin J., Arganda-Carreras I., Frise E. Fiji: an open-source platform for biological-image analysis. Nature methods 2012; 9(7): 676-682
48. Hu K., Olsen B.R. The roles of vascular endothelial growth factor in bone repair and regeneration. Bone 2016; 91:30-38
49. Raghavendra S., Wood M.C., Taylor T.D. Early wound healing around endosseous implants: a review of the literature. Int J Oral Max-illofac Implants 2005;20(3):425-431
50. Berner A., Reichert J.C., Woodruff M.A., Saifzadeh S., Morris A.J., Epari D.R., Nerlich M., Schuetz M.A., Hutmacher D.W. Autologous vs. allogenic mesenchymal progenitor cells for the reconstruction of critical sized segmental tibial bone defects in aged sheep. Acta Biomaterialia 2013; 9:7874-7884
51. Cipitria A., Reichert J.C., Epari D.R., Saifzadeh S., Berner A., Schell H., Mehta M., Schuetz M.A., Duda G.N., Hutmacher D.W. Polycaprolactone scaffold and reduced rhBMP-7 dose for the regeneration of critical-sized defects in sheep tibiae. Biomaterials 2013; 34: 9960-9968
52. Reichert J.C., Cipitria A., Epari D.R., Saifzadeh S., Krishnakanth P., Berner A., Woodruff M.A., Schell H., Mehta M., Schuetz M.A., Duda G.N., Hutmacher D.W. A Tissue Engineering Solution for Segmental Defect Regeneration in Load-Bearing Long Bones. Science translational medicine 2012; 4(141): 141ra93
53. Niemeyer P., Schonberger T.S., Hahn J., Kasten P., Fellenberg J., Suedkamp N., Mehlhorn A.T., Milz S., Pearc S. Xenogenic transplantation of human mesenchymal stem cells in a critical size defect of the sheep tibia for bone regeneration. Tissue Engineering, Part A: Tissue Engineering 2010; Vol.16(1), p.33(11)
54. Cornell C.N., Lane J.M. Current understanding of osteoconduction in bone regeneration. Clinical Orthopaedics and Related Research 1998; 355(S):267-273

55. Kamei N., Atesok K., Ochi M. The Use of Endothelial Progenitor Cells for the Regeneration of Musculoskeletal and Neural Tissues. Hindawi Stem Cells International 2017; 2017:1-7
56. Bessa P.C., Casal M., Reis R.L. Bone morphogenetic proteins in tissue engineering: the road from the laboratory clinic, part I (basic concepts). J Tissue Eng Regen Med 2008; 2:1-13
57. Bessa P.C., Casal M., Reis R.L. Bone morphogenetic proteins in tissue engineering: the road from the laboratory clinic, part II (BMP delivery). J Tissue Eng Regen Med 2008; 2:81-96
58. Jones A.L., Bucholz R.W., Bosse M.J., Mirza S.K., Lyon T.R., Webb L.X., Pollak A.N., Golden J.D., Valentin-Opran A. Recombinant human BMP-2 and allograft compared with autogenous bone graft for reconstruction of diaphyseal tibial fractures with cortical defects. A randomized, controlled trial. J Bone Joint Surg Am 2006; 88:1431–144
59. Ishihara A., Shields K.M., Litsky A.S., Mattoon J.S., Weisbrode S.E., Bartlett J.S., Bertone A.L. Osteogenic Gene Regulation and Relative Acceleration of Healing by Adenoviral-Mediated Transfer of Human BMP-2 or -6 in Equine Osteotomy and Ostectomy Models. J of Orthop Res 2008; 6:764-771
60. Perrier M, Lu Y, Nemke B, et al: Acceleration of second and fourth metatarsal fracture healing with recombinant human bone morphogenetic protein-2/calcium phosphate cement in horses. Vet Surg 2008; 37:648
61. Langenfeld E.M., Langenfeld J., Bone morphogenetic protein-2 stimulates angiogenesis in developing tumors, Mol. Cancer Res. 2 (2004) 141-9.
62. Rothhammer T., Bataille F., Spruss T., Eissner G., Bosserhoff A.K., Functional implication of BMP4 expression on angiogenesis in malignant melanoma, Oncogene 26 (2007) 4158–4170.
63. Mattar T., Friedrich P.F., Bishop A.T. Effect of rhBMP-2 and VEGF in a Vascularized Bone Allotransplant Experimental Model Based on Surgical Neoangiogenesis. Journal of Orthopedic Research 2013; 31(4):561-566;
64. Lv J., Xiu P., Tan J., Jia Z., Cai H., Liu Z. Enhanced angiogenesis and osteogenesis in critical bone defects by the controlled release of BMP-2 and VEGF: implantation of electron beam melting-fabricated porous Ti6Al4V scaffolds incorporating growth factor-doped fibrin glue. Biomed Mater 2015; Jun 24; 10(3): 035013;
65. Hankenson K.D., Dishowitz M., Gray Ch., Shenker M. Angiogenesis in bone regeneration. Injury 2011: 42(6); 556-561;
66. Clarkin C.E., Gerstenfeld L.C. VEGF and bone cell signaling: an essential vessel for communication? Cell Biochem Funct 2013; 31:1-11; DOI: 10.1002/cbf.2911
67. Werther K., Christensen I.J., Nielsen H.J. Determination of vascular endothelial growth factor (VEGF) in circulating blood: significance of VEGF in various leucocytes and platelets. Scand J Clin Lab Invest 2002; 62:343-350;

68. Steflik D.E., Corpe R.S., Young T.R., Sisk A.L., Parr G.R. The biologic tissue responses to uncoated and coated implanted biomaterials. Adv Dent Res 1999;27–33.
69. Kim H.W., Knowles J.C., Kim H.E. Hydroxyapatite/poly(epsiloncaprolactone) composite coatings on hydroxyapatite porous bone scaffold for drug delivery. Biomaterials 2004;25(7–8):1279–87
70. Zakaria S.M., Zein S.H.S., Othman M.R., Yang F., Jansen J.A. Nanophase Hydroxyapatite as a Biomaterial in Advanced Hard Tissue Engineering: A Review. Tissue Engineering Part B 2013; 19(5):431-441
71. Gabriel L.P., dos Santos M.E., Jardini A.L., Bastos G.N.T., Dias C.G.B.T., Webster T.J., Filho R.M. Bio-based polyurethane for tissue engineering applications: How hydroxyapatite nanoparticles influence the structure, thermal and biological behavior of polyurethane composites. Nanomedicine: Nanotechnology, Biology, and Medicine 2017; 13:201–208
72. Yu J., Xia H., Teramoto A., Ni Q.Q. The effect of hydroxyapatite nanoparticles on mechanical behavior and biological performance of porous shape memory polyurethane scaffolds. J Biomed Mater Res Part A 2018:106A:244–254.
73. Rogers L., Said S.S., Meguanint K. The effects of fabrication strategies on 3d scaffold morphology, porosity, and vascular smooth muscle cell response. J. Biomater. Tissue Eng. 2013; 3(3):300–311.
74. Tsai S.W., Huang S.S., Yu W.X., Hsu Y.W., Hsu F.Y. Fabrication and Characteristics of Porous Hydroxyapatite-CaO Composite Nanofibers for Biomedical Applications. Nanomaterials 2018,8,0:1-9
75. Fuerstenberg C.H., Wiedenhoefer B., Putz C., Burckhardt I., Gantz S., Kleinschmidt K., Schroeder K. Collagen hydroxyapatite (Healos) saturated with gentamicin or levofloxacin. In vitro antimicrobial effectiveness – a pilot study. Orthopade 2010; 39(4):437-43
76. Andronescu E., Ficai A., Albu M.G., Mitran V., Sonmez M., Ficai D., Ion R., Cimpean A. Collagen-hydroxyapatite/Cisplatin Drug Delivery Systems for Locoregional Treatment of Bone Cancer. Technology in Cancer Research & Treatment 2013; 12(4): 275-284
77. Zhou H., Lee J. Nanoscale hydroxyapatite particles for bone tissue engineering. Acta Biomater 2011; 7: 2769
78. Venkatesan J., Kim S.K. Nano-Hydroxyapatite Composite Biomaterials for Bone Tissue Engineering – A review. Journal of Biomedical Nanotechnology 2014; 10: 3124-3140

CHAPTER FIVE
EFFECTS OF NOVEL 3D BONE SCAFFOLD ON THE HEALING OF EQUINE IV METACARPAL BONES.

Abstract

Background

Bone regeneration remains a challenge in horses. Scenarios in which horses may benefit from enhanced bone healing include comminuted fractures, subchondral bone cysts, osteoarthritis and bone infections. This study aimed to assess bone regenerative capacity of a nano Hydroxyapatite polyurethane bone scaffold. The scaffolds were evaluated in five horses. Study design included 10 splint-bone defects assigned to scaffold (n=5) and control treatment group (n=5). Two cm full-thickness defects were created in both fourth metacarpal bones in each horse. Bone healing assessment conducted over the ensuing 60 days included high definition infrared thermography camera, ultrasonography, radiography, and computed tomography. Histological evaluation of the tissue filling each defect was conducted at the termination of the study.

Results

The analysis of radiography revealed a significantly higher percentage of new bone formation (67.42% of the defect size) within defects containing bone scaffold as compared to defects left unfilled (35.88% of the defect size). Further analysis of computed tomography images revealed that defects containing bone scaffold had a significantly higher density as compared to the control (807.80 HU and 464.80 HU in defects with bone scaffold and control respectively). Neither ultrasound nor thermography revealed signs of adverse effects associated with bone scaffold implantation. Histological evaluation confirmed significant bone formation within the pores and channels as well as on the surface of the bone scaffold.

Conclusions

The novel bone scaffold technology showed to be osseointegrative in current research model. The implant can be utilized to enhance the bone regeneration in horses affected by subchondral bone cysts, comminuted fractures with bone loss or in horses requiring arthrodesis. The unique design and composition of the implant allows for potential use as a drug delivery device.

Introduction

Bone injuries resulting in tissue loss and mechanical impairment are common in equine athletes. Examples include fractures (1-4), subchondral bone cysts (5-10), and bone infection (11-14). Fractures have been estimated to cause up to 63% of fatal injuries in the racing industry (1-3) and approximately 34% of them are comminuted with a variable degree of bone loss (2,4). Bone regeneration remains challenging in equids due to delayed or poor healing, repair failures resulting from high-stress loads, and infection (11-14). Prolonged convalescence is further associated with life-threatening complications, such as contralateral limb laminitis or colitis caused by an extended course of medication (15,16).

To date, autologous cancellous bone graft (autograft) is the gold standard to fill in the void in bone because of the low rejection risk as well as high osteoprogenitor cell concentration (17,18). Limitations of autografts include the necessity of a second surgery site, increased risk of infection, and a limited amount of donor tissue available (19,20). Because of the limitations, an ideal substitute for an autograft is desirable. It should be osteoinductive, osteoconductive and osseointegrative (21). Several allogenic materials have been tested in horses; they are however lacking three-dimensional structure and adequate mechanical properties (22-25)

The objective of this study was to evaluate regenerative capacity of a three-dimensional hydrophilic polyurethane platform coated with hydroxyapatite nanoparticles (nHA) and decellularized bone particles (DBP) (26). Hydrophilic polyurethane (PU) is a biocompatible synthetic polymer with stable biological and mechanical properties (26). Nanostructured hydroxyapatite has been shown to promote fibroblastic and osteoblastic cell adhesion and proliferation (osteoinduction and osteoconduction), provide calcium-containing minerals, and change the energy of coated materials to control initial protein adsorption as well as change the conformation to inhibit inflammatory cell functions (27-31).

The bone scaffold was evaluated in defects that were created in the fourth metacarpal bones of horses. This has been established as an acceptable model of equine bone healing (22,32-38). The hypothesis was that the bone scaffold will be osteoinudctive, osteoconductive and osseointegrated, and therefore will enhance bone regeneration within the implanted defects as compared to the contralateral non-implanted control.

Materials and Methods

Study Population and Study Design

The study was conducted on mares acquired for this study from local vendors and owned by the University of Tennessee, College of Veterinary Medicine (UTCVM). The study was approved by the University of Tennessee Institutional Animal Care and Use Committee and was conducted according to the IACUC protocol #2609-0518. Horses were screened for general health as well as orthopedic conditions. Horses which showed signs of systemic diseases (e.g. bronchitis, pneumonia, chronic weight loss, colitis, etc.), were lame or had palpable abnormalities the fourth metacarpal (MC IV) bones, were not included in the study. The fourth metacarpal bones of each horse were randomly assigned to one of two treatment groups, S – bone scaffold[a] (n=5) and C – control (n=5).

Study Timeline

Horses were quarantined 14 days prior to the study. Each horse was transported from the farm to the veterinary teaching hospital 48 hours before the scheduled surgery. The surgeries were performed on day 0 followed by 5 days of

postoperative care which involved physical examinations and perioperative medications. The horses' activity was restricted to stall rest for 14 days after surgery so as not to compromise surgical site healing and to prevent bone scaffold[a] displacement. After 14 days, sutures were removed, and the horses were allowed access to small runs in front of the stalls for an additional 14 days. Forelimbs were kept bandaged for 21 days following the surgery after which the wounds were covered with standing wrap bandages for another 9 days. Thirty days after surgery, the horses were turned out on pasture for an additional 30 days before tissue biopsy was performed.

Bone scaffold implantation surgery

Perioperative treatment included gentamicin sulfate[b] (6.6 mg/kg IV, q24h), penicillin procaine G[c] (22,000 IU/kg IM, q12h), and a non-steroidal anti-inflammatory – firocoxib[d] (0.3 mg/kg IV, q24h). The horses were sedated with acetylpromazine maleate (0.04 mg/kg IM) followed approximately 30 min later by xylazine hydrochloride[e] (1.0 mg/kg IV). Anesthesia was induced with ketamine hydrochloride[f] (2.2 mg/kg, IV) and midazolam[g] (0.05 mg/kg, IV). Anesthesia was maintained with isoflurane[h] in oxygen (3 L/min) and xylazine hydrochloride[e] (1 mg/kg/h). Horses were placed in dorsal recumbency and both forelimbs were clipped from the hoof to above the carpus. The surgical site was aseptically scrubbed and draped for aseptic surgery. A 5 cm long incision was created over the middle third of the left MCIV. Subcutaneous tissue was bluntly separated to expose the bone. A 2 cm long fragment of the MCIV was removed using an oscillating bone saw. Care was taken not to injure the underlying suspensory ligament during the procedure. The created defect was either filled with bone scaffold[a] or left unfilled according to the treatment group assignment. Prior to implantation, the bone scaffolds[a] were soaked in 1 ml of sterile saline to allow the implant to absorb the fluid and increase its volume (Figure 5-1, all figures and tables are placed in the appendix). Subcutaneous tissue was closed in a simple continuous pattern using absorbable suture[i] and skin was closed in the simple continuous pattern using non-absorbable suture[j]. Surgery on the right MCIV was performed in the same manner as on the left MCIV. Sterile wraps were temporarily placed on both forelimbs and CT was performed to establish the baseline of defect density. Following CT, sterile distal limb bandages were placed, and the horse was allowed to recover from general anesthesia. Antibiotics as previously described were administered for an additional 48 hours. NSAID's as previously described were administered for an additional 72 hours.

Data acquisition throughout the study

The amount of postoperative inflammation surrounding the implant, including soft tissue swelling and local fluid accumulation, was assessed with ultrasonography and thermography. Thermography[k] was recorded in degrees Celsius (°C) by the same investigator (RG) in two projections, anteroposterior and lateral-medial projection, maintaining the same distance (0.5 m) during each recording. The

camera was adjusted to the environmental temperature and humidity and the recording was performed 5 min after bandage removal to allow the limb to cool down. Thermography was performed on the days 1, 3, 5,7,10,14,21,30 and 59 following surgery. One 45° dorsolateral-palmaromedial oblique (DLPMO) projection of each MC IV bone was recorded using a portable radiograph machine[l] on standing horses day 1 (Figure 5-2) after surgery followed by day 14, 30 and 59. Ultrasonography was performed by one investigator (RG) using a portable ultrasound machine[m] on standing horses day 1 (Figure 5-3) after surgery followed by day 14, 30 and 59. The CT was carried out using a 40-slice helical CT scanner[n] immediately after implantation surgery and again 60 days post-implantation immediately before tissue biopsy (Figure 5-4). Transverse images were reconstructed in 0.67- and 5-mm slice thickness, and sagittal and dorsal multiplanar reconstructed (MPR) images were generated. Images were sent to picture archive and communication system[o]. The biopsied tissue was submitted for histological evaluation.

Data Analysis

The data collected from bone healing assessment was organized in Excel[p] spreadsheets. Radiographs and CT images were evaluated by a board-certified radiologist (SH) and scored for osteotomy gap filling as well as opacity of a new bone (Tables 5-1 and 5-2). The two individual scores were summarized for an overall radiographic healing score of each defect. Quantitative assessment of defect filling with new bone was performed on the radiographs using the NIH Fiji software[q] by the principal investigator (RG). Quantification was conducted through the generation of binary masks (black background and white color for bone) for images and drawing the region of interest (ROI) covering entire defect. The defect filling was calculated as the amount of white color (bone) within the ROI and expressed as percent of the defect area. The CT images were scored for new bone formation (Table 5-3) and the visibility of graft material on the CT images were recorded as being present or absent. A transverse slab was reconstructed spanning the length of the defect for both the study and control leg, and density of the defect was measured quantitatively with the results being expressed in Hounsfield Units (HU). Ultrasonography images were descriptively evaluated for any signs of inflammation surrounding the filled or unfilled defects.

Tissue Biopsy

At the termination of the study (60 days post implantation), the horses underwent CT and tissue biopsy. The perioperative treatment was as previously described. General anesthesia was induced as previously described. Horses had CT of both forelimbs performed and then both forelimbs were prepared for aseptic surgery in the same manner as previously described. A 5 cm long incision was created above the location of the previously created defect in both forelimbs and subcutaneous tissue was bluntly separated to present the defect. A 5 mm thick biopsy was performed at the center of the defect using a scalpel blade or osteotome if required.

Care was taken not to injure the underlying suspensory ligament during the procedure. Subcutaneous tissue and skin were closed as previously described. Sterile distal limb bandages were applied to both forelimbs and the horse was allowed to recover. Tissue was subsequently submitted for the histological evaluation. Postoperative care was as previously described.

Histology

Histology was performed on decalcified specimens. Each tissue specimen was preserved in 10% neutral buffered formalin (NBF)$_r$ for 48 h after tissue biopsy and was then decalcified with 15% formic acid for up to 14 days after tissue harvest. Specimens were cut with a scalpel and were stained with Hematoxylin and Eosin (H&E) for histologic evaluation. Histologic sections were analyzed using a light microscope at 10, 20 and 100 X magnification. The area available for tissue in-growth was analyzed and described.

Statistical Analysis

The analysis was performed using SPSS statistical software$_s$ and PS power and sample calculation software$_t$. Descriptive statistics were determined for the continuous variables including thermography, percentage of defect filling as well as defect density after bone scaffold$_a$ implantation and before biopsy. The normality of data distribution of each variable was performed using a Kolmogorov-Smirnov test of normality. The variables with continuous data were compared between the treatment groups using a paired-samples student T-test. The variables with categorical data were compared between the treatment groups using the Wilcoxon Signed Ranks test. The statistical significance was assumed at $\alpha = 0.05$. The calculated power of the study design and carried out evaluations to detect the true difference in the filling of the defect with the new bone was $\beta = 0.9$.

Results

The study included five adult mares (4 -10 years of age) with a mean weight of 437.7 kg (± 29 kg). The breeds of the horses included Thoroughbred (n=1), Quarter Horse (n=1), Rocky Mountain Horse (n=1), Standardbred (n=1) and unknown (n=1). The bone scaffolds, after being soaked in sterile saline, increased by 100% of its original volume, however, the soaking did not compromise their integrity. The bone scaffold$_a$ remained mechanically tunable and handling, as well as the implantation process, were accomplished with no damage to bone scaffold$_a$ (Figure 5-1). None of the adverse effects were detected after implantation, including excessive swelling, seroma formation, or surgical site infection. The analysis of the high definition infra-red (HD-IR) thermography did not reveal significant differences between the treatment groups in the temperature of the superficial tissues over the surgery site immediately after the surgery ($p>0.05$). The temperature gradually decreased over 60 days after surgery equally in both treatment groups (Figure 5-7).

Radiographically, the defects with bone scaffolds contained a significantly higher percentage of bone 60 days after the implantation, as compared to controls [67.42% (±26.7%) in the bone scaffold$_a$ group and 35.88% (±32.69%) in the control group (p=0.013)] (Figure 5-2, Table 5-4). In one of the five horses, the bone scaffold$_a$ was slightly displaced in the proximal aspect, but this did not interfere with bone formation within the defect. The qualitative assessment of the radiographs failed to show a statistically significant difference between the treatment groups (p>0.05). However, the bone scaffold$_a$ treatment group showed a trend of a higher median gap-filling and new bone opacity score as compared to the control (Figure 5-8). The qualitative assessment of the CT images, including the amount of newly formed bone within the defect was significantly higher in the bone scaffold$_a$ group as compared with the control group (p=0.038). Quantitatively, the density of new bone filling the defects in the bone scaffold$_a$ group was significantly higher than that in the control, revealing 807.80 HU (±129.63 HU) and 464.80 HU (±81.27 HU) respectively (p=0.002) (Figure 5-4 and Figure 5-9). Fourteen days following the implantation, ultrasonography revealed mild to moderate homogeneous fluid accumulation around the bone scaffold$_a$ and soft tissue swelling (Figure 5-3). Neither the fluid accumulation nor the soft tissue swelling was different from that of the defect in the control group. Serial ultrasonographic evaluation confirmed gradual bone formation around the bone scaffold, which was evident as a smooth hyperechogenic line at the surface of the implant (Figure 5-3). Histology confirmed significant bone formation within the pores and channels of the implant and around the implant (Figure 5-5). Analysis of the histological slides revealed several cartilage clusters within the bone tissue. In contrast, the center of the control was filled with connective tissue with no signs of bone formation (Figure 5-6).

Discussion

The study presented promising results in the enhancement of bone regeneration using the bone scaffold$_a$ in equids. The results were statistically and clinically significant as well as the calculated power of the study (β=0.9) revealed that 90% of the outcome was not related to a chance. The surgeries were rapid and scaffold manipulation as well as implantation was feasible in all cases. The bone scaffolds absorbed entire 1 ml of sterile saline after being soaked before the surgery. The fluid absorption increased the size of the implant by approximately 100%, however this did not compromise its integrity. The proximal aspect of one out of five implants was mildly displaced within the defect in the abaxial direction, however it did not interfere the bone healing. None of the horses developed adverse effects associated with the scaffold implantation.

The defects containing the scaffolds in all 5 horses were filled in with a higher amount of the new bone as compared to the negative control on the contralateral limb. The amount of new formed bone varied similarly within the treatment groups as it was shown with the similar standard deviations. The original hypothesis that

the bone scaffold is osseointegrative in equids was accepted. These terms mean that the scaffold did stimulate the primitive, undifferentiated and pluripotent cells to produce the bone lineage (osteoinduction) as well as attracted the cells to the material allowing them to produce the bone on its surface (osteoconduction) (21). Both processes resulted in implants satisfying osseointegration grade which was associated with the direct formation of bony tissue around the implant without the layer of fibrous tissue on the implant-bone surface (21).

Up to date, there are several bone scaffolds which have been researched on horses (22-25). The features of bone scaffold used in this study are unique from other synthetic scaffolds (26). Most important is related to its hydrophilic structure which allows for implant swelling and filling non-uniform bone voids and incongruencies. Further advantage is related to its mechanical integrity. The combination of soft (PU) and hard components (nHA, DBP) gives it overall mechanical stability and stiffness greater than that of the individual components. The scaffold is being implanted into the defect in press-fits matter, and the flow of blood and cellular components leads to immediate hydration. Unique porosity, with pore size ranging between 50 and 800 μm and interconnected pore distribution, implant induces advanced and early neovascularization. is ideal for new bone formation based on the fact that the small pores facilitate early vascularization, and the larger ones facilitate larger blood vessel formation – resulting in rapid vascularization of the graft, which is responsible for fast and reliable new tissue formation (26).

Horses may benefit from enhanced bone regeneration for several reasons. The most common include long and flat bone fractures (1-4), subchondral bone cysts (5-10), bone infections (11-14), and arthrodesis (46-51). Bone regeneration remains challenging in equids and the fractures have been associated with up to 63% of fatal injuries in the racing industry (1-3). It is not uncommon that the fractures are open and comminuted (2,4,11-14). The current success rate of subchondral bone cyst treatment varies between 56-75% in the return to the previous level of performance (5-10). All the methods described in the literature are aimed at reducing the inflammation within the cyst as well as filling and decompressing the bone void (5-10). The rate of surgical site infection following the long bone fracture repair and arthrodesis has been reduced over the years and currently reported as 14% in one of the veterinary teaching hospitals (11-14). The chronic degenerative osteoarthritis often requires arthrodesis which success rate varies between 46-75% in the return to the previous level of performance (46-51). In all of these cases, the bone scaffold[a] used in this study could serve as a bone filler and enhance bone regeneration, potentially increasing the positive outcome of the treatment. Additionally, the implant may serve as a drug delivery device in infected tissue.

This novel technology was tested in the equine splint-bone model, which has been a well-established model to research bone healing in horses (32-38). The splint-

bone partial ostectomy procedure is considered a safe method with minimal soft tissue disruption, which does not cause exostosis or sequestration formation (32). Furthermore, this procedure did not impair the perfusion and integrity of the distal fragment, which was most likely maintained from the periosteal and soft tissue vasculature (32). The horses tolerated the procedure well with the lack of noticeable pain, discomfort, or gait impairment. Because of the thick interosseous ligament between the fourth and third metacarpal bones, the osteotomies provide relatively stable, uncomplicated, and appositional bone healing models with the advantage of not requiring an internal fixator (32-38). Each horse can serve as its control because of multiple splint bones and therefore reducing the intra-individual healing variability (35). The limitation of this model is related to the fact that the fourth and second metacarpal bones are not fully weight-bearing bones as well as they do not contain a medullar cavity, therefore the entire healing process occurs from the periosteum. To the best of our knowledge, this is only one full-thickness long bone healing model described in horses.

Conclusions

The bone scaffold enhanced the splint bone regeneration after 60 days post implantation in the splint-bone healing model. The results were repeatable among the horses with relatively small inter-individual variation. Because of the unique design of this bone regenerative technology the implant can be further used as the drug delivery device. The future research direction therefore will include delivery of bioactive agents into the defect, such as commonly used platelet rich plasma gels (PRP) and mesenchymal stem cells (MSC).

Tables

Table 5-1. Radiographical ostectomy gap filling scoring system.

Ostectomy Gap Filling	
Score	**Ostectomy gap filling**
0	No interval change compared to immediate post-operative radiographs
1	New bone filling <25% of ostectomy gap
2	New bone filling 26-50% of ostectomy gap
3	New bone filling 51-99% of ostectomy gap
4	Ostectomy gap completely filled and/or bridging callus present on at least 3 cortices

Table 5-2. Radiographical opacity scoring system.

Ostectomy Opacity	
Score	**Opacity of new bone**
0	No interval change compared to immediate post-operative radiographs
1	New bone less opaque than normal cortex
2	New bone of similar or greater opacity compared to normal cortex

Table 5-3. CT ostectomy gap filling scoring system.

CT Ostectomy Gap Filling	
Score	**Ostectomy gap filling**
0	No evidence of new bone formation adjacent to graft or within osteotomy gap
1	New bone filling <25% of ostectomy gap
2	New bone filling 26-50% of ostectomy gap
3	New bone filling 51-99% of ostectomy gap
4	Ostectomy gap completely filled and/or bridging callus present on all cortices

Table 5-4. Percent of defect filling.

Comparison of defect filling in scaffold and control		
No	**Defect filling in scaffold (%)**	**Defect filling in control (%)**
1	62.31	39.01
2	27.92	1.79
3	81.59	31.68
4	65.35	18.37
5	99.92	88.58
Mean	67.42	35.89
St Dev	±26.68	±32.69

Figures



Figure 5-1. Bone scaffold.

The figure presents two images, the image on the left side shows the 2 cm long bone scaffold and image on the right side shows bone scaffold placed within the defect created in the fourth metacarpal bone. (c) 2020 Photographs of bone filler scaffold used with permission of NuShores Biosciences LLC).

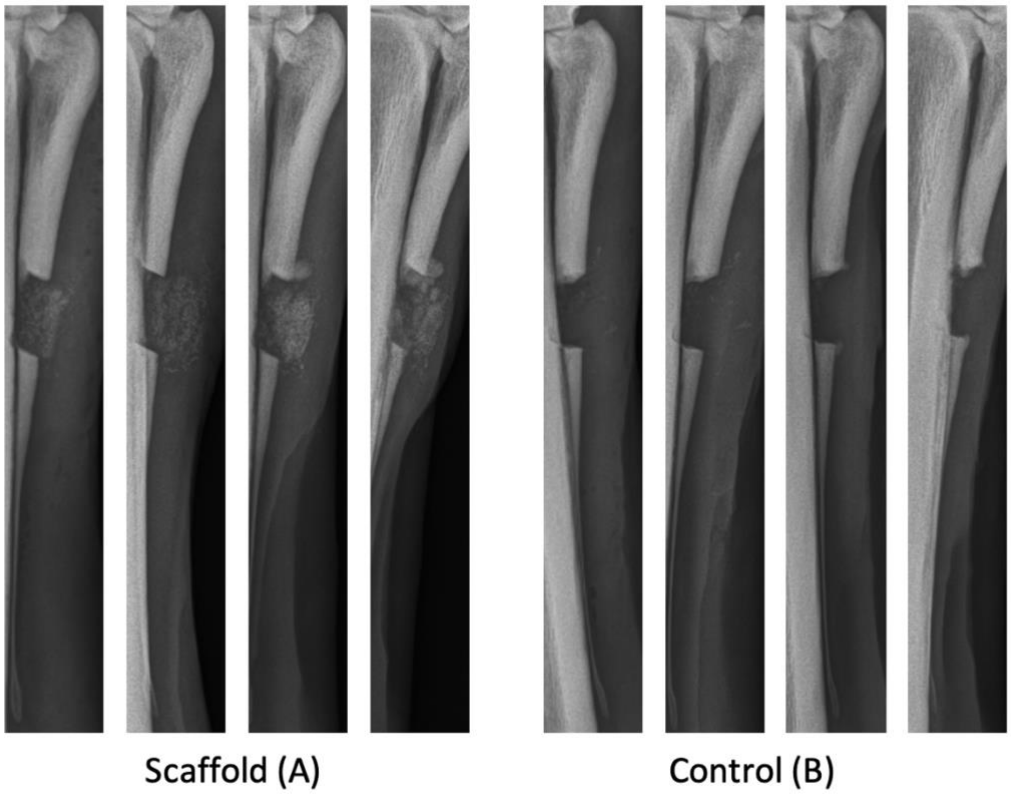


Figure 5-2. Radiographic assessment of healing.

The figure shows a representative sequence of radiographs taken throughout the study of the defect filled with the bone scaffold (A) and the control (B). The defects were created in the fourth metacarpal bones in same horse. Each sequence within the bone scaffold and control treatment group consist of four images which were recorded at 24h (starting from the left side), 14, 30 and 60 days after the implantation surgery. This figure shows gradual filling of defects containing bone scaffold with a new bone (A) as compared to the control, where the bone regeneration was minimal (B).

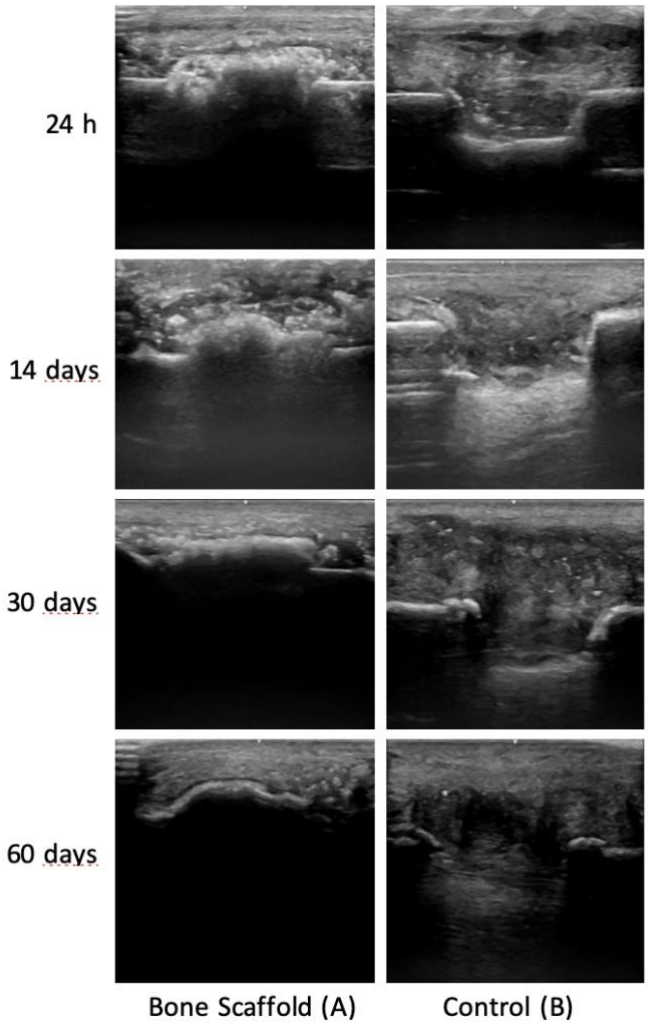


Figure 5-3. Ultrasonographic assessment of healing.

The figure shows a representative sequence of ultrasonography images recorded throughout the study of defect filled with bone scaffold (A) and the control (B). Both defects were created in the same horse. Each sequence within bone scaffold and control treatment group consist of four images which were recorded at 24h (starting from top to bottom), 14, 30 and 60 days after the implantation surgery. The images show increased soft tissue swelling as well as fluid accumulation 14 days after implantation (second row of images from the top) that was similar in both treatment groups. The bone scaffold is being gradually covered with bone presented as the smooth hyperechogenic line (A). In the control defect, bone formation was minimal and occurred only at the margins of the defect (B).

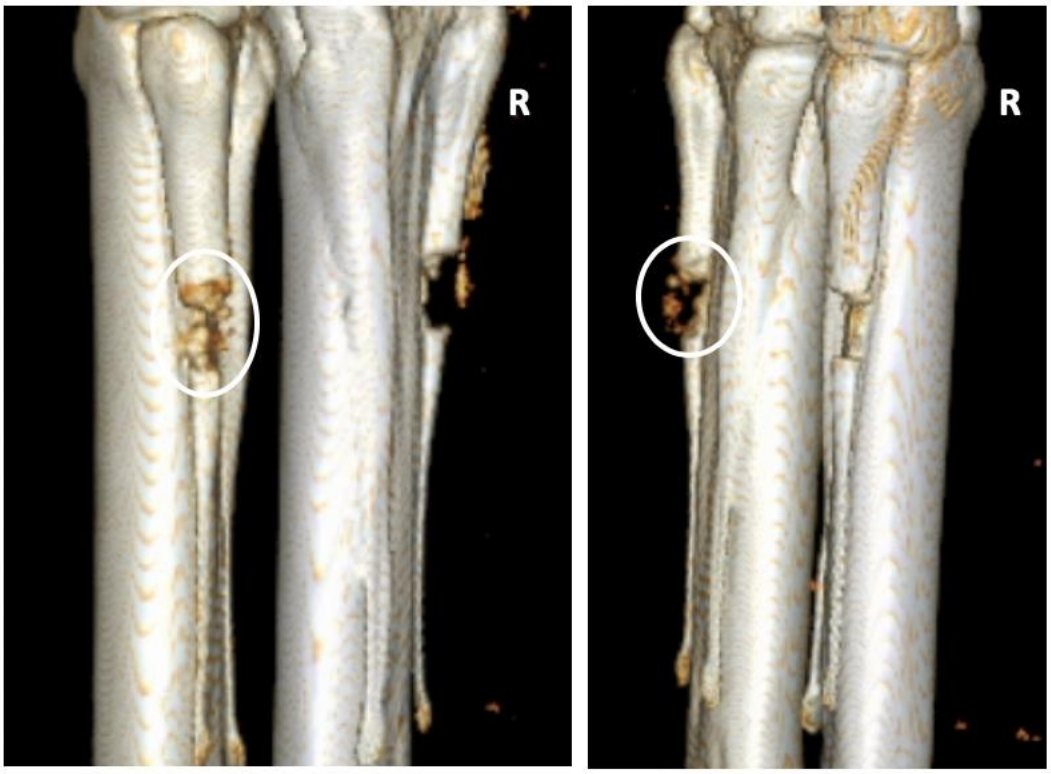
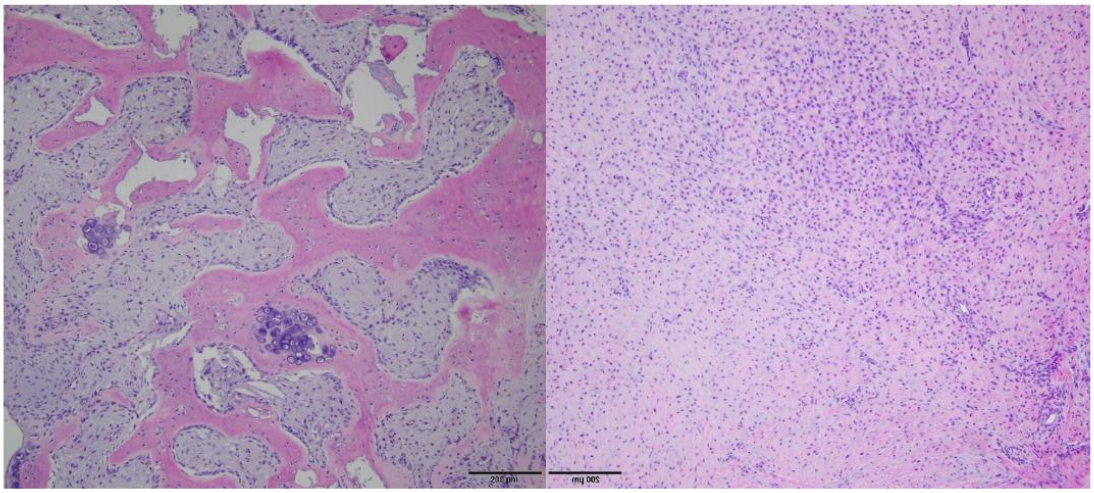


Figure 5-4. 3D CT reconstruction.

The figure presents representative 3-D reconstructed computed tomography (CT) images of the fourth metacarpal bones in same horse. CT images were taken 60 days after implantation and were used for illustration only. The image analysis was performed on 2D and slab reconstructed images. The defect filled with bone scaffold is labeled with a white circle. The CT confirmed significant bone formation within the defect containing bone scaffold as opposed to the control, where bone formation was minimal.



Bone Scaffold (A) Control (B)

Figure 5-5. Scaffold and control histology.

The figure shows histology at 10x magnification of a section harvested from the middle of defect filled with bone scaffold (A) and the control (B). The section harvested from bone scaffold shows bone formation adjacent to pores of bone scaffold. The tissue harvested from middle of the control defect represents connective tissue without signs of new bone formation.

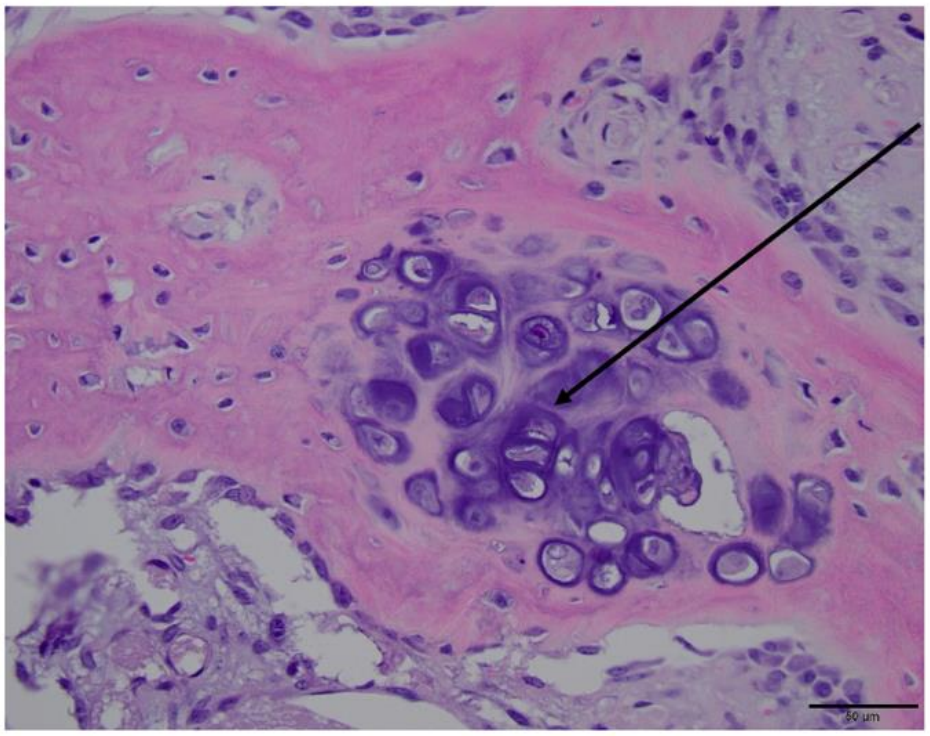


Figure 5-6. Hyaline cartilage formation.

The figure shows a histology image at 100x magnification of a section harvested from the middle of defect containing bone scaffold. The image shows a new bone formation with a central island of new cartilage formation (black pointing arrow).

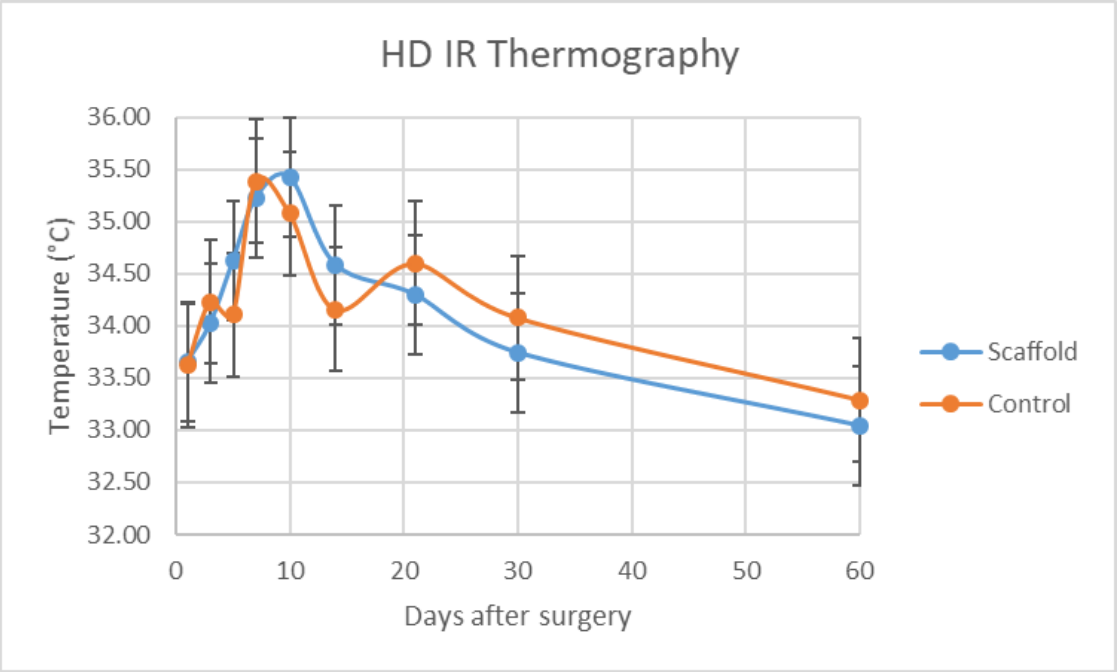


Figure 5-7. Thermography graph.

The graph shows changes in cutaneous temperature (°C) associated with local tissues adjacent to created defects. Temperature was measured with infrared camera over time after surgery.

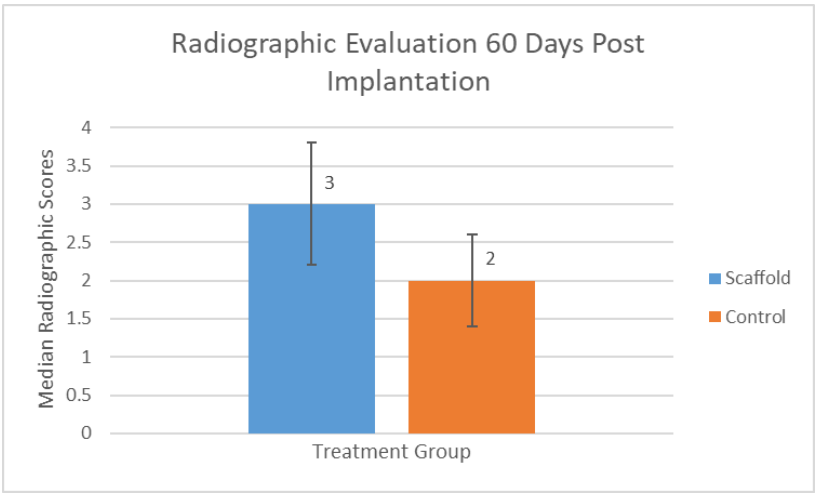


Figure 5-8. Radiographic evaluation 2M after surgery.

The comparison between treatment groups in the median values of radiographic scoring 60 days after implantation surgery

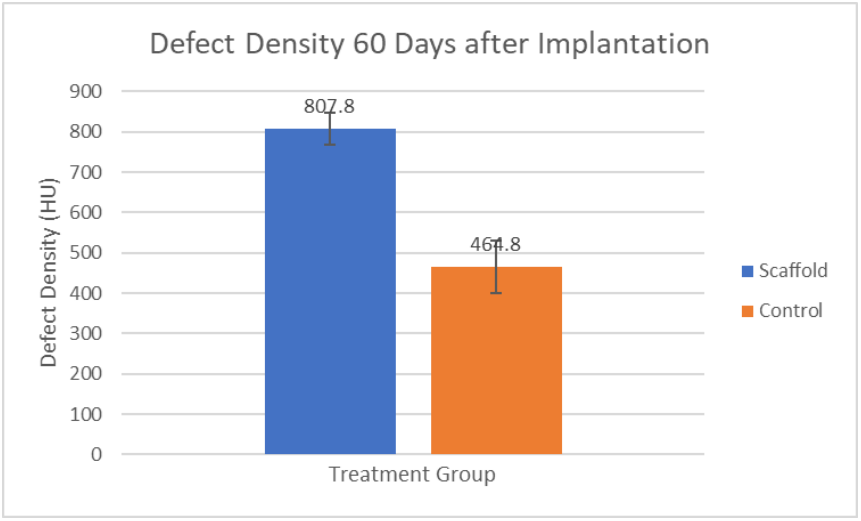


Figure 5-9. Defect density 2M after surgery.

The comparison between treatment groups in mean density the defect measured in Hounsfield Units (HU) from CT images.

Abbreviations

CT – Computed Tomography
DBP – Decellularized Bone Particles
DICOM – Digital Imaging and Communications
DLPMO – Dorso-lateral Palmaro-medial Oblique
HU – Hounsfield Units
H&E - Hematoxylin and Eosin
MC IV – fourth metacarpal bone
NBF – Neutral Buffered Formalin
nHA – nanophase Hydroxyapatite
PACS – Picture Archival and Communication System
PU – Polyurethane
ROI – Region of Interest

Footnotes

a. NuCress™ bone scaffold, NuShores Biosciences LLC, AR
b. Gentamicin sulfate,100mg/ml, VetOne®, Boise, ID
c. Penicillin Procaine G injectable suspension, 300.000 units/ml, VetOne®, Boise, ID
d. Firocoxib, Equioxx injectable, 20 mg/ml, Boehringer Ingelheim Animal Health USA Inc., Duluth, GA
e. Xylazine hydrochloride, Xylamed, 100 mg/ml, VetOne®, Boise, ID
f. Ketamine hydrochloride, Zetamine, 100 mg/ml, VetOne®, Boise, ID
g. Midazolam, 5 mg/ml, Akorn, Ann Arbor, MI
h. Isoflurane, 250 ml, VetOne®, Boise, ID
i. PDS II - Polydioxanone #2-0 (3.0 metric) suture with CT-1 36 mm 1/2c taper needle, Ethicon, Guaynabo, Puerto Rico
j. Surgipro™ – Polypropylene monofilament #0 (3.5 metric) suture with C-17 39 mm 3/8 cutting needle, Covidien, Mansfield, MA
k. Fluke VT04A Visual IR Thermometer, Fluke Corporation, Everett, WA
l. NEXT Equine DR™, Sound Technologies, Carlsbad, CA
m. Logic™ e Vet NextGEN®, Sound Technologies, Carlsbad, CA
n. Philips® Brilliance-40™, Philips International B.V., Amsterdam, Netherlands
o. Sectra® PACS™ IDS7, Sectra AB, Linkoeping, Sweden
p. Microsoft Office Professional Plus 2016, Microsoft, Redmond, WA
q. Fiji, ImageJ, National Institute of Mental Health, Bethesda, MD
r. Neutral Buffered Formalin, Decalcifying solution protocol A, Fisher Scientific Co LLC, Hampton, NH
s. IBM® SPSS Statistics™ v.25 Software, IBM, New York, NY
t. PS Power and Sample Size Calculation, ver 3.0, 2009

Bibliography

References

1. Clegg P.D. Musculoskeletal disease and injury, now and in the future. Part 1: Fractures and fatalities. Equine Vet J 2011: 43(6): 643-649
2. Smith M.R.W., Corletto F.C., Wright I.M. Parasagittal fractures of the proximal phalanx in Thoroughbred racehorses in the UK: Outcome of repaired fractures in 113 cases (2007–2011). Equine Vet J 2017;49(6): 784-788
3. Samiullah M.H., Varma V.S., Nguhiu-Mwangi J., Mogoa E.G.M. Incidence, types and outcomes of distal limb fractures of racehorses in Kenya: A retrospective study of radiographs (2005-2014). International Journal of Veterinary Science 2017; 6(2): 81-85
4. Donati B., Furst A.E., Hassig M., Jackson M.A. Epidemiology of Fractures: The role of kick injuries in equine fractures. Equine Vet J 2018; 50(5):580-586
5. McIllwraith C.W. Management of subchondral cystic lesions of medial femoral condyle – an evolution based on research and clinical evidence. Pferdeheilkunde 2010; 26(4):591
6. McIllwraith, C.W. Subchondral bone cysts in the horse: aetiology, diagnosis and treatment options. Equine vet. Educ. 1998; 6, 313-317.
7. Baxter, G.M. (1996) Subchondral cystic lesions in horses. In: Joint Disease in the Horse, Eds: C.W. McIlwraith and G.W. Trotter, W.B. Saunders Co., Philadelphia. pp 384-397
8. Ortved K.F., Nixon A.J., Mohammed H.O., Fortier L.A. Treatment of subchondral cystic lesions of the medial femoral condyle of mature horses with growth factor enhanced chondrocyte grafts: A retrospective study of 49 cases. Equine Vet. J. 2012; 44:606-613
9. Fortier, L.A. and Nixon, A.J. New surgical treatments for osteochondritis dissecans and subchondral bone cysts. Vet. Clin. N. Am.: Equine Pract. 2005; 21, 673-690
10. Santschi E.M., Williams J.M., Morgan J.W., Johnson C.R., Bertone A.L., Juzwiak J.S. Preliminary investigation of the treatment of equine medial femoral condylar subchondral cystic lesions with a transcondylar screw. Vet Surg. 2015; 44:281-288.
11. Glass K., Watts A.E. Septic Arthritis, Physitis, and Osteomyelitis in Foals. Vet Clin North Am Equine Pract. 2017; 33(2):299-314
12. Curtiss A.L., Stefanovski D., Richardson D.W. Surgical site infection associated with equine orthopedic internal fixation: 155 cases (2008-2016). Veterinary Surgery 2019; 48:685-693
13. Auer J.A., Grainger D.W. Fracture management in horses: Where have we been and where are we going? The Veterinary Journal 2015; 206:5-14
14. Ahern B.J., Richardson D.W., Boston R.C., Schaer T.P. Orthopedic infections in equine long bone fractures and arthrodeses treated by internal fixation:192 cases (1990-2006). Vet Surg 2010; 39:588–593.

15. Uzal F.A., Diab S.S. Gastritis, Enteritis, and Colitis in Horses. Vet Clin North Am Equine Pract. 2015; 31(2):337-58
16. Welsh C.E., Duz M., Parkin T.D.H., Marshall J.F. Disease and pharmacologic risk factors for first and subsequent episodes of equine laminitis: A cohort study of free-text electronic medical records. Prev Vet Med. 2017; 136:11-18.
17. Fillingham Y., Jacobs J. Bone Grafts and Their Substitutes. Bone Joint J. 2016; 98-B (1 Suppl A):6-9
18. Millis D., Martinez S.A. Bone Grafts in Slatter DH (ed): Textbook of Small Animal Surgery. 3rd Ed. Saunders, Philadelphia, 2003: 1875
19. Auer J.A., von Rechenberg B., Bohner M., Hofmann - Amtenbrink M. Bone Grafts and Bone Replacements in Auer J.A. and Stick J.A. Equine Surgery Fourth Ed. Elsevier Saunders St Louis, MI 2012:1081-1094
20. Younger E.M., Chapman M.W. Morbidity at bone graft donor sites. J Orthop Trauma 1989; 3:192–195.
21. Albrektsson T., Johansson C. Osteoinduction, osteoconduction and osseointegration. Eur Spine J 2001; 10: S96-S101
22. Cohen J.M., Southwood L.L., Engiles J., Leitch M., Nunamaker D.M. Effects of a novel hydrogel on equine bone healing: A pilot study. Vet Comp Orthop Traumatol 2012; 3:185-191
23. David F., Levingstone T.J., Schneeweiss W., de Swarte M., Jahns H., Gleeson J.P., O'Brien F.J. Enhanced bone healing using collagen-hydroxyapatite bone scaffold implantation in the treatment of a large multiloculated mandibular aneurysmal bone cyst in a thoroughbred filly. J Tissue Eng Regen Med. 2015; 9(10):1193-9
24. Stack J.D., Levingstone T.J., Lalor W., Sanders R., Kearney C., O'Brien F.J., David F. Repair of large osteochondritis dissecans lesions using a novel multilayered tissue engineered construct in an equine athlete. J Tissue Eng Regen Med. 2017; 11(10):2785-2795.
25. Korthagen N.M., Brommer H., Hermsen G., Plomp S.G.M., Melsom G., Coeleveld K., Mastbergen S.C., Weinans H., van Buul W., van Weeren P.R. A short-term evaluation of a thermoplastic polyurethane implant for osteochondral defect repair in an equine model. Vet J. 2019; 251:105340.
26. Alghazali, K., Srivatsan, M., Trigwell, S., Bumpass, D., Mannen, E., McCarthy, R., Anderson, D.E., Biris, A.S., (2019). Bone scaffold as a spine fusion novel solution. Abstract presented at Defense TechConnect Innovation Summit October 8-10, National Harbor, MD
27. Oh S.H., Park S.C., Kim H.K., Koh Y.J., Lee J.H., Lee M.C., Lee, J.H. Degradation behavior of 3D porous polydioxanone-b-polycaprolactone bone scaffolds fabricated using the melt-molding particulate-leaching method. J. Biomater. Sci. Polym. 2011; 22(1–3):225-237
28. Steflik D.E., Corpe R.S., Young T.R., Sisk A.L., Parr G.R. The biologic tissue responses to uncoated and coated implanted biomaterials. Adv Dent Res 1999;27–33.

29. Kim H.W., Knowles J.C., Kim H.E. Hydroxyapatite/poly (epsiloncaprolactone) composite coatings on hydroxyapatite porous bone scaffold for drug delivery. Biomaterials 2004;25(7–8):1279–87
30. Zakaria S.M., Zein S.H.S., Othman M.R., Yang F., Jansen J.A. Nanophase Hydroxyapatite as a Biomaterial in Advanced Hard Tissue Engineering: A Review. Tissue Engineering Part B 2013; 19(5):431-441
31. Gabriel L.P., dos Santos M.E., Jardini A.L., Bastos G.N.T., Dias C.G.B.T., Webster T.J., Filho R.M. Bio-based polyurethane for tissue engineering applications: How hydroxyapatite nanoparticles influence the structure, thermal and biological behavior of polyurethane composites. Nanomedicine: Nanotechnology, Biology, and Medicine 2017; 13:201–208
32. Jenson P.W., Gaughan E.M., Lillich J.D., Bryant J.E. Segmental ostectomy of the second and fourth metacarpal and metatarsal bones in horses: 17 cases (1993-2002). JAVMA 2004; 224(2): 271-274
33. Southwood LL KCMCFD: evaluation of an equine metacarpal IV fracture defect model. Vet Surg 2006; 35, E1-E28
34. Ishihara A., Shields K.M., Litsky A.S., Mattoon J.S., Weisbrode S.E., Bartlett J.S., Bertone A.L. Osteogenic Gene Regulation and Relative Acceleration of Healing by Adenoviral-Mediated Transfer of Human BMP-2 or -6 in Equine Osteotomy and Ostectomy Models. J of Orthop Res 2008; 6:764-771
35. McDuffy L.A., Pack L.A., Lores M., Wright G.M., Esparza-Gonzalez B., Masaoud E. Osteoprogenitor Cell Therapy in an Equine Fracture Model. Vet Surg 2012; 41:773-783
36. Ishihara A., Zekas L.J., Litsky A.S., Weisbrode S.E., Bertone A.L. Dermal Fibroblast-Mediated BMP2 Therapy to Accelerate Bone Healing in an Equine Osteotomy Model. J of Orthop Res 2010; 28:403-411
37. Perrier M., Lu Y., Nemke B., Kobayashi H., Peterson A., Markel M. Acceleration of Second and Fourth Metatarsal Fracture Healing with Recombinant Human Bone Morphogenetic Protein-2/Calcium Phosphate Cement in Horses. Vet Surg 2008:37;648-655.
38. Southwood L.L., Kawcak C.E., Hidaka C., McIlwraith C.W., Werpy N., Macleay J., Frisbie D. Evaluation of Direct In-vivo Gene Transfer in an Equine Metacarpal IV Ostectomy Model Using an Adenoviral Vector Encoding the Bone Morphogenetic Protein-2 and Protein-7 Gene. Vet Surg 2012; 41:345-354Rossi F., Santoro M., Perale G. Polymeric bone scaffolds as stem cells carriers in bone repair. J Tissue Eng Regen Med 2015; 9:1093-1119
39. Yu J., Xia H., Teramoto A., Ni Q.Q. The effect of hydroxyapatite nanoparticles on mechanical behavior and biological performance of porous shape memory polyurethane bone scaffolds. J Biomed Mater Res Part A 2018:106A:244–254.
40. Rogers L., Said S.S., Meguanint K. The effects of fabrication strategies on 3d bone scaffold morphology, porosity, and vascular smooth muscle cell response. J. Biomater. Tissue Eng. 2013; 3(3):300–311.

41. Tsai S.W., Huang S.S., Yu W.X., Hsu Y.W., Hsu F.Y. Fabrication and Characteristics of Porous Hydroxyapatite-CaO Composite Nanofibers for Biomedical Applications. Nanomaterials 2018,8,0:1-9
42. Fuerstenberg C.H., Wiedenhoefer B., Putz C., Burckhardt I., Gantz S., Kleinschmidt K., Schroeder K. Collagen hydroxyapatite (Healos) saturated with gentamicin or levofloxacin. In vitro antimicrobial effectiveness – a pilot study. Orthopade 2010; 39(4):437-43 46.
43. Andronescu E., Ficai A., Albu M.G., Mitran V., Sonmez M., Ficai D., Ion R., Cimpean A. Collagenhydroxyapatite/Cisplatin Drug Delivery Systems for Locoregional Treatment of Bone Cancer. Technology in Cancer Research & Treatment 2013; 12(4): 275-284 47.
44. Zhou H., Lee J. Nanoscale hydroxyapatite particles for bone tissue engineering. Acta Biomater 2011; 7: 2769 48.
45. Venkatesan J., Kim S.K. Nano-Hydroxyapatite Composite Biomaterials for Bone Tissue Engineering – A review. Journal of Biomedical Nanotechnology 2014; 10: 3124-3140
46. Schaer T.P., Bramlage L.R., Embertson R.M., Hance S. Proximal interphalangeal arthrodesis in 22 horses. Equine Vet. J. 2001; 33(4): 360-365
47. Herthel T.D., Rick M.C., Judy C.E., Cohen N.D., Herthel D.J. Retrospective analysis of factors associated with outcome of proximal interphalangeal joint arthrodesis in 82 horses including Warmblood and Thoroughbred sport horses and Quarter Horses (1992–2014). Equine Vet J 2015; 48:557-564
48. Carpenter R.S., Galuppo L.D., Simpson E.L. Clinical evaluation of the locking compression plate for fetlock arthrodesis in six thoroughbred racehorses. Vet Surg 2008; 37(3):263-268
49. Biedrzycki A.H., Grant B.G., Nemke B. In vitro biomechanical evaluation of four surgical techniques for fusion of equine centrodistal and tarsometatarsal joints. Am J of Vet Res 2016; 77(10):1071-1081
50. Moore B.R., Reed S.M., Robertson J.T. Surgical treatment of cervical stenotic myelopathy in horses: 73 cases (1983-1992). J Am. Vet. Med. Assoc. 1993; 203(1):108-12
51. DeBowes R.M., Grant B.D., Bagby G.W., Gallina A.M., Sande R.D., Ratzlaff M.H. Cervical vertebral interbody fusion in the horse: a comparative study of bovine xenografts and autografts supported by stainless steel baskets. Am J. Vet. Res. 1984; 45(1):191-9

VITA

Remigiusz M. Grzeskowiak was born on September 29th in 1988 in Poznan, Poland. He wrote the dissertation and all included manuscripts. Remigiusz graduated in 2013 from the Wroclaw University of Environmental and Life Sciences in Wroclaw, Poland. During veterinary school, he was awarded two years scholarship at the University of Veterinary Medicine in Vienna, Austria, where he did a one-year rotating internship in equine medicine at the Veterinary Teaching Hospital. Following the internship, he worked as an associate veterinarian in equine private practice for six months which was succeeded by two years of advanced equine surgery internship at Hagyard Equine Medical Institute in Lexington, Kentucky. After this internship, Remigiusz moved down to Knoxville, Tennessee to pursue the Ph.D. program in Comparative and Experimental Medicine at the University of Tennessee, College of Veterinary Medicine. Already during veterinary school, Remigiusz showed significant interest in equine medicine as well as in orthopedic research.